FABRICATION AND CHARACTERIZATION OF AN UPSIDE-DOWN CNT MEA

NIKOLAS GAIO

MASTER OF SCIENCE THESIS

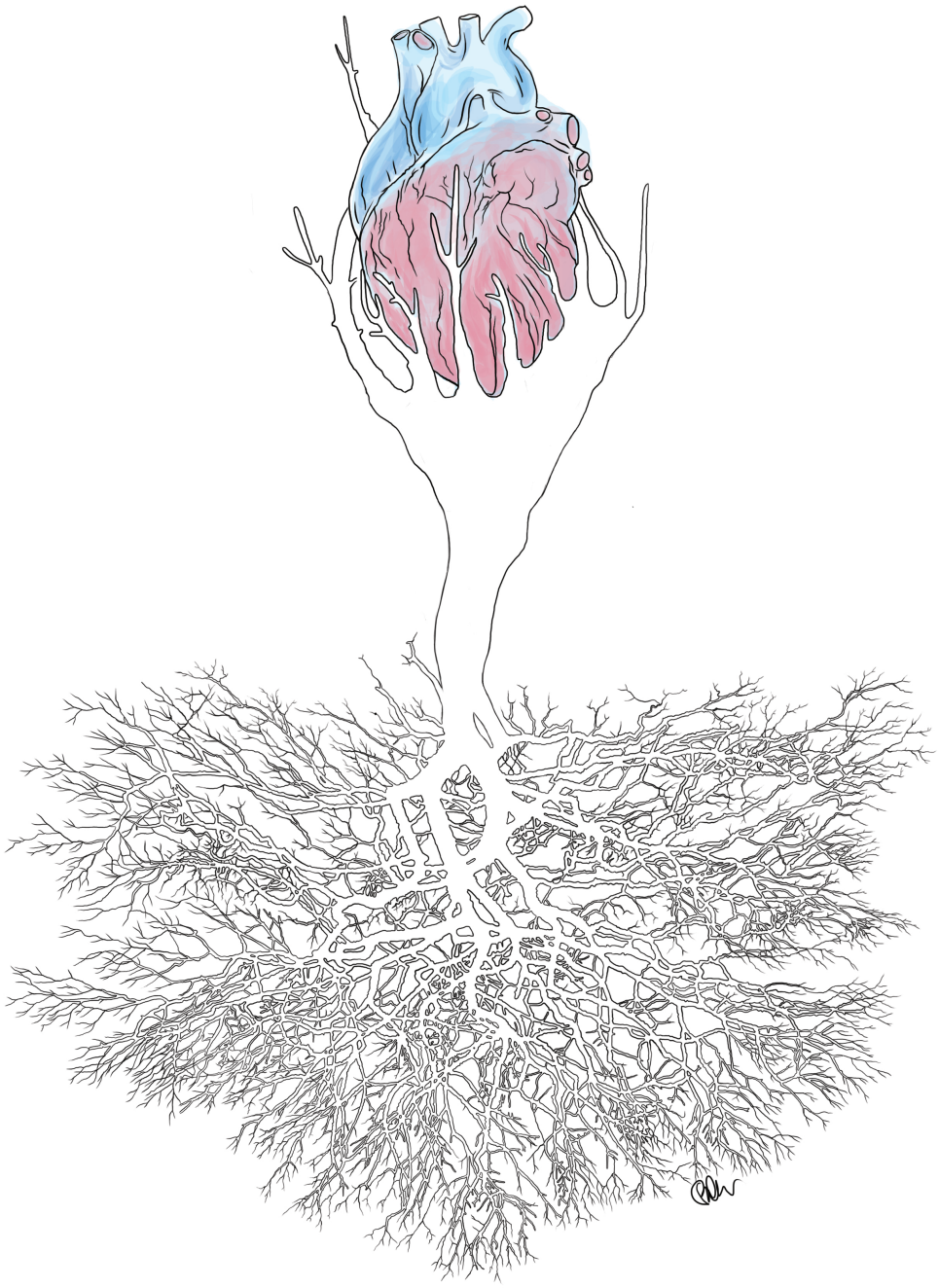

TU Delft Delft University of Technology

BIOMEDICAL ENGENEERING, 3ME

Fabrication and characterization of an Upside-down CNT MEA

Master of Science Thesis

For the degree of Master of Science in Biomedical Instrumentation at Delft University of Technology

Nikolas Gaio

March 18, 2015

Faculty of Mechanical, Maritime and Materials Engineering (3mE) · Delft University of Technology


TU Delft
Delft
University of
Technology

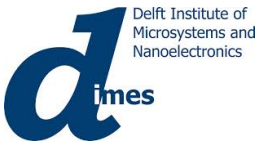
Delft Institute of
Microsystems and
Nanoelectronics
dimes

Delft University of Technology
Department of
Biomedical engineering

The undersigned hereby certify that they have read and recommend to the Faculty of Mechanical, Maritime and Materials Engineering (3mE) for acceptance a thesis entitled

Fabrication and characterization of an Upside-down CNT MEA

by

Nikolas Gaio

in partial fulfillment of the requirements for the degree of

Master of Science Biomedical Instrumentation

Dated: March 18, 2015

Supervisor(s):

Prof. Dr. Ronald Dekker

Prof. Dr. Lina Sarro

Reader(s):

Prof. Dr. Paddy French

Abstract

Over the last few years the need of new alternatives to traditional disease modelling, drug screening and toxicity tests has boosted the development of a new class of devices called Organ on Chip. These usually consist in a substrate or a well in which cells are cultured with the aim of differentiating them in a particular tissue lineage. With sensors and actuators integrated in the device, a culturing environment, as close as possible to *in vivo* one, is reproduced. This stimulates both cell differentiation and viability, boosting model reliability in this way.

An instance of this class of devices is the Heart on Chip developed by Philips Research in collaboration with TU Delft. This device, also know as Cytostretch device, is a stretchable polydimethylsiloxane (PDMS) membrane embedding a micro-electrode array meant to measure the electrical activity of cardiomyocytes grown on the top of the membrane. Unlike most of previous organ-on-chip designs, the Cytostretch device was developed aiming at fabricating a clean-room compatible product. This should guarantee a large-scale fabrication and a rapid commercialization. Besides this, Philips Research team focused on the mechanical properties of the membrane by opting for a polymer-last approach. These design choices led to the fabrication of multi-electrode array characterized by an electrode-electrolyte impedance too high for the detection of the low-amplitude biopotential signals coming from the cells.

In order to solve this problem, the integration of carbon nanotube (CNT) electrodes into the Cytostretch device will be considered; CNT forests have been widely used to coat biopotential electrodes since they guarantee intrinsically large surface area as well as low electrode-electrolyte impedance. To the best of authors knowledge, this is the first attempt to embed CNT electrodes in an Organ on Chip. Moreover, this is the first work which aims to produce a CNT multiple electrode array with a large-scale fabrication, a fully clean-room compatible process and a polymer-last approach.

This project had three main goals. Firstly, it aimed to characterize Cobalt-grown CNTs as bio-electrode coating. Secondly, it verified the feasibility of a novel fabrication process which allows to embed CNT electrodes in a PDMS membrane without the need to perform critical manual steps and last but not least, it aimed to prove the biocompatibility of CNTs as bio-electrode coating in *in vitro* tests including human induced pluripotential stem cells.

Table of Contents

Acknowledgements **xiii**

1 Introduction **1**

1-1 Organ on Chip . . . 2

1-2 Cytostretch device . . . 3

1-2-1 Design . . . 3

1-2-2 Fabrication . . . 6

1-3 Contribution of this project: introduction of CNT electrodes in the Cytostretch device . . . 7

1-3-1 Thesis outline . . . 7

2 Cytostretch and CNT MEA **9**

2-1 Electrogenetic cells . . . 9

2-2 Bio-electric signal detection . . . 9

2-2-1 Cytostretch micro-electrode array (MEA) . . . 12

2-3 Electrochemical-performance improvements . . . 13

2-4 Carbon Nanotubes (CNTs) . . . 15

2-4-1 Growth mechanism . . . 16

2-4-2 CNT characterization . . . 17

2-4-3 Cobalt-grown CNT on TiN support . . . 18

2-5 CNT MEA . . . 22

2-5-1 Flexible CNT MEAs . . . 23

2-6 Metal-CNT contact characterization . . . 26

3 Device fabrication **29**
3-1 Overview . . . 29
3-2 Fabrication sequence . . . 30
3-3 Standard CNT/TiN MEA . . . 32
3-4 Rigid Upside-down CNT MEA. . . . 34
3-4-1 CNT growth . . . 34
3-4-2 Contamination prevention . . . 35
3-4-3 Metal interconnects and membrane fabrication . . . 35
3-4-4 CNT electrodes releasing . . . 38
3-5 Stretchable Upside-down CNT MEA. . . . 40

4 Electrochemical Characterization **41**
4-1 Methods . . . 41
4-2 Electrochemical impedance spectroscopy (EIS) set up . . . 44
4-3 Standard MEA EIS . . . 45
4-4 Upside-down MEA EIS . . . 46
4-5 Discussion . . . 47

5 Cell-device interaction **51**
5-1 Induced pluripotential stem cells (iPSC) . . . 51
5-2 CNT toxicity . . . 52
5-3 IPSC-derived cardiomyocytes on CNTs . . . 54
5-3-1 Substrate samples . . . 55
5-3-2 Sample sterilization and coating . . . 55
5-3-3 IPSC-derived cardiomyocyte plating . . . 56
5-3-4 Protocol definition . . . 57
5-3-5 IPSC-derived cardiomyocytes on CNT pattern . . . 58
5-4 Extracellular recording . . . 60
5-5 Discussion . . . 61

6 Conclusion **63**
6-1 Recommendations and future work . . . 64

A Standard MEA **67**
A-1 Starting material . . . 67
A-2 Flowchart summary . . . 68
A-3 Detailed flowchart . . . 69

B Upside-down CNT MEA **77**
B-1 Starting material . . . 77
B-2 Flowchart summary . . . 78
B-3 Detailed flowchart . . . 80

C Mask set **95**

Bibliography **99**

Glossary **105**

List of Acronyms 105

List of Symbols 106

List of Figures

1-1 (a) Cytostretch device die and (b) optical image of the TiN micro-electrodes [1]. 4

1-2 (a) Second principal strain magnitude FEM with highlighted zero-crossing trajectory of the second principal strain in an inflated membrane without interconnects; (b) second principal strain magnitude in an inflated membrane with interconnects [1]. 5

1-3 Fabrication steps of the Cytostretch device [2] 6

2-1 (b) Equivalent circuits for electrode-electrolyte interfaces. This can be approximated by Capacitive and Faradaic models ((a) ideally polarizable and (c) nonpolarizable) [3]. 11

2-2 (a) Cross-sectional view of the EIS measurement set up used in [1]: two Pt wire electrodes (counter and reference electrodes) are immersed in a PBS droplet on top of the working electrodes; (b,c) the magnitude and phase of the double-layer impedance of five TiN electrodes measured in parallel [1]. 12

2-3 Bode plot of Cytostretch EIS and fitted plot. 13

2-4 Considered patterned electrode. 15

2-5 Graphene, SWCNT, and MWCNT representation (from the right) [4]. 15

2-6 Topside view of CNT forest. 16

2-7 CNT wettability tuned by means of UV/ozone, oxygen plasma and vacuum annealing treatments [5]. 18

2-8 CNT forests grown at (a) 350, (b) 400, (c) 500 and (d) $650°$C. 19

2-9 (a) Root and tip growth models [6]; (b,c) SEM images of CNTs synthesized at a two growth temperatures (2' at $500°$C and 2' $600°$C). 20

2-10 Fitted Raman spectra of CNT grown on 5 nm Co at $500°$C. Original spectrum: solid black line; fitting peaks: dashed green line. 20

2-11 Drop test on top of CNT forests grown at different temperatures. 22

2-12 Survey, presented in [7], including micro-electrode impedances at 1 kHz vs geometric surface surface area. 23

2-13 (a) High resolution SEM image of a neuronal cell on random aligned CNT forest (bar is 1 μm); (b) signals recorded from cultured neurons with a CNT MEA; (c) signals recorded from cultured neurons with a commercial TiN MEA [8]. 24

2-14 (a) Fabrication schematic and (b) photo of flexible CNT electrode array devices presented in [9]. 25

2-15 (a) Optical image of the sample pieces obtained after the failed cross section; (b-c) SEM images of the backside of the free standing aluminum layer after the failed cross section. In (c) the CNT attached on the bottom of the aluminum layer can be seen. 26

2-16 (a) Sketch of a four point probe measurement structure used to characterize CNT-METAL contact; (b) SEM top-side-view image of the structure; (c) I-V characteristics obtained with CNTs grown at 500°C on TiN support and covered with 100 nm of TiN and 2 μm of Al. 27

3-1 Sketch of Standard CNT MEA. 29

3-2 Sketch of Upside-down CNT MEA: (a) backside, (b) frontside. 30

3-3 Process flow for the fabrication of Standard MEA. 30

3-4 Process flow for the fabrication of Upside-down CNT MEA on rigid membrane. . 31

3-5 Process flow for the fabrication of Upside-down CNT MEA on stretchable membrane. 32

3-6 Optical image of the hole right (a) before and (b) after HF etching; (c) SEM image of the Standard TiN electrode; (d) SEM image of the Standard CNT electrode. 33

3-7 (a,b) CNT grown in TEOS hole. 34

3-8 (a,b) Metallization layer composed of 100 nm of TiN and 2 μm of Al on top of CNTs. 35

3-9 (a) SEM images during SiN etching (photoresist not stripped); (b,c) SEM image of metal interconnects 2 μm thick and sputtered at 25°C; (d) 4 μm thick Al layer on top of 2 μm step; (e) 4 μm thick Al layer on top of 2 μm step with scratch caused by measurement needle. 36

3-10 (a) SiN residues on the edge of the circular structure for spacer fabrication; (b-c) 4 μm Al layer sputtered at 350°C; (d) test hole to verify step coverage in hole 1 μm deep and with a 8 μm diameter. 37

3-11 (a) Picture of the final device; (b) optical image of CNT electrode with support TiN circle detaching from CNT roots; (d-f) SEM images of Upside-down electrode. 38

3-12 (a) Optical image of CNT island detached from the electrode; (b) SEM image of failed electrode without CNT; (c) SEM image of failed electrode with CNT island inside cavity; (d) cross section SEM image of failed electrode with CNT island inside cavity. 39

4-1 (b) CVs different materials in PBS at a sweep rate of 20 mV s^{-1} [10]; (b) CV scans of CNT coated electrodes conducted at 20, 140 and 300 mV s^{-1} in PBS [8]. . . 42

4-2 Bode plots of EIS of gold, CNT and plasma-treated CNT micro-electrodes ((a) impedance and (b) phase). Micro-electrodes have a geometric area of 116 μm^2 geometric surface area. Gold electrodes, CNT electrodes and Plasma-treated CNT electrodes show respectively an impedance of 1.3 MΩ, 260 kΩ and 79.4 kΩ. . . . 43

4-3 Rendles circuit used to model CNT electrodes. This correspond to the circuit often used to model metal electrodes with porous organic coating. 43

4-4 Picture of the EIS set up on a Standard CNT MEA. Three electrodes method composed by a reference, a counter and a working electrode were used. 44

4-5 EIS measurement input and output (ca 6 kHz): Voltage stimulation signal (blue) applied across the metal/electrolyte interface and correspondent output current signal (red). 45

4-6 Bode graphs ((a) amplitude and (b) phase) of Standard CNT (red) and TiN (blu) electrodes. Markers show measured data, and solid lines show the fitting curve of the equivalent circuit. 45

4-7 Representative CNT electrode impedance vs time. 46

4-8 Bode plots ((blu) amplitude and (red) phase) of impedance spectra of CNT Upside-down CNT micro-electrodes. Markers show measured data, and solid lines show the fitting curve of the equivalent circuit. 47

4-9 Effect of IPA on 1 μm high CNT forest: sample SEM (a) before and (b) after IPA treatment. 47

4-10 Bode plots of impedance spectra of CNT micro-electrodes after and before IPA treatment. 48

5-1 Adult somatic cells can be reprogrammed in iPSCs; after this, they can be differentiated and used for different application s.a.: (a) disease modeling, (b) drug screening and discovery and (c) toxicity tests [11]. 52

5-2 Receptor-mediated endocytosis and nanopenetration are suggested as two possible mechanisms for CNT interactions with cells [12]. 54

5-3 CNT patterns to verify cell migration: (a) macroscale CNT island (1/1.5 cm diameter) and (b) microscopic CNT island (60 μm diameter). 55

5-4 12-well plate containing CNT samples during cell culture protocol. 56

5-5 Merged fluorescent images of cardiac iPSCs stained with DAPI (blue) and CY3 (red) and plated (a) on top and (b) in proximity of CNTs. 59

5-6 Merged fluorescent images of cardiac iPSC plated on patterned CNTs ((a): macroscopic pattern, (b) microscopic pattern) and stained with DAPI (blue) and CY3 (red). 60

5-7 Optical images of cardiac iPSC (a) on top of cytrostretch device and (b) Upside-down CNT MEA. 61

5-8 Field potential of cardiomyocytes recorded using (a,b) Upside-down CNT MEA and (c,d) Cytostretch device. Signals were obtained after filtering the signal measured by MEA amplifier to remove 50 Hz noise, the frequencies above 200 Hz and below 2 Hz. 62

C-1 Mask: METAL. Blue area not exposed. 95

C-2 Mask: CNT/SiN. CNT: d=12 μm, SiN: d= 6 μm. Blue area not exposed. Mask METAL reported with black dotted lines. 96

C-3 Mask: Ti/Ti2. Ti: d=14 μm, Ti2: d= 24 μm. Blue areas not exposed. Mask METAL reported with black dotted lines. 96

C-4 Mask: BACK. Blue area not exposed. Scribe lines reported in black. 96

C-5 Mask: METAL2. Blue area not exposed. 97

C-6 Maks: ORGAN_V3. Blue area not exposed. 97

List of Tables

2-1 EIS spectra fitting values (Pt, Ti, rough and smooth TiN data: [13]). 14

2-2 Raman data obtained from CNT grown at different temperatures 21

4-1 Average Fitting Parameters for TiN, Standard CNT, and Upside-down CNT Electrodes 49

5-1 List of sample used during protocol definition 57

5-2 Qualitative observations about cell state 36 hours after cell plating (where ✓stands for successful, ✗stands for failed, + stands for positive result and - stands for negative result). 58

A-1 Wafer Specifications 67

A-2 Process conditions from chamber recipe URK_ETCH 69

A-3 Process conditions from chamber recipe TiTiNTi1 71

A-4 Process conditions from chamber recipe xxxnmTEOS 72

A-5 Process conditions from chamber recipe Stdsio2 73

A-6 Process conditions from chamber recipe: SiO_2 etching (Alcatel) 74

B-1 Process conditions from chamber recipe TiTiNTi2 82

B-2 Process conditions from chamber recipe xxxsiostd 85

B-3 Process conditions from chamber recipe al2T01gf 87

B-4 Process conditions from chamber recipe xxxnmsinstd 88

B-5 Process conditions from chamber recipe: SiN etching (Alcatel) 88

B-6 Process conditions from chamber recipe AL4MU350 91

B-7 Process conditions from chamber recipe $zero\_stress\_sio2$ 91

Acknowledgements

I would like to thank Prof. Ronald Dekker for his support and encouragement throughout my time in the Electronic Components, Technology and Materials (ECTM) group. He was open to my unconventional ideas and I consider myself extremely lucky because of that. Special thanks should go to my project supervisor Dr. Gregory Pandraud for his support and correct guidance to keep me on the right track. I am also thankful to Dr. Tom Schotels for his assistance in the clean room. As promised, I am willing to wash his car as a reward for his precious suggestions. Moreover, special thanks go to Dr. Giampaolo for his helpful input, and good suggestions about technology and life.

I am greatly thankful to Dr. Sten Vollebregt; his guidance has been indispensable during this long project. His knowledge of CNTs is an extremely important resource of Dimes. I am thankful to Saeed Pakazad for his suggestions during the electrochemical characterization of the devices. I would also like to thank Berend van Meer for his incredible support in the physiological tests performed on CNTs and I am looking forward to collaborate with him in the future. A special thanks to the PhDs in Delft Institute for Microsystems and Nanoelectronics (DIMES): Cinzia, Giuseppe and Bruno. They have always been available to help me during my technical dramas. Also, the thanks should go to technicians Mario Laros, Silvana Milosavljevic and Johan Wingerden of DIMES.

Finally, I would like to thank all the amazing people I met during this long journey: my classmates (Joaquin, Jose', Dhati, Andita, Shruti), my partners in crime (Liang, Yinxin and Josie) and the colleagues in DIMES (Salvatore, Yorick, AslIhan, Teng, Manju, William, Yelena, Ifi, Jian, Daniel, Yingjie, Ramin and Marta). I am also thankful to Marco, who bore my weekly crises via Skype and last but not least, I would like to thank my family for their never-ending patience and support. Grazie.

Delft, University of Technology — Nikolas Gaio
March 18, 2015

Chapter 1

Introduction

Testing medicine, chemicals and consumer products s.a. cosmetics and soaps is mandatory before their commercialization to guarantee consumer safety. This kind of testing, which mainly relies on information gathered by means of animal experimentations, is defined by specialized national regulators (s.a. the European Medicines Agency (EMA) in Europe). Animal tests used to predict toxicity, corrosivity, and other safety variables, are based on the assumption that small animals can be used as an approximation for the human body. However, this kind of procedure contains several drawbacks and issues: in fact these tests are considered to be unreliable, unpractical and high-cost. The reliability is affected by the genetic differences between small animals and humans: human-specific viruses cannot be tested in these models, for example. Moreover, animal testing involves ethical-related issues. The latter has promoted the definition of a set of principles that are supposed to guarantee animal rights without causing any limitations on testing. [14].

In 1959 Russell and Burch defined the Rs principles, the goals of which are the following: reducing the number of animals used during drug tests, replacing actual tests with non-animal-test alternatives and redefining them to reduce animal pain as much as possible. A complete replacement of animal tests will only be feasible when *in vitro* tests will become as reliable as animal tests. Untill this has been achieved, *in vitro* tests need to be validated with animal models. Even though the full replacement of animal tests is considered not feasible by a large amount of the scientific community, the three principles have been used as starting point for the definition of several animal test legislations in Europe and U.S.A. [14].

Several efforts have been made in Europe to guarantee animal welfare over the last 20 years [15]. Laboratories, s.a. the EURL ECVAM (the European Union Reference Laboratory for Alternatives to Animal Testing), aim to define, validate and promote new non-animal tests by following the Rs principles pursued in the european Directive 2010/EU/63. Animal tests, also called *in vivo* tests, could be partially replaced by employing *in vitro* or *in silico* tests. *In vitro* tests are performed outside a living system rather than in a whole living organism. *In silico* tests consist of mathematical simulations to produce and screen drug candidates. *In vitro* testing will be thoroughly explored in the next paragraphs.

Over the last few years, *in vitro* tests moved from simple and not reliable tissue models

composed of a single cell layer, to more realistic 3D models. This improvement has been possible even though *in vitro* testing is strictly limited due to the trade-off between simplicity and lack of realism. In fact, in order to obtain a realistic *in vitro* test, every cell type which composes a specific tissue should be included in the model. However the insertion of several cell types often leads to uncertainties, complications and unpredictable behaviour [16]. Even though 3D models are available and often used in tissue engineering, in several drug-test applications the complexity of the model is kept as low as possible by employing 2D models. This guarantees the accessibility of the entire cell culture either by means of microscope or chemicals. Moreover, 2D models provide a biologically simple structure and therefore a more predictable behaviour.

The unrealistic behaviour of these simple models was overcome: not only have the biochemical factors, commonly required for cell culturing and to promote cell viability, been dealt with, but also other aspects s.a. geometrical, electrical and mechanical factors. Devices which employ such a technique are referred as Organ on Chips. Their use enables to mimic the behaviour of *in vivo* cells in a more precize way without increasing the biological complexity and unpredictability of models [16].

1-1 Organ on Chip

Van de Stolpe et al. [17] define Organ on Chip as "3D (mini-) organs or tissues consisting of multiple and different cell groups interacting with each other under closely controlled conditions, grown in a microfluidic chip, and mimicking the complex structures and cellular interactions in and between different cell types and organs *in vivo*, enabling the real time monitoring of cellular processes". As can be inferred by the definition, although designs vary from application to application, each of them is composed of one or more cell types cultured on a structure based on microchip technology [16, 17].

In this way it is possible to embed sensors and actuators in the culture environment to assess cell state and stimulate the cells in the model. The latter is employed with the aim to promote both viability and differentiation in the necessary lineage (in case of stem cells). These stimuli, in combination with the interactions among different cells types, recreate organ functionality.

Besides biochemical stimuli performed by means of substances (e.g. drugs and nutrients) usually provided via fluxes, mechanical and electrical stimuli can be exploited. Mechanical stimuli are produced by means of micro-fluidic systems (composed by pumps, valves and channels) and stretchable surfaces. Electrical stimuli are provided by means of electrodes reaching the cells from the culturing substrate. As already stated, these stimuli do not affect the biological complexity. On the contrary, they affect device fabrication and full system complexity.

Another common feature is the use of microscopy as accessibility method: due to this feature, most of the time the structure needs to be transparent or at least partially transparent. Another method for gathering information from cells can be derived from exploitation of the electrical behaviour of cells.

During the past decade the number of publications related to organ-on-chip designs has seen an increase worth noting. These differ in system complexity, technologies employed, measurement methods, stimuli, materials and last but not the least mimicked organ. So far

the majority of the publications has focused on the reproduction of a single tissue or a single organ. Lung, heart, artery, etc. have been reproduced over the last two years [16, 17]. Moreover, even more complex systems, aiming at reproducing the interactions among organs, have been designed. These devices, usually called Human on Chip, milliHuman or microHuman, consist of different Organ on Chips interfacing among each other by means of microfluidic systems.

Organs interaction is supposed to boost the resemblance between the model and *in vivo* conditions. Zhang et al. [18] describe the development of a multichannel system which includes four interconnected micro-enviroments representing liver, lung, kidney and adipose tissue on the same chip. Previous works, s.a. [19], presented different laws to define the dimensions of the different organs in a Human on Chip: wrong relative sizes could lead to unreliable system behaviour. Also, the fluid flowing through the organs plays a critical role concerning the system reliability: for instance, a too large fluid volume could lead to insufficient and delayed organ-organ interactions.

1-2 Cytostretch device

Since almost 40% of clinical introductions of new drugs fail because of cardiac complications, cardiotoxicity tests play a critical role in the toxicity and safety assessment of medicine [20]. Cardiac and non-cardiac drugs can easily cause unexpected drug-induced ventricular arrhythmias leading to cardiac deaths s.a. Torsades de Pointes or ventricular fibrillation. These particular complications are usually related to the interface between the drug and cardiomyocyte ion channels which affects polarization and depolarization phase of cell membranes [21].

Under these circumstances, the development of efficient and low cost cardiac *in vitro* tests is essential to avoid life-threatening drug reactions. Organ on Chips and, in this particular case, Heart on Chips can satisfy this demand by providing an environment which promotes the viability and the differentiation of stem cells into cardiac cells. Moreover, they could increase the reliability of eventual *in vitro* testing by including model dependent conditions which reproduce the *in vivo* environment. The Cytostretch device developed by Pakazad et al. [1] can be used for this particular purpose.

This device is an *in vitro* environment composed by a micro-electrode array embedded in a PDMS membrane; this can be employed to merge the need of mechanical stimulation and electrical characterization of cardiomyocyte cell cultures [2]. Mechanical stimuli are provided by means of a pneumatic system which stretch the surface periodically. As proven in previous works [22, 23, 24], cardiac cell differentiation can be improved by means of mechanical stimuli. These replace the mechanical inputs that each heart cell receives from the surrounding cells. Moreover, the PDMS surface also presents radial micro-grooves which stimulate cell alignment: this, as mentioned in [25], improves the directional contraction of the heart.

1-2-1 Design

This section provides a detailed description of the Cytostretch design. This multielectrode array (MEA) has been developed for biomedical applications s.a. myocardial cell culturing.

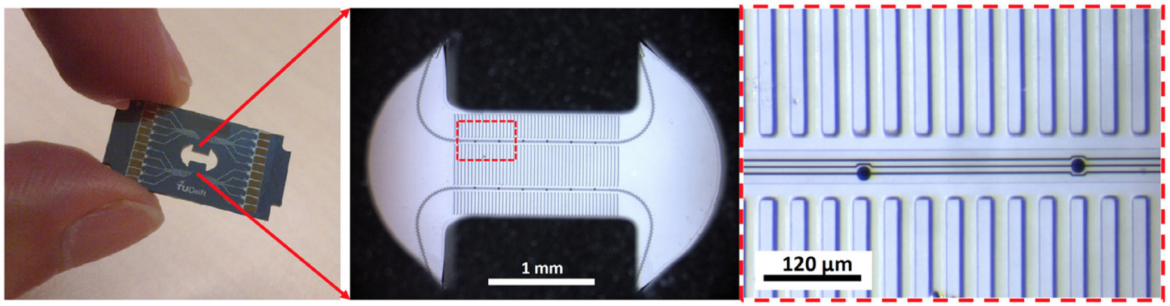

Figure 1-1: (a) Cytostretch device die and (b) optical image of the TiN micro-electrodes [1].

The Cytostretch is composed of a freestanding PDMS membrane which covers a dog-bone hole in a silicon (Si) substrate. The 12 μm thick PDMS membrane includes 12 micro-electrodes placed on two lines in the rectangular part of the dog-bone shape, as shown in Fig. 1-1. This area is considered to be the active part of the device above which cardiomyocyte cells are cultured.

Micro-electrodes and electrical interconnects are made of Titanium Nitride (TiN). This material, commonly used for bio-electrodes, provides several advantages s.a. good biocompatibility, intrinsic chemical and mechanical stability and a very high specific surface area (providing a very low electrolyte-electrode impedance as a consequence). Moreover TiN is easy to deposit and pattern. The interconnects on the Si chip are made of Aluminum (Al).

For the fabrication of the Cytostretch device a "polymer last approach" was chosen. This design differs from previous works due to its fabrication procedure. In fact, previous stretchable MEAs simply consisted of electrodes and interconnects deposited on top of a PDMS surface. Mechanical properties of the PDMS are dependent on several processing parameters: as reported in [2], it provides a low stiffness and has a high thermal expansion and swelling. This means that the number of steps performed after PDMS spinning should be reduced to the minimum.

Pakazad and colleagues in [1] claimed to be able to limit this problem with their procedure in which the deposition of the electrodes and the interconnects precedes PDMS spinning. The fabrication starts with the deposition and patterning of the electrodes, the interconnects and the contact pads on a Silicon Dioxide (SiO_2) layer grown on a Si wafer. After that, the PDMS membrane is applied on top of the wafer and is then released by etching the SiO layer beneath the PDMS. The active area of the membrane is on the backside of the wafer in this case. Device fabrication is covered in more details in Section 1-2-2. The Cytostretch device is completely fabricated in a clean-room environment, moreover, the lack of manual steps enables a large-scale fabrication of the device.

Mechanical Design

An extensive mechanical optimization was performed to guarantee that the interconnects included in PDMS can withstand the strain during membrane expansion. Several alternatives to improve the stretchability of classic metal interconnects are available: these are necessary since metals and metal alloys are not inherently stretchable. Alternative stretchable materials are available, e.g. liquid metals, liquid metal alloys, elastomers doped or implanted

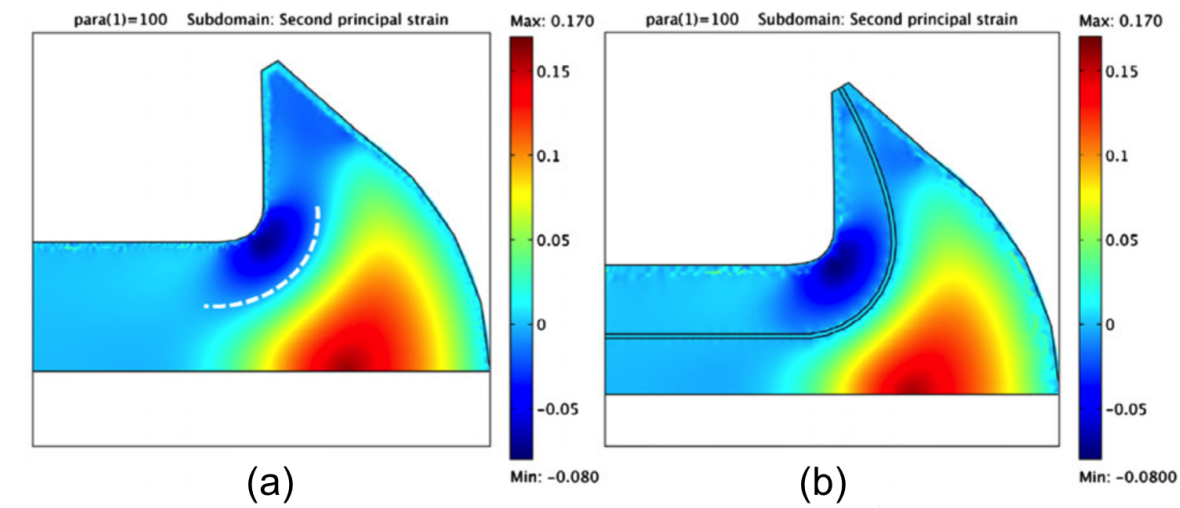

Figure 1-2: (a) Second principal strain magnitude FEM with highlighted zero-crossing trajectory of the second principal strain in an inflated membrane without interconnects; (b) second principal strain magnitude in an inflated membrane with interconnects [1].

with conductive particles, and metal deposition on elastomers as reported in [2]. However, these options are not compatible with a large-scale fabrication. The second option to reduce interconnect stress consists in patterning the interconnects in a wavy or serpentine shape. Such a design reduces the strain during membrane inflation promoting the bending in-plane or out-of-plane of the metal interconnects. However, because this design occupies a higher surface area, the surface topography and the mechanical properties of the membrane drastically change. Moreover, the fatigue life time is affected by the mechanical bending of the interconnects.

Since both solutions have been considered unsuitable for this process, Pakazad et al. [1] opted for an optimization of the topography and trajectories of the interconnects, aiming at reducing forces and strain applied on the interconnects as much as possible. For this purpose, stress and strain on the membrane during inflation were evaluated by means of finite-element model (FEM) mechanical simulations. In particular, they were placed in such a way that their trajectories are always perpendicular to the first principal strain direction and looking for those trajectories where second principal strain was minimum. By following these design principles, interconnects need only to bear second principle strain longitudinally.

The dog-bone shape of the PDMS structure was chosen to reduce the mechanical effects on the electrical interconnects during membrane inflation. The functional area of the MEA, which consists in the rectangular area of the dog bone membrane, experiences almost unidirectional strain during inflation because of its semi-cylindrical shape. This provides directional stretching of the cells, improving in this way cell alignment and guaranteeing a negligible second principal strain. The circular region provides a path for the electrical interconnects which guarantees the minimal strain for the metal.

As can be conveyed from Fig. 1-2a, the second principal strain on the membrane goes from negative to positive values in specific areas. The zero-crossing line is the trajectory where the interconnects experience the minimum second principal strain, which should be theoretically zero along those trajectories. Authors verified that the presence of the interconnects in the

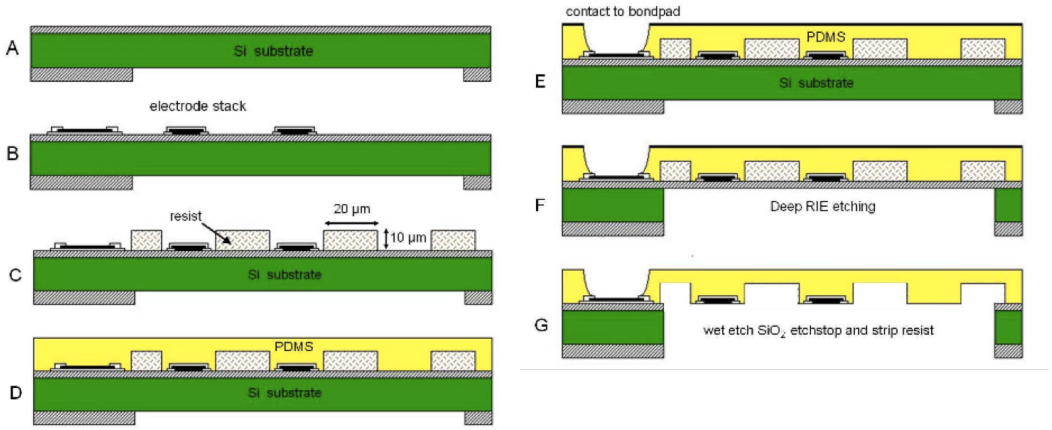

Figure 1-3: Fabrication steps of the Cytostretch device [2]

simulations does not move the zero-crossing line (Fig. 1-2b). This is due to the fact that the interconnects in that position do not take up longitudinal stress. Moreover, it was proved that zero crossing path is not affected by the movement of the membrane: in fact, the position of the line does not change when the membrane is inflated. As a consequence of this extensive mechanical design, the interconnects tilt out of plane rather than being stretched when the membrane is inflated.

1-2-2 Fabrication

The fabrication of the Heart on Chip starts with a four inches Si wafer with 1 μm of thermal SiO_2 on both sides: the oxide on the frontside will be used as a support for the following steps and as a landing layer for the final through-silicon-wafer etching step. An additional oxide layer is deposited on the backside of the wafer by means of plasma enhanced chemical vapour deposition (PECVD). As shown in Fig. 1-3a, the backside is patterned by means of dry etching, defining shape and dimensions of the final membrane. After this, electrodes and interconnects are deposited on the surface; these consist in a 100 nm thick layer of sputtered TiN enclosed in two layers of parylene (1-3b). Both first and second insulating layers are deposited by vapour phase deposition until they reach a thickness of 2 μm and then they are patterned by means of dry etching.

After this, a 10 μm thick photoresist is spun and patterned: this is employed as a mold for the micro patterning formation on the PDMS membrane. Then, PDMS is spun on the wafer and metal openings for electrical measurements are patterned on the front side, as shown in Fig. 1-3e. The membrane is freed from the substrate by means of deep reactive ion etching (DRIE); Si wafer etching pattern is defined by the SiO_2 hard mask on the backside. In the end, SiO_2 and resist are removed from the backside and the frontside of the membrane respectively.

1-3 Contribution of this project: introduction of CNT electrodes in the Cytostretch device

The aim of this thesis is to enhance the electrochemical performance of Cytostretch device by increasing the specific surface area (SSA)[1] of its micro-electrodes. This MEA has in fact shown poor performance in the detection of the bio-signals coming from cells cultured on top of the device. Since this problem has been ascribed to the high electrode-electrolyte impedance of Cytostretch electrodes [1], the thesis mainly focuses on researching a valid solution to reduce this value. During the literature review, the integration of Carbon Nanotube (CNT) electrodes in the device has been identified as one of the most suitable solution to improve its performance. In order to embed this material in the device, four main objectives were identified:

- Characterize the CNTs that will be used to increase the performance of the device. For this particular project, CNTs will be catalyzed on top of Cobalt (Co) supported by TiN.
- Characterize the electrochemical performance of Co-grown CNT electrodes.
- Embed CNT electrodes in a membrane and characterize the MEA.
- Assess the biocompatibility of CNTs used as bio-electrode coating.

1-3-1 Thesis outline

The thesis is structured as follows: Chapter 2 starts describing the theory behind generation and detection of the potential field variations caused by cardiomyocytes. From this, it can be inferred that, to improve micro-electrode performance, it is necessary to increase their SSA. The second part of this chapter presents CNTs as a suitable material for this purpose. Moreover, the characterization of the CNTs used in this thesis will be presented.

Chapter 3 describes the fabrication of two MEAs: one to characterize Co-grown CNT electrodes and the other to prove that it is possible to embed CNT electrodes in a PDMS membrane guaranteeing a large-scale-fabrication process. The latter can be considered a completely novel device. Chapter 4 presents the characterization of the devices just mentioned: this includes the electrochemical impedance spectroscopy tests performed on the electrodes.

Chapter 5 consist of a brief discussion about CNT and catalyst toxicity followed by a biocompatibility assessment of CNT forests as culture substrate for human induced pluripotential cells. This ends presenting the extracellular recordings performed on cardiomyocytes cultures. In Chapter 6 conclusions are drawn and eventual future works presented. Appendixes A and B present detailed fabrication flowcharts defined during this master project and Appendix C includes the mask set used for the fabrication of the devices.

[1] Total surface area of a material per unit of mass, solid or bulk volume, or cross-sectional area

Chapter 2

Cytostretch and CNT MEA

2-1 Electrogenetic cells

Cardiac cells, muscle and neuronal cells, are said to be electrogenic since they generate ion flow across the tissues which include them. The electrical signal coming from cells is mediated by their membrane and the potential across it (V_m). The source of this potential is the difference in ion concentration (K^+, Na^+ and Ca^{2+}) between the cytoplasm and the extracellular space. Cell membrane consists in a phospholipid bilayer completely impermeable to ions. Nevertheless, variations of the membrane potential are due to migration of ions inwards and outwards the cell; this is enabled by ion channels included in the bilayer structure. In fact, in order to cross this layer ions have to pass through specialized transporter or channel proteins embedded in the cell membrane.

By measuring the membrane potential, it is possible to verify that neurones and cardiac cells are electrically excitable. Under chemical or electrical depolarization, V_m is altered: when it becomes more positive than a threshold voltage (V_t), cell reacts with an all-or-none response called action potential (or spike). In case of action potential, the membrane potential rapidly rises (starting from a resting potential around -80 mV and reaching a value between +10 and +40 mV). After this, the cell experiences a slow repolarization step which brings the membrane potential back to the initial value.

2-2 Bio-electric signal detection

Membrane potential variations can be measured by means of intracellular electrodes, spectroscopic technique and extracellular electrodes. The first technique measures V_m by inserting a sharp micro-electrode inside a cell. Membrane potential is evaluated by measuring the voltage difference between the internal electrode and another electrode placed close to the cell. The second technique detects potential variations by dying cell membranes. Both intracellular recording and spectroscopy techniques are unsuitable for dynamic measurements [26].

The third option available to study this electrical activity is detecting the field potential

variations in the extracellular volume in proximity of a group of cells by means of a micro-electrode. As opposed to intracellular recording the source consists in a group of cells. For this reason it is necessary to improve measurement spatial resolution by reducing micro-electrode geometric surface area (GSA) as much as possible.

Biopotential electrodes work as transducers, transforming the ionic current flowing in the extracellular space into an electron current in the electrode metal: this is then read out by means of an external circuit. In case of devices meant to stimulate cells with electrical signals, s.a. cochlear implants and brain stimulators, electrodes perform the same transformation but in the opposite direction. This signal transformation is ascribed to the interface of two phases (metal-solution) created when the electrode is soaked in a physiological solution s.a. extra-cellular fluid. Thus, the electrochemical interface between the electrode and electrolyte plays a critical role in the stimulation and the detection of cell electrical activity.

The transformation of an ion flow into an electron flow is mainly due to following reactions: Faradaic and Capacitive. The former includes oxidation and reduction phenomena at the metal-electrolyte interface. In case no current is flowing across the interface, these reactions still occur but oxidation and reduction rate are equal, thus, the total charge transfer is equal to zero. However, if current is flowing across the interface, either oxidation or reduction is dominating.

On the other side, Capacitive reactions are related to ions displacement on top of the electrodes when the MEA is soaked in an electrolyte. Several theories were developed to describe the ion distribution at the metal-electrolyte interface: all of them end describing this distribution as a separation of charges called electric double layer at the metal-electrolyte interface. This is composed by a layer of charge on the surface of the metal and the opposite kind of charge distributed in excess in proximity of the metal. The charge separation is equal to the Helmholtz double layer thickness which is defined as half of the diameter of the absorbed solvated ions [16].

The behaviour of the interface when a current is flowing between the electrolyte and the electrode depends on the electrode material: these variations allow to subdivide electrodes in polarizable and non-polarizable. In case of perfectly polarizable electrodes the current flowing in the electrolyte does not cross the interface by means of chemical reactions (redox). On the contrary the current is generated in the electrode by means of charge displacement. In this case the interface is behaving as a capacitor: the conversion of ion signal into electron signal is performed by means of charging and discharging of this capacitor. In order to obtain Faradaic reactions on these electrodes it is necessary to provide enough energy in form of over potential at the interface.

In case of perfectly non-polarizable electrodes, the current passes through the interface by means of reduction/oxidation reactions without any need of additional energy. Even if neither of the two ideal types can be fabricated, some materials show similar behaviour. For example, inherent materials s.a. Platinum (Pt) do not oxidise, reduce and dissolve: for this reason Pt, if used as electrodes, will detect the biological signal only by means of charge-displacement currents. Silver/Silver Chloride (Ag/AgCl) electrodes on the contrary detect cell activity through Faradaic reactions [27].

The signal coming from Capacitive reactions has smaller amplitude than one coming from Faradaic reactions, nevertheless, polarizable electrodes are the best choice since they avoid electrode surface oxidation and reduction; these reactions can indeed be partially irreversible causing tissue and electrodes damages [10]. In case of Capacitive electrodes, it is possible

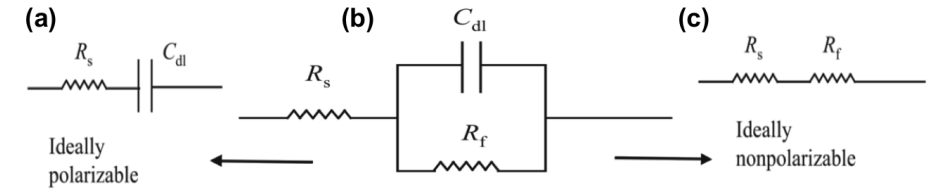

Figure 2-1: (b) Equivalent circuits for electrode-electrolyte interfaces. This can be approximated by Capacitive and Faradaic models ((a) ideally polarizable and (c) nonpolarizable) [3].

to increase signal amplitude by enlarging C_{dl} increasing either the GSA or the SSA of the electrodes.

The electrode-electrolyte interface can be represented with an equivalent circuit, known as Randles circuit. In Fig. 2-1b the Randles circuit used for metal electrodes is reported. This circuit includes a capacitor which corresponds to the double layer capacitor mentioned in the previous paragraphs. This is shunted by a Faradaic resistance; the parallel of the two elements is in series with a resistance representing the solution. Faradaic resistance is dependent on which kind of material the electrode is made of. In case of a Capacitive material R_f is large and the circuit can be simplified obtaining Fig. 2-1a. In case of Faradaic reactions the circuit can be simplified to R_s and R_f in series like in Fig. 2-1c [3].

In case of rough surfaces, for a more practical representation of the electrode-electrolyte interface, the capacitance in the circuit Fig. 2-1 is substituted by a constant phase element (CPE) given by:

$$Z_{\mathrm{CPE}} = \frac{1}{K_{dl}(i\omega)^{\alpha_{dl}}} \tag{2-1}$$

where i is the imaginary number, ω the angular frequency, K_{dl} is a constant, and α is a mathematical expression the value of which varies between 0 and 1. For an ideal capacitor α_{dl} is equal to 1 and K_{dl} correspond to the capacitance. This variation is included in the model to represent the non ideal behaviour of the capacitance in case of rough material. Electrode roughness can increase the surface area of the electrode (increasing the double layer capacitance value); however, because of the impedance of the solution inside the pore, the high frequency AC signals have a low penetration depth compared to the low frequency ones [13].

The total impedance of the electrode-electrolyte interface, also known as electrode impedance, has to be designed to be as low as possible during cell recording and stimulation. In case of stimulation with a high impedance electrode, to reach a sufficient current density it is necessary to apply a high-amplitude voltage; this could cause harmful electrochemical reactions in proximity of the cells [28]. In case of recording, a high impedance electrode leads to high Johnson noise and thus low signal to noise ratio (SNR) [29, 7]. Thermal noise is related to electrodes impedance by the Nyquist equation:

$$V_{th}^2 = 4kTBR(V) \tag{2-2}$$

where K is Boltzman constant, T is the temperature (K), B the bandwidth (Hz), and R is the real part of the electrode-eletrolyte impedance (Ω) [30].

2-2-1 Cytostretch micro-electrode array (MEA)

As mentioned in Section 1-2-1, the Cytostretch device interfaces with cardiomyocyte cells via TiN electrodes; this material presents several advantages:

- Sputtered TiN presents a high porous surface geometry called fractal which guarantees a low electrode-electrolyte impedance;
- TiN guarantees mechanical and chemical stability and a good biocompatibility;
- Easy sterilization is available.

The Cytostretch electrochemical impedance spectroscopy (EIS) measured in [1] is shown in Fig. 2-2: this technique is briefly introduced here, but a more detailed description will be given in Chapter 4. A standard three point set up was used; in this case two electrodes (reference and counter electrode) were soaked in a drop of PBS covering five device electrodes rather than filling completely the backside hole. The cross section of the device is shown in Fig. 2-2a. This set up was used to avoid the parasitic capacitance generated by the Si substrate in contact with the electrolyte on the metal contact pads.

The impedance measurement was performed by using a Metrohm Autolab instrument with a PGSTAT12 module. Sinusoidal excitation with amplitude equal to 20 mV and frequency ranging between 100 Hz and 600 kHz were applied across the reference and the test electrode. The correspondent current generated at the electrode-electrolyte interface flow through the test and the counter electrode. The impedance amplitude measured at 1 kHz is 800 kΩ. This is the parallel of five electrode impedances, thus, the value of one electrode is around 4 MΩ.

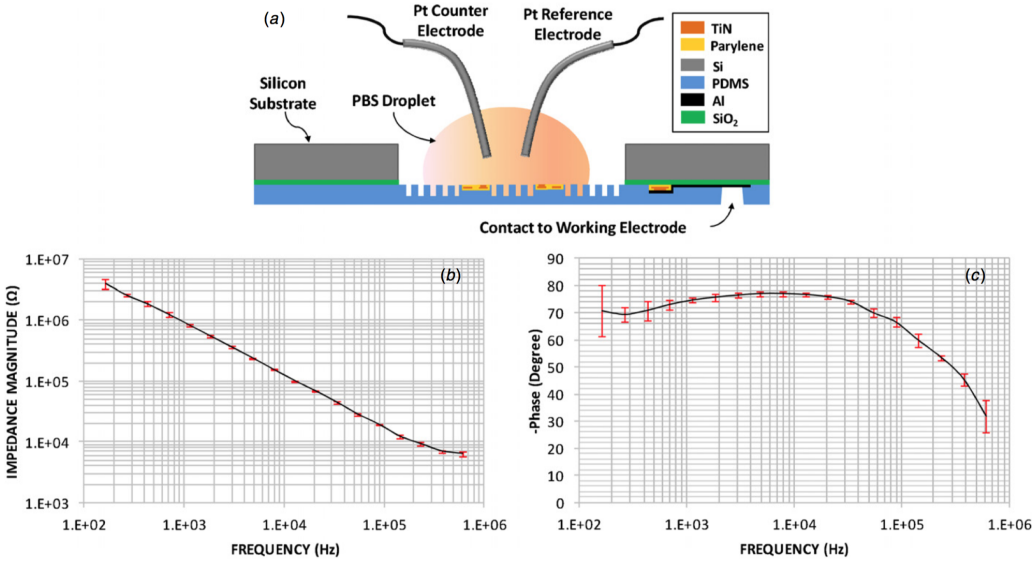

Figure 2-2: (a) Cross-sectional view of the EIS measurement set up used in [1]: two Pt wire electrodes (counter and reference electrodes) are immersed in a PBS droplet on top of the working electrodes; (b,c) the magnitude and phase of the double-layer impedance of five TiN electrodes measured in parallel [1].

Though TiN has been chosen as electrode material, this impedance measurement is unsatisfactory for a device meant to detect low voltage bio-signals. In comparison, the conventional MEA device from Multi Channel Systems MCS GmbH presents an impedance one order of magnitude lower than those of the Cytostretch device. This problem is mainly due to the "polymer last approach" design chosen for the Cytostretch device: TiN presents a fractal geometry on the side facing the source during deposition. On the contrary, close to the substrate, TiN layer has a less porous surface. In the Cytostretch device, cells are in contact with this smooth surface rather than the fractal one. The flat surface of those electrodes, combined with the small dimensions of the electrodes, leads to the high impedance measured in [1] and reported in Fig. 2-2b,c.

2-3 Electrochemical-performance improvements

For this project the Capacitive behaviour of the electrodes included in the PDMS membrane will be guaranteed. Although this characteristic is not mandatory for an *in vitro* test, maintaining the safety and the stability guaranteed by a double layer capacitor could imply additional applications for this flexible MEA. In fact, implantable devices s.a. chochlear implants, implantable brain stimulators and recorder and visual prothesis would benefit from the development of novel low-impedance and Capacitive electrode array embedded in PDMS membrane. Avoiding Faradaic reactions makes the list of alternative materials quite limited. Material with a high charge injection capacitance s.a. Platinum-Iridium alloys, activated

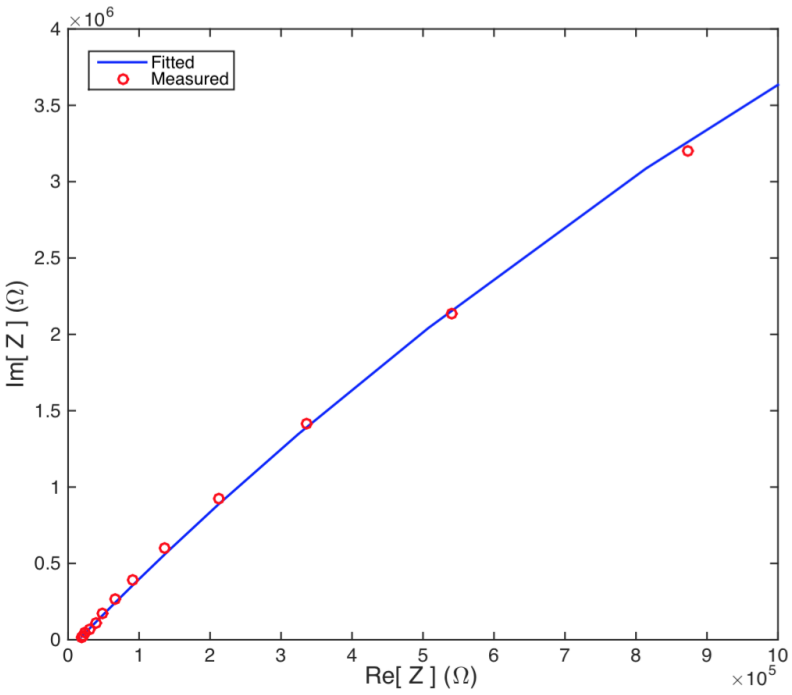

Figure 2-3: Bode plot of Cytostretch EIS and fitted plot.

	Rp (Ωcm^2)	K_{dl} ($(\Omega s^{-\alpha_{dl}})/cm^2$)	α_{dl}
Smooth Pt	7.4-8.6 $\cdot 10^5$	4.3-5.7 $\cdot 10^{-5}$	0.91
Smooth Ti	2.3-3.4$\cdot 10^7$	1.6-1.7$\cdot 10^{-5}$	0.97
Smooth TiN on Ti	2.1-5.6$\cdot 10^7$	4.7-5.5$\cdot 10^{-5}$	0.91-0.94
Rough TiN	6.6-8.8$\cdot 10^3$	1.8-2.2$\cdot 10^{-2}$	0.82
Cytostretch	21.9	3.7$\cdot 10^{-4}$	0.87

Table 2-1: EIS spectra fitting values (Pt, Ti, rough and smooth TiN data: [13]).

Iridium Oxide and sputtered Iridium Oxide could increase the SNR without the need of increasing SSA. However, they will be not considered for this application due to their Faradaic nature.

The other solution that can be employed to increase the double layer capacitor is increasing the SSA of TiN electrodes by patterning the electrodes. Data provided by Pakazad et al. [1] were fitted with the circuit shown in Fig. 2-1; measurement and fitting Bode graphs are shown in Fig. 2-3. From the extrapolated parameters included in Table 2-1, it can be seen that Cytostretch electrodes exhibit a Capacitive behaviour with a K_{dl} of 3.7$\cdot 10^{-4}$ $(\Omega s^{-\alpha_{dl}})/cm^2$. Considering that this was obtained from the EIS of five electrodes in parallel, the value of the K_{dl} is in the same order of the smooth TiN electrodes presented in [13] and three order of magnitude higher than the rough TiN electrodes (values included in Table 2-1). This implies that, in order to obtain the same performances guaranteed by a rough TiN electrode, it would be necessary to increase the area by at least 100 times.

In order to understand whether patterning the electrode could be a feasible idea, a 12 x 12 μm squared electrode will be considered. By pattering the electrode with the columnar structure shown in Fig. 2-4, the area of the electrode is equal to:

$$A = A_g + N \cdot h \cdot 4 \cdot w \tag{2-3}$$

Where A is the SSA of the electrode, A_g is the GSA of the electrode (144 μm^2), N is the number of columns, w is the width of the columns (and the distance between two adjacent columns) and h is the height of the columns. The width of the squared column has been chosen to be equal to 0.5 μm since this is the minimum resolution that can be obtained with the ASLM-STEPPER PAS 5500/80 available in Cleanroom 100 Delft Institute for Microelectronics and Submicron technology (DIMES).

With this structure, a 100 times larger surface area could be obtained only with h equal to 50 μm, and thus, with an aspect ratio of 100. This value is unrealistic for a metal structure and not compatible with Cytostretch fabrication process: for this reason other alternatives need to be considered. The last option considered in this project is the use of CNTs as electrode coating. This material provides an almost ideal Capacitive behaviour as shown in [31]; moreover, it is composed by high aspect ratio tubes which guarantee an impressive high SSA. These, and other properties, make CNTs an interesting possibility to improve the electrical performance of Cytrostretch electrodes.

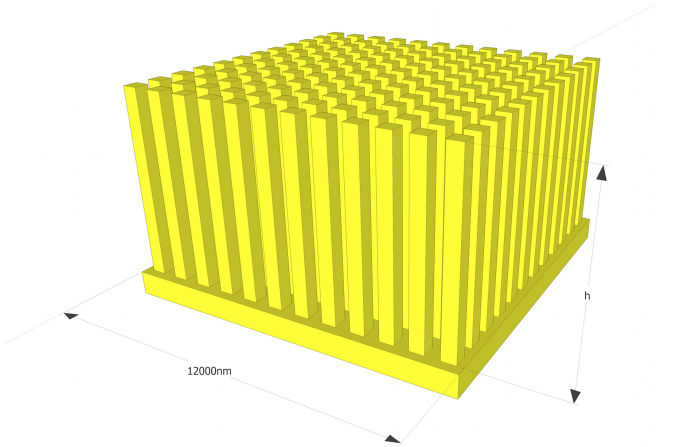

Figure 2-4: Considered patterned electrode.

2-4 Carbon Nanotubes (CNTs)

CNTs are an allotrope form of Carbon (C): the structure of a single CNT can be seen as a graphene layers rolled up forming an allow tube. Graphene, as shown in Fig. 2-5, consists of a monoatomic layer composed by sp2 hybridized C atoms displaced in an hexagonal net. A CNT can be either composed by a single layer of graphene (single walled CNT), or more concentric layers (multi walled CNT). A top view of a CNT forest is shown in Fig. 2-6. CNT characterization often defines the number of layer composing the tubes, their length, their diameter and density, their quality and their chirality. CNT diameter goes from 1 to 100 nm and they can be grown few centimetres long; this implies an extremely high aspect ratio in the order of 10^7.

CNT chirality is expressed as the indexes of the chiral vector (c_h) when compared to the unit vectors (a_1, a_2) of the graphene unit cell, as presented in [4]. These vectors graphically show how a graphene layer should be rolled up to obtain a specific CNT configuration and their vector indexes not only define the appearance of a CNT (zigzag, armchair and chiral structures), but also its electrical properties. In fact, different indexes correspond to a semiconductor or metallic behaviour [4]. The quality of the material is dependent on the crystallinity of CNTs: low crystallinity implies a high number of defects in C net.

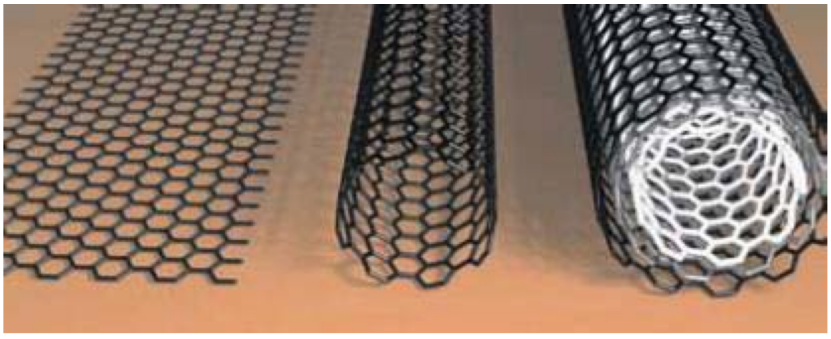

Figure 2-5: Graphene, SWCNT, and MWCNT representation (from the right) [4].

The outstanding electrical, mechanical, chemical and thermal properties of this material have promoted the use of CNTs in an impressive number of publications over the last 20 years [32]. CNTs can stand high current densities (in the order of 109 A/cm^2); this property promoted the use of CNTs as vertical interconnection in 3D integrated circuits. Current flows in CNTs near the limit of the ballistic transport, thus, impedance is independent on their length up to few micrometers. Besides their electrical properties, CNTs excel for their high thermal conductivity (up to 3500 W/mK for MWCNT and 6000 W/mK for SWCNT), strength (tensile strength around 150 GPa, Young's modulus around 1 TPa) and good chemical and environmental stability [33, 34]. These properties make CNTs an interesting material for several applications besides microelectronic, s.a. aerospace structures, body armors, sport equipments and so on [35].

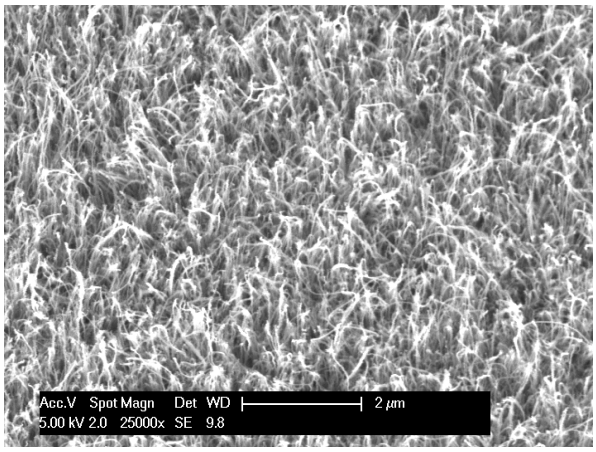

Figure 2-6: Topside view of CNT forest.

2-4-1 Growth mechanism

Different mechanisms are available to synthesize CNTs: Chemical Vapour Deposition (CVD), laser ablation and arc-discharge. In this work, only the first technique will be considered since it guarantees low-temperature, cheap and controlled growth.

CVD growth is performed inside a CVD reactor. CNT growth requires a precursor gas (s.a. Tetrafluoromethane (CH_4) or Acetylene (C_2H_2)), an energy source and a layer of catalyst nanoparticles. The precursor is absorbed in the catalyst particles where the hydrogen is dissociated. Due to energy minimization nanotubes nucleate on top of the particles. Different catalysts are available s.a. Fe, Ni, Co, Pd and Cu. The catalyst is deposited on a barrier layer, also called support layer, which prevents the diffusion of the catalyst in the wafer; usually a nm-thin layer is deposited on the barrier layer and the nanoparticles are formed by heating the sample. This procedure breaks the thin layer of catalyst by minimization of surface energy.

CNTs can be grown in such a way that the single tubes are aligned among each other; these CNTs are usually called vertically aligned CNT (VACNT). This alignment can be promoted by depositing a highly dense catalyst layer; in this way CNTs will grow in a dense structure and the self alignment will be guaranteed by the van der Waals interactions among CNTs.

Alternatively, it is possible to force the vertical alignment by means of an electrical field. CNT properties are directly dependent to fabrication conditions. CNT length is dependent on the growth time and CNT diameter is related to the catalyst nanoparticles used. Moreover, CNT crystallinity is influenced by the temperature at which they were grown; higher temperature implies higher crystallinity.

2-4-2 CNT characterization

A brief analysis of CNTs can be obtained with a scanning electron microscope (SEM). With this technique it is possible to measure CNT length and determine eventual CNT alignment. Further information can be obtained by transmission electron microscopy (TEM) with which it is possible to measure CNT diameters and count the number of graphene layers composing the single tubes. TEM images give also information about CNTs quality, however this technique is considered expensive and time consuming. In order to quantify CNT quality, Raman spectroscopy can be used. This technique is faster and cheaper than TEM; moreover, Raman spectroscopy is non-destructive and provides a more quantitative approach [34].

Raman spectroscopy, also called Raman scattering, is a vibrational spectroscopy based on inelastic scattering of a monochromatic laser. The light, interacting with molecular vibrations, is shifted in frequency; these phenomena can be studied by analysing the spectrum of the signal after interfacing with the sample. Intensity and full width at half maximum (FWHM) of the peaks in the spectrum can be analyzed to assess CNT crystallinity.

Two regions can be identified in Raman spectra: first-order and second order region. In the first order region two strong bands can be found: D band around 1350 cm^{-1} and G band around 1582 cm^{-1}. The first originates from defect vibrations; the second one originates from the stretching modes in the graphite plane. The third feature of the first order region is called D' and is also disorder generated; this is weaker than the other two and can be found as a shoulder of G. In the second-order region only one sharp band, called G' band, can be found. This is placed around 2700 cm^{-1} and is generated by two inelastic phonon scattering processes.

Absolute and relative amplitudes and bandwidths of these peaks provide information about CNT crystallinity. CNTs grown at higher temperature present higher crystallinity: this change in CNT quality can be verified by studying the variations in Raman spectrum (peaks and bandwidths) at different temperatures. $I_{D/G}$, $I_{D'/IG'}$ and $I_{G'/G}$ are commonly used to assess CNT quality. I_D and I'_D are influenced by the disorder in CNT crystal: as a consequence, $I_{D/G}$ and $I_{D'/IG'}$ decrease for increasing crystallinity. $I_{G'/IG}$ ratio increases for increasing quality. Last but not least, also the FWHM can be used to assess sample quality: wider bands correspond in fact to lower-quality CNTs.

Another important parameter that needs to be characterized, is the wettability of CNT forests. Pristine CNTs are in fact highly hydrophobic; this characteristic limits the contact surface between a solution and a CNT surface. In order to quantify the wettabilty of a CNT surface, drop test can be performed: this consists in measuring the contact angle of a drop of water on top of a CNT surface. As already mentioned in Section 2-3, CNTs have been chosen for their high SSA; this property is limited by the high hydrophobicity of the material. Several publications, s.a. [31, 7, 36], focused on overcoming this problem by means of low power plasma treatments; either treating CNTs with H_2O plasma, like in [31], or with O_2

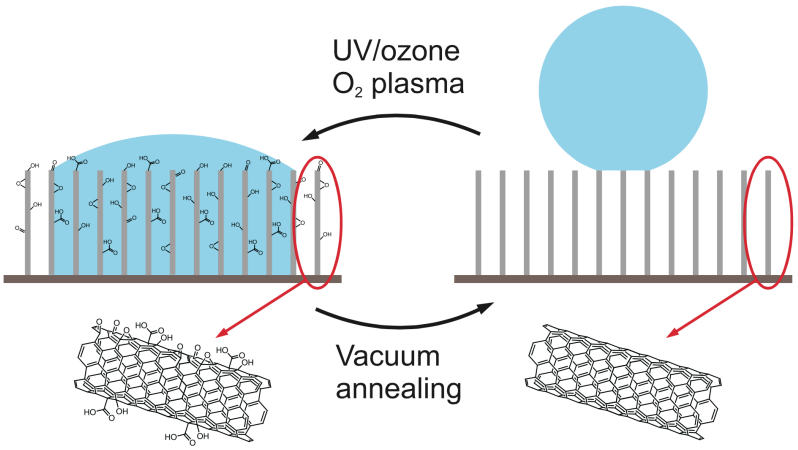

Figure 2-7: CNT wettability tuned by means of UV/ozone, oxygen plasma and vacuum annealing treatments [5].

plasma, like in [7, 36], leads to a substantial improvement of CNT wettability. UV light can also be employed to tune CNT wettability as shown in [5] (Fig. 2-7).

Although oxygen plasma treatment provides a much faster oxidation process, it can completely oxidize CNTs into CO, COH, and COOH groups. This process is reversible in case of low Oxigen(O)/C ratio (less than 18%): in fact, CNT hydrophobicity can be recovered by means of vacuum annealing as shown in Fig. 2-7. A higher O/C concentration, corresponds to heavy functionalization of the walls with stable oxygenated group that are considered difficult to remove. At much higher O/C ratios (higher than 40%), etching process occurs, creating holes, exfoliations and amorphous deposition on the CNT forest [5].

2-4-3 Cobalt-grown CNT on TiN support

Sample preparation: During this work, only Cobalt (Co) will be considered as catalyst. Even if Co is considered a highly cytotoxic material, it has been chosen because it guarantees CMOS compatibility, as opposed to Cu and Fe. This is mainly due to the fact that Co does not lead to deep-level traps in Si and has a lower diffusion coefficient than Cu and Fe. This means that Co is not detrimental for eventual CMOS circuits integrated in the Si bulk of the device [37]. The effect of Co cytotoxicity on a cell culture will be presented and discussed in Chapter 5.

Along this work, the same CNT growth presented in [34] was used. CNT samples were prepared by sputtering 10 nm of Ti and 50 nm of TiN on top of four inches Si wafers. The purpose of the bottom layer is to improve the adhesion between TiN and Si; the top layer is used as support layer. Five nanometers of Co were then evaporated with a CHA Solution Std; this layer works as catalyst during the syntetization. CNT growth was performed in an AIXTRON Blackmagic CVD reactor.

Before loading the samples in the machine, the CVD reactor needs to be warmed up with a dummy run. After sample loading the system is pumped down to < 0.1 mbar. 700 sccm of H_2 are then injected in the reactor meanwhile temperature and pressure are ramped to

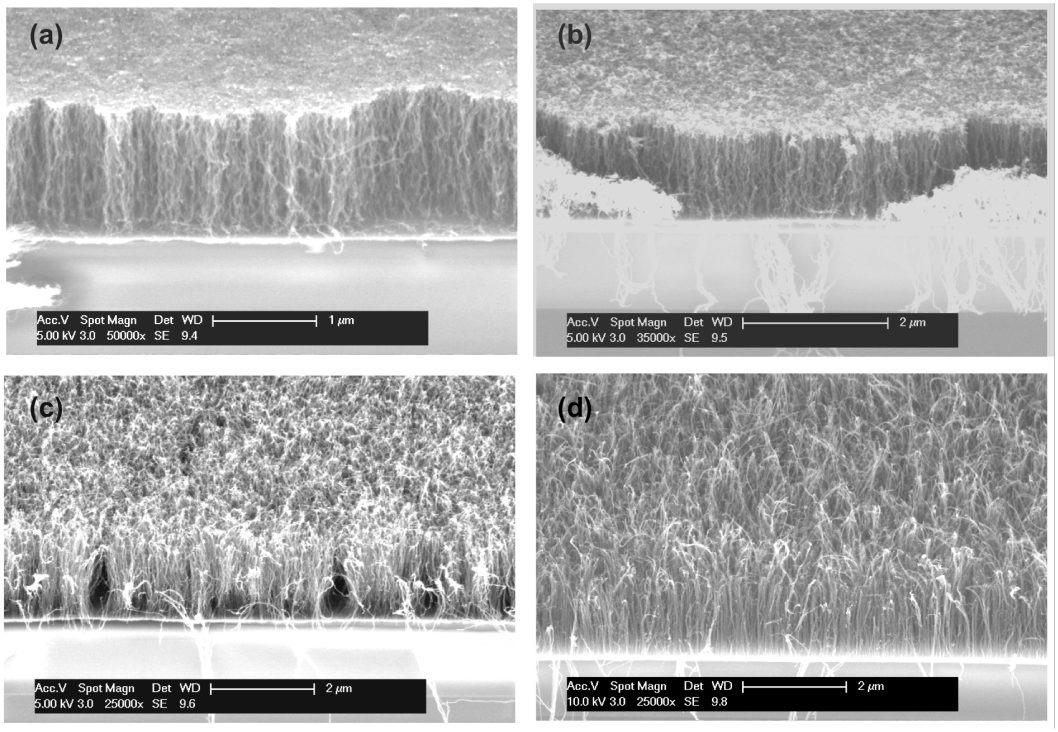

Figure 2-8: CNT forests grown at (a) 350, (b) 400, (c) 500 and (d) 650°C.

500°C and 80 mbar, respectively. This step is followed by a three minutes annealing and the warm up of the chamber to growth temperature. After this, 50 sccm of C_2H_2 are added and CNTs are synthesized on top of the catalyst particles. The process ends with the cut-off of gasses and heater and the pump down. Untill it is cooled down below 400°C and purged by means of N_2, the chamber cannot be open.

Characterization: Four different growth temperatures were considered: 350, 400, 500 and 650°C. 350°C can be considered an extremely low temperature for CNT growth. This is feasible because of the low activation energy of Co catalyst growth [34]. By growing CNTs for different times, and checking the samples with SEM analysis, the growth rates were determined: 0.285, 1.977, 30.83, 163 nm/sec for 350, 400, 500 and 650°C respectively. As can be conveyed, lower temperatures imply lower growth rates. In case of CNT grown in cavity the rate slightly decreases. For example, in order to fill a hole (deepness: 1 μm, diameter: 12 μm) with CNTs at 500°C, it is necessary to grow the CNTs for 38" rather than 33.

SEM images of 1 μm long CNTs are shown in Fig. 2-8; samples were synthesized at four growth temperatures. CNT grown at 650°C showed a higher alignment compared to lower temperatures. However, the high temperatures also implies a worse uniformity in growth rate across CNTs; this can be inferred by the fact that some of them look longer than the others. CNTs grown at 350 and 400°C showed similar alignment.

In order to understand whether Co-grown CNTs on TiN support are synthesized with a tip or a root growth (Fig. 2-9a), a double temperature growth was performed. CNTs were grown for two minutes at 500°C; then temperature was increased to 600°C and CNT growth

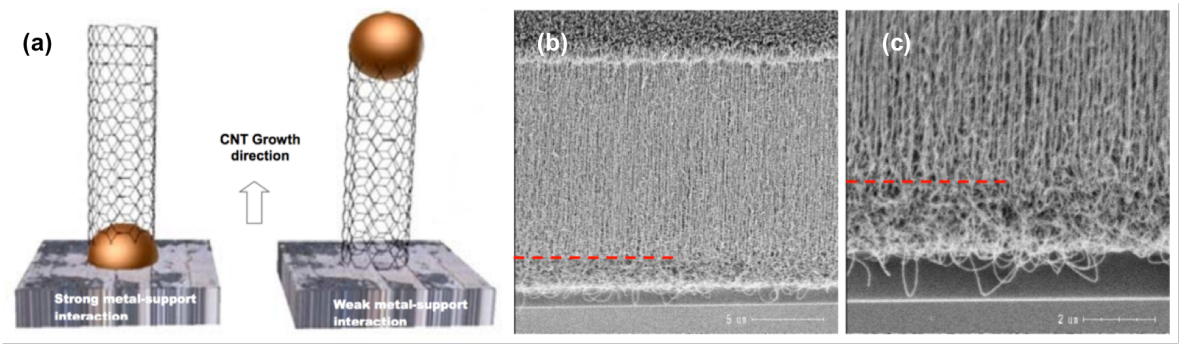

Figure 2-9: (a) Root and tip growth models [6]; (b,c) SEM images of CNTs synthesized at a two growth temperatures (2' at 500°C and 2' 600°C).

continued other two minutes. The SEM images of this sample are shown in Fig. 2-9b,c. As can be seen (and highlighted by the red dotted line) CNTs presented two distinct phases. The top side of the CNT forest was well aligned as opposed to the bottom side; the bottom part corresponded to the low temperature growth step. From this result, it can be inferred that, differently from what claimed in [34], this catalyst/support combination implies a tip growth process: this is probably due to a weak interaction between TiN surface and Co particles.

Raman spectroscopy tests were performed on samples grown at different temperatures with a Renishaw inVia Raman spectroscope with 514 nm laser. First and second order bands of Raman spectrum obtained from a CNT sample grown at 500°C degrees are shown in Fig. 2-10 (black). The Matlab script presented in [34] was used to fit the spectra with eight Lorentzian curves and two Gaussians. The different elements composing the fitting are represented in Fig. 2-10 with green dotted lines. The values obtained from Raman spectra fitting for different Co-grown samples synthesized at different temperatures are shown in Table 2-2; single Raman spectroscopy graphs are not reported.

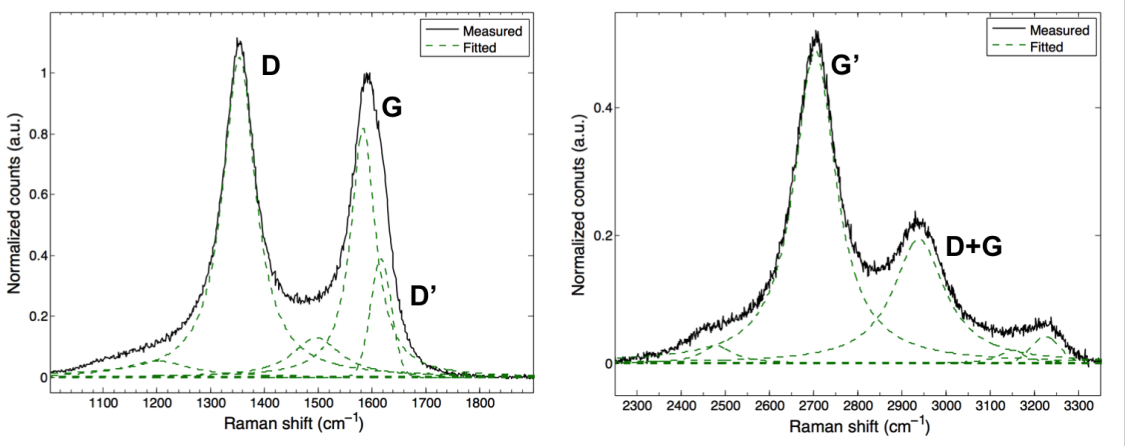

(a) First order region **(b)** Second orders region

Figure 2-10: Fitted Raman spectra of CNT grown on 5 nm Co at 500°C. Original spectrum: solid black line; fitting peaks: dashed green line.

Temp.	$I_{D/G}$	$I_{D'/G}$	$I_{G'/G}$	FWHM $[cm^{-1}]$ D	G	D'	G'
350 °C	1.11	0.49	0.18	145	61.34	43.99	221.15
400 °C	1.14	0.34	0.26	100.49	60.83	41.00	169.31
500 °C	1.27	0.46	0.6	73.68	55.27	45.89	112.77
650 °C	1.02	0.36	0.83	56.64	45.45	41.93	88.41

Table 2-2: Raman data obtained from CNT grown at different temperatures

Almost all the quality indicator trends show an increase in quality as the temperature increases. D, G and G' FWHMs decrease as the temperature increases. The $I_{D/G}$ ratio showed an initial increase followed by a decrease. This behaviour is due to the low temperature at which samples were grown. In CNT samples with low crystallinity, I_D is influenced not only by the number of defect in CNTs, but also by the number of six-fold rings. As the crystallinity increases, the probability of finding a six-fold ring increases causing an increase of D band magnitude. Reached a high level of crystallinity, the probability of encountering six-fold rings becomes constant; at this point only the number of defects influences I_D. $I_{G'}/I_G$ also confirms the increase in quality for higher temperature samples [34]. The absence of a well defined trend for D', $I_{D'}/I_{G'}$ and D' FWHM is probably caused by fitting inaccuracies of D' peak.

The wettability of Co-grown CNT samples was assessed with a Dataphysics OCA20 contact angle system. 5-10 μl of distilled water were drop on the samples. In order to guarantee equilibrium condition, angle measurements were performed 10" after the water entered in contact with the CNT forest. As expected, CNT forests showed an hydrophobic behaviour. CNTs grown at 500 and 650°C can be considered superhydrophobic since the contact angle value was close or higher than 150°.

The drop test pictures on CNT samples are shown in Fig. 2-11 with the correspondent synthetization temperature. As can be seen, as the temperature (and the quality) increases the hydrophobicity increases as well. CNT wettability can be used as quick quality test only for low quality ranges since at high growth temperature the static contact angle saturates to a maximum.

CNT wettability was altered by means of a brief oxygen plasma treatment. CNT samples (1 μm and 5 μm long) grown at 500°C were placed in an Europlasma stripper and treated with low RF power (50 W) oxygen plasma for 10". For both CNT lengths, oxygen treatment altered CNT wettability moving them from a superhydrophobic to a superhydrophilic regime. The latter corresponds to a static contact angle close to 0° (picture not reported). The eventual increase of defect density induced by the oxygen plasma was verified by means of Raman spectroscopy. Oxygen plasma treatments caused relatively small increases in $I_{D/G}$ (less than 10% variations). This small change in $I_{D/G}$ ratio ensures that oxygen treatments did not cause severe local or complete CNT exfoliation as reported by [5].

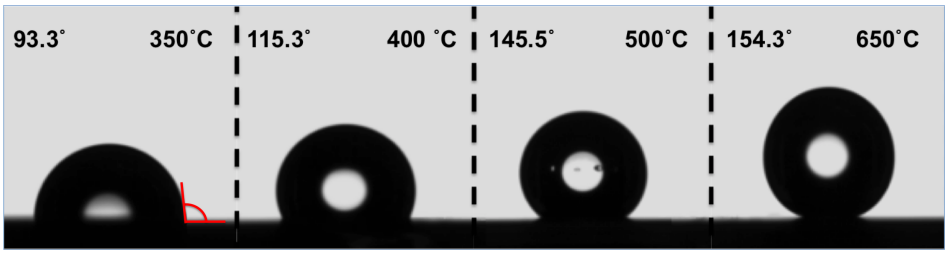

Figure 2-11: Drop test on top of CNT forests grown at different temperatures.

2-5 CNT MEA

CNT is considered an attractive material to improve the electrochemical impedance of micro bio-electrodes. This material in fact provides a large double-layer charge capacity as a consequence of its high SSA/GSA. Moreover, CNT electrodes showed an almost ideal Capacitive behaviour, preventing in this way unwanted and irreversible effects [10]. CNTs have been widely used in MEAs electrodes; in this section the literature about this topic will be reviewed.

Like in the case of the Cytostretch device, standard MEAs present micro-electrodes whose electrochemical impedance is limited by their small dimensions. In the last decade, several publications, s.a. [8, 38, 39], show that CNTs used as electrode coating can eventually solve this problem. Moreover, when in contact with *in vitro* cell cultures, CNTs can also provide additional advantages s.a. promoting cell adhesion.

The fabrication of rigid MEAs often consists in the procedure presented in [8]: the process starts with a Si wafer with 500 nm of SiO_2 on the front side. On top of SiO_2, a metal layer is deposited and patterned, composing electrodes, contacts pads and interconnects. This layer can be made of a single metal (s.a. TiN) or a stack of metal layers (s.a. Ti and TiN [7]); in both cases the top layer needs to be made of a material suitable as support layer. The metal layer is then passivated by means of a dielectric, s.a. Silicon Nitride (Si_3N_4) and SiO_2; electrodes and contact pads are then opened by etching the insulator in correspondence of the electrodes and the pads. After this, a catalyst layer is evaporated on top of the wafer and patterned either by additive or subtractive process. Fabrication ends growing a CNT forest on top of the electrodes.

In literature, MEAs differ for CNT growth technique, dimensions, intra-electrode distances and number of electrodes. In most of the cases, these are used with the purpose of detecting bio-electrical signals generated by neural cells. Electrode impedance values found in different publications are shown in Fig. 2-12. This graph highlights how CNTs outperform common materials used for micro-electrodes s.a. gold (Au) and Pt [7]. The propensity for growing neurons on top of CNT electrode is due to the strong coupling between these cells lineage and CNTs; in fact, it was shown that neurons preferentially adhere to randomly oriented CNTs [39]. Gabay et al. [8] grew on top CNT electrodes cortical neurones without any coating (Fig. 2-13). The rough surface provided by CNT island promotes migration and adhesion of neuronal cells on top of CNT electrodes [8, 7].

The extracellular signal measured by Gabay et al. [8] is reported in Fig. 2-13b. This is compared with the signal detected with a commercial 30 μm TiN electrode array (Fig. 2-13c); as can be noticed, CNT electrodes showed a higher-quality signal in term of SNR.

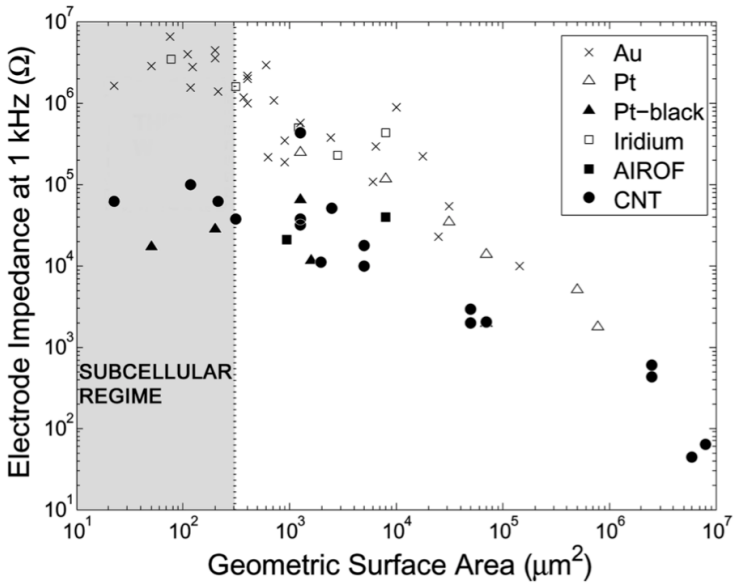

Figure 2-12: Survey, presented in [7], including micro-electrode impedances at 1 kHz vs geometric surface surface area.

This should guarantee an easier recognition of the signals originated from a cell culture. This drastic improvement is due to the smaller electrochemical impedance of CNT electrodes and the improved electrode-cell coupling shown in Fig. 2-13a.

2-5-1 Flexible CNT MEAs

Besides Organ on Chips, MEAs can be employed to record and stimulating neuronal cells *in vivo*. Brain implantable MEAs have been widely used to treat deafness, parkinson, halzheimer, schizophrenia and so on [28]. The substrates of the MEAs presented in Section 2-5 are made of Si; the brittleness of this material makes this kind of devices unsuitable for these applications since they can easily break. For this reason polymer materials are usually employed as MEA substrate guaranteeing higher flexibility and biocompatibility [40]. The outstanding adhesion between neurons and CNTs mentioned in Section 2-5 and the fact that flexible solutions are easier to handle in neural recordings have promoted the development of different techniques to embed CNT electrodes into flexible polymer substrates.

Previous works, s.a. [41], focused on growing CNTs directly on a polymer membrane. This option is limited by the temperature at which CNTs are grown. In the particular case of the device presented in [41], CNTs were grown on a gold layer sputtered on a flexible paralyne. CNT growth was performed at 350°C on account of the fact that paralyne can stand higher temperatures than PDMS (which is cured at 90°C). Though this could be a valid option to improve Cytostretch electrodes, this work aims to maintain the mechanical features defined by Saeed et al. [1]. For this reason, the possibility of changing the membrane material will be not taken in to account for now.

The thermal budged limitations imposed by the use of PDMS can be avoided by growing first CNTs and then, embedding them into a polymer support by means of transfer. This

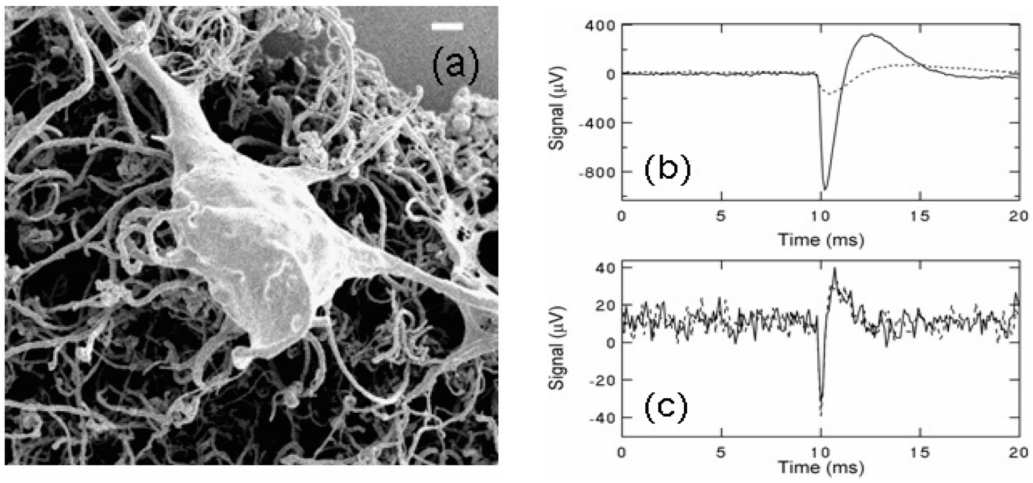

Figure 2-13: (a) High resolution SEM image of a neuronal cell on random aligned CNT forest (bar is 1 μm); (b) signals recorded from cultured neurons with a CNT MEA; (c) signals recorded from cultured neurons with a commercial TiN MEA [8].

technique was already used in previous works s.a. [9, 40]. David-Pur et al. [9] presented a flexible neuronal micro-electrode array device completely based on CNT films embedded in a polymeric support. Device fabrication is presented in Fig. 2-14: this starts patterning Ni catalyst layer by means of resist lift off on a Si wafer. In this case, electrodes, interconnection tracks and contact pads are composed by a CNT layer. CNTs are grown on the patterned catalyst layer by means of chemical vapour deposition. After this, a flexible layer is placed on top of the CNT forest; several materials have been considered for this purpose: adhesive medical tape, parylene C and PDMS. The adhesive medical tape is attached to the CNT pattern by means of manual pressure; parylene C can be deposited by means of vapour deposition and polymide and PDMS can be spun on the surface. After this step the polymeric surface is pealed off transferring the patterned CNT forest.

The fabrication of this device ends by isolating CNT interconnects. A passivation PDMS membrane, patterned with holes corresponding to the contact pads and the electrodes, is bonded on top of the membrane embedding the CNTs. Even if this fabrication process produces flexible CNT MEAs, several limits make it unsuitable to be employed in the Cytostretch fabrication. First of all, the interconnect tracks, completely made of a CNT film, are affected by poor conductivity when compared with a metal line; this is mainly influenced by the contact impedance among the single tubes composing the film. Second, this process is limited by a series of manual steps: these can be considered critical and could drastically reduce device throughput.

The interconnect passivation was faced by Lin [40] and colleagues in a different way. In this case, after membrane peeling off, PDMS was dispensed on the interconnects with a commercial pneumatic dispensing system (systemUltra 2400 Series Dispensing Workstation). The manual control of the pneumatic system makes this solution unusable in Cytostretch device.

Even if the solutions presented in [9, 40] cannot be considered completely compatible with the Cytostretch fabrication, they can be used as starting points for the integration of CNTs in the device. Both these works embed CNT electrodes on a polymer surface in the following way: first, CNTs are grown; second, a polymer layer is placed on top of the CNTs. This

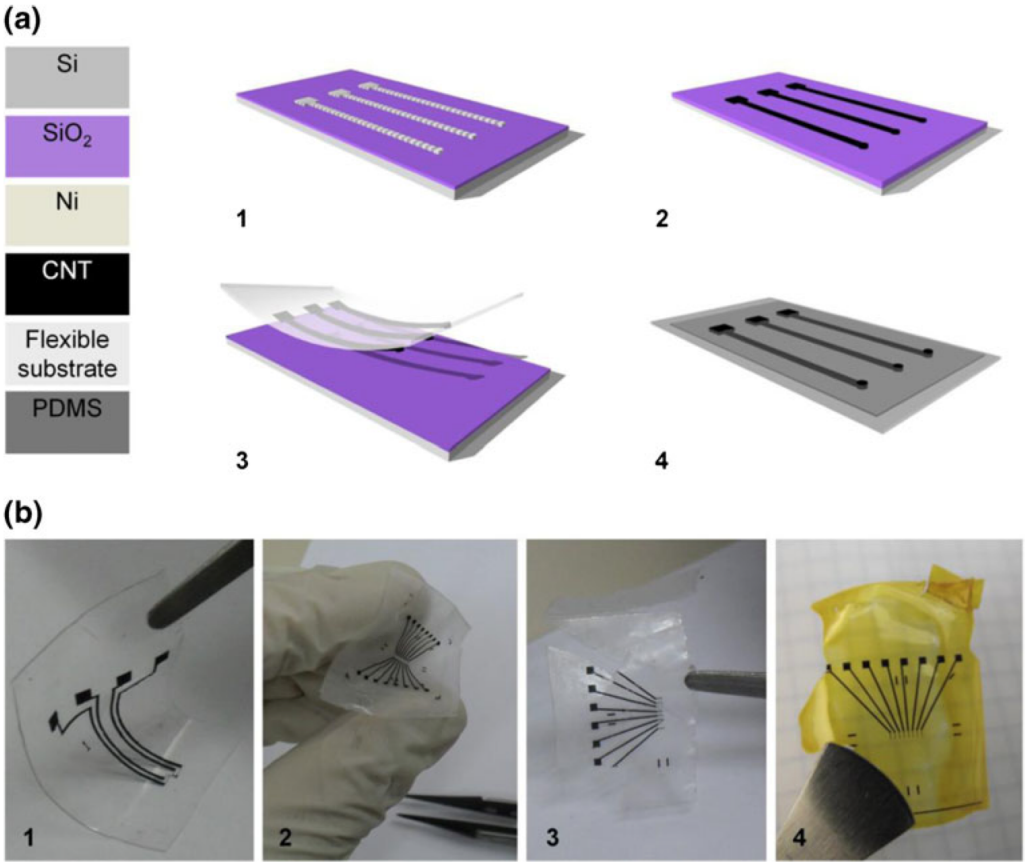

Figure 2-14: (a) Fabrication schematic and (b) photo of flexible CNT electrode array devices presented in [9].

procedure is compatible with the "polymer-last approach" used for Cystostretch fabrication. Second, by exploiting the good adhesion between CNTs and polymers, CNTs are detached from the support layer where they have been grown. This good adhesion can be found also with different materials s.a. sputtered metals. As can be conveyed from different images reported in [34], CNTs tend to detach from the TiN support where they have been grown rather than from the top-side metallization. This means that the metal layer is tightly in contact with the CNTs tips like PDMS was in [9, 40]. Since the metallization chosen for this project is different from that one used in [34], metal/CNT contact will be characterized in the following section.

These concepts promoted the design of a new Cytrostretch module composed by CNT electrodes. The fabrication of this module will be the main topic of Chapter 3. The module is supposed to improve the electrical properties of the device without affecting its mechanical properties; moreover, by using Co as catalyst, the integration of the CNTs will not affect the high-scale-fabrication compatibility of the device and the possibility to place eventual integrated circuits closed to the membrane.

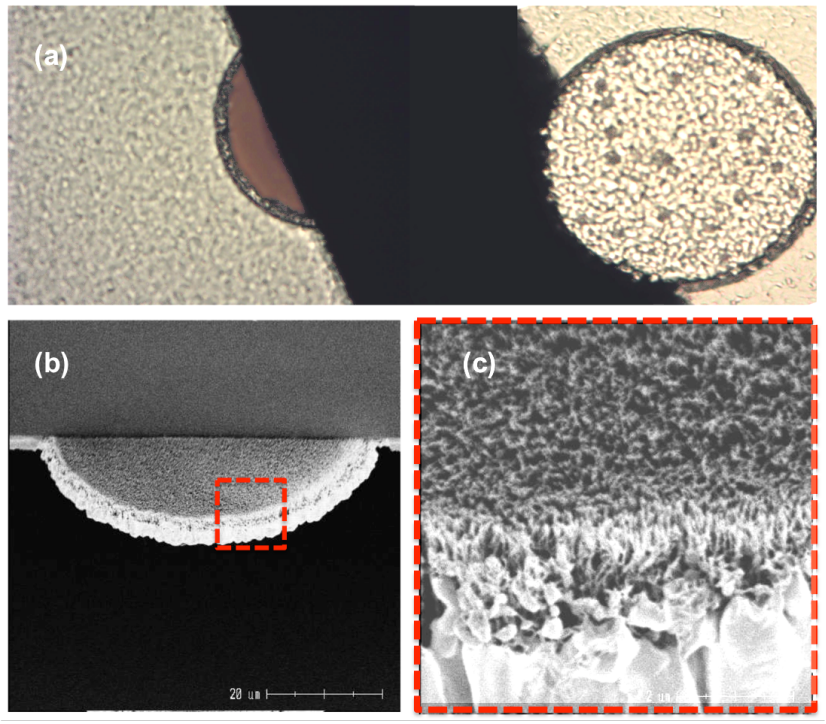

Figure 2-15: (a) Optical image of the sample pieces obtained after the failed cross section; (b-c) SEM images of the backside of the free standing aluminum layer after the failed cross section. In (c) the CNT attached on the bottom of the aluminum layer can be seen.

2-6 Metal-CNT contact characterization

Since the novel structure that is going to be presented in Chapter 3 relies on the contact between a CNT forest and a layer of metal sputtered on top of it, two tests, aiming at studying both mechanical and electrical properties of the contact, were performed. These tests were performed to confirm that, replacing the Ti layer used by Vollebregt et al. [34] with a layer of TiN, the contact is not altered.

First, VACNTs were grown in TEOS holes and covered with 100 nm of TiN and 2 μm of Al. The vertical alignment of CNTs in this case is critical since it guarantees that all the tips are in contact with the metal layer: for this reason, CNTs were grown at 500°C. This structure was meant to be used to obtain a cross-sectional SEM image of a CNT forest covered with metal. However, by performing the cross section manually, the metal on top of CNTs tended to break along the hole perimeter rather than along the cut line, obtaining the structure shown in Fig. 2-15a. The freestanding metal structure was checked with SEM analysis. As can be seen in Fig. 2-15b,c, CNTs are still under the metal proving the good adhesion between CNTs and metal layers.

The electrical contact between CNTs and metal was characterized by fabricating the structure presented in [34] and shown in Fig. 2-16a,b. This test via structure was obtained with a top down approach. This was composed by a layer of TiN sputtered on top of a SiO_2 layer. On top of the metal, TEOS was deposited and etched fabricating vertical interconnections through it. CNTs were then grown in these holes up to the edge of the TEOS layer and

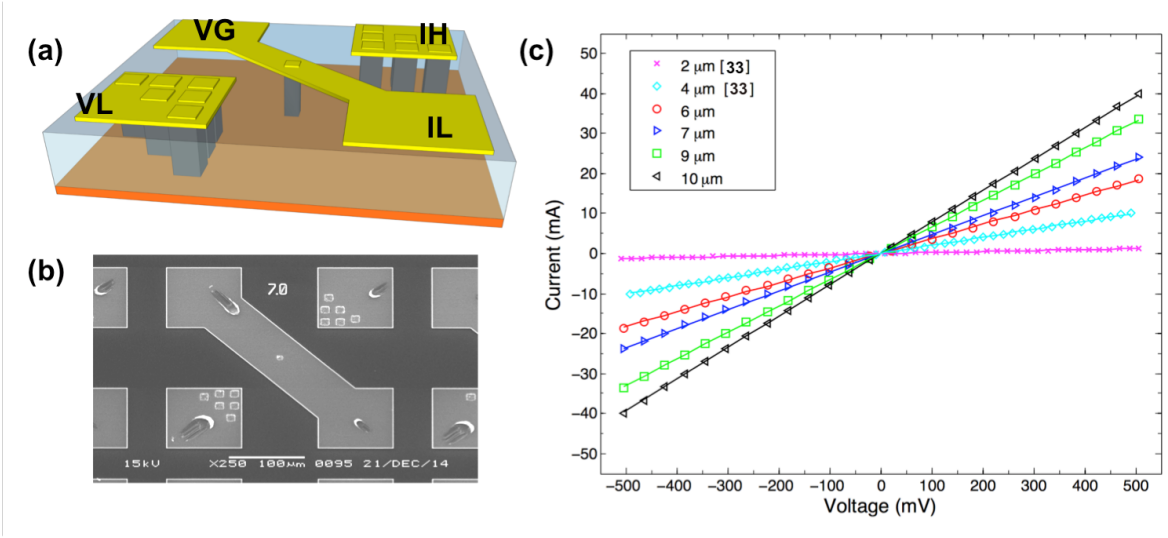

Figure 2-16: (a) Sketch of a four point probe measurement structure used to characterize CNT-METAL contact; (b) SEM top-side-view image of the structure; (c) I-V characteristics obtained with CNTs grown at 500°C on TiN support and covered with 100 nm of TiN and 2 μm of Al.

then covered with 100 nm of TiN and 2 μm of Al. These two layers were etched creating the four measurement pads shown in Fig. 2-16a. This structure was used in [34] to measure the resistance of the central CNT bundle for different bundle diameters. In this work, it was used to verify whether the contact between metal and CNT presents an ohmic behaviour.

In order to assess the I-V characteristics of the CNT bundles in series with the metal stack, four point probe method was used; this configuration employed two set of probes: two probes drove a known voltage (VF and VG) and the other two present an almost infinite input impedance (IH, IL) guaranteeing no current flows through these contacts. The current was then measured across the first couple of electrodes and shown in a graph vs voltage variations (shown in Fig. 2-16c).

I-V characteristics for different CNT via diameters highlights a linear relation indicating ohmic contact between the two metal layers (support and top layer) and the CNTs. In Fig. 2-16c, the results presented in [34], are also shown. It can be conveyed that the behaviour of the metallization used for this project is in line with the results collected by Vollebregt and colleagues [34]. The linear behaviour implies that between the top metal and the CNTs there is no Schottky barrier, problem that could strongly affect the measurements through CNT electrodes. Some of the tested structures presented this problem. This behaviour was seen in some areas of the wafer where they have been fabricated on. These performance variations could be due to disuniformity in CNT growth.

Chapter 3

Device fabrication

3-1 Overview

Two devices were fabricated for this project. The first one consists in a Standard CNT MEA composed of 12 electrodes covered by 3 μm long VACNTs (Fig. 3-1). This maintains the same dimensions and intra-electrode distance of the Cytostretch device. This was meant to be used to test the electrochemical performance of Co-grown CNTs as bio-electrode coating. From now on this device will be referred as Standard MEA.

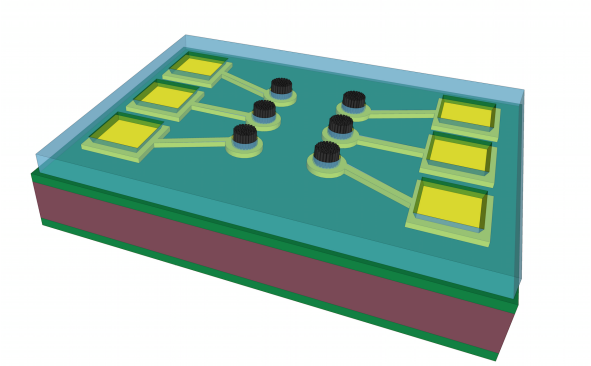

Figure 3-1: Sketch of Standard CNT MEA.

The second device consists in a CNT MEA placed on the backside of a membrane (Fig. 3-2). The pads to access the CNT electrodes are placed on the frontside of the device. The fabrication of this device consists of two main steps: the CNT growth followed by the membrane fabrication. In this way, synthetization temperature is not limited by the polymers which compose the membrane. CNT electrodes are released with the membrane during backside etching; they do not detach from the structure as a consequence of the good adhesion between CNT tips and the metal layer deposited on top of the CNT forest (as proven in Section 2-6). The membrane can either be made of PDMS, like in a Cytostretch device, or

simply PECVD SiN and SiO_2. The flexible device could not be fully carried out during this project. For this reason only a rigid solution has been implemented with the aim of proving the concept. From now on this device will be referred as Upside-down MEA. The fabrication of flexible and rigid Upside-down MEAs will be discussed even if only the rigid one will be covered in details.

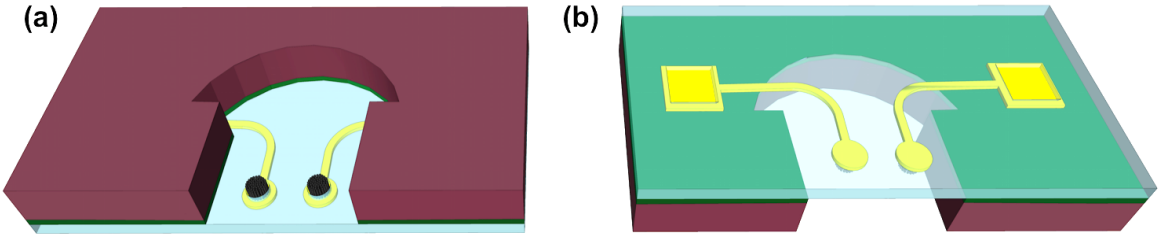

Figure 3-2: Sketch of Upside-down CNT MEA: (a) backside, (b) frontside.

3-2 Fabrication sequence

Standard MEA process is listed schematically in Fig. 3-3; the detailed fabrication sequence is listed in Appendix A. Rigid and flexible Upside-down MEA processes are depicted respectively in Fig. 3-4 and 3-5; the detailed fabrication sequence of the rigid Upside-down MEA is presented in Appendix B. A flexible Upside-down MEA can be fabricated with a combination of the processes presented in [4] and [1]. In the first one, a CNT forest is grown in a TEOS hole and then covered with a metal layer; in the second one Cytostretch membrane is fabricated and then released. The latter has been already presented in Section 1-2-2. In this chapter, the details and information collected during the fabrication of Standard MEAs and rigid Upside-down MEAs will be presented.

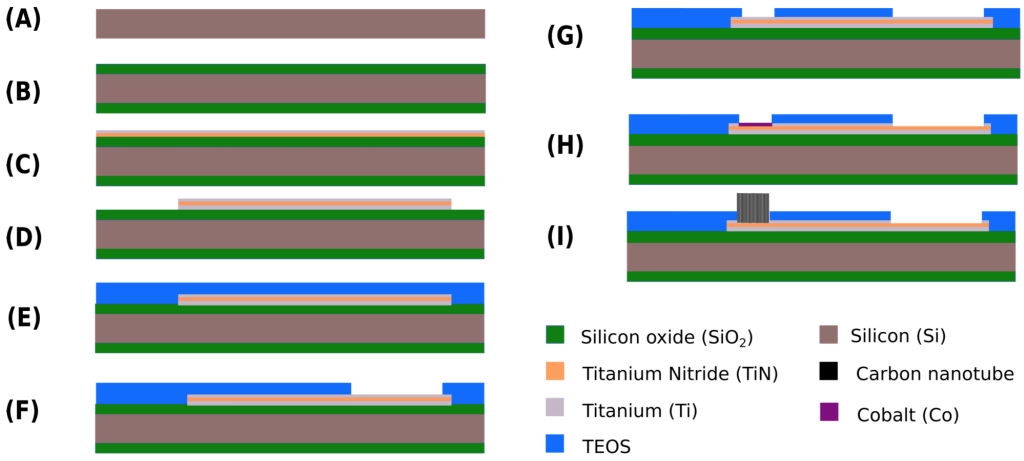

Figure 3-3: Process flow for the fabrication of Standard MEA.

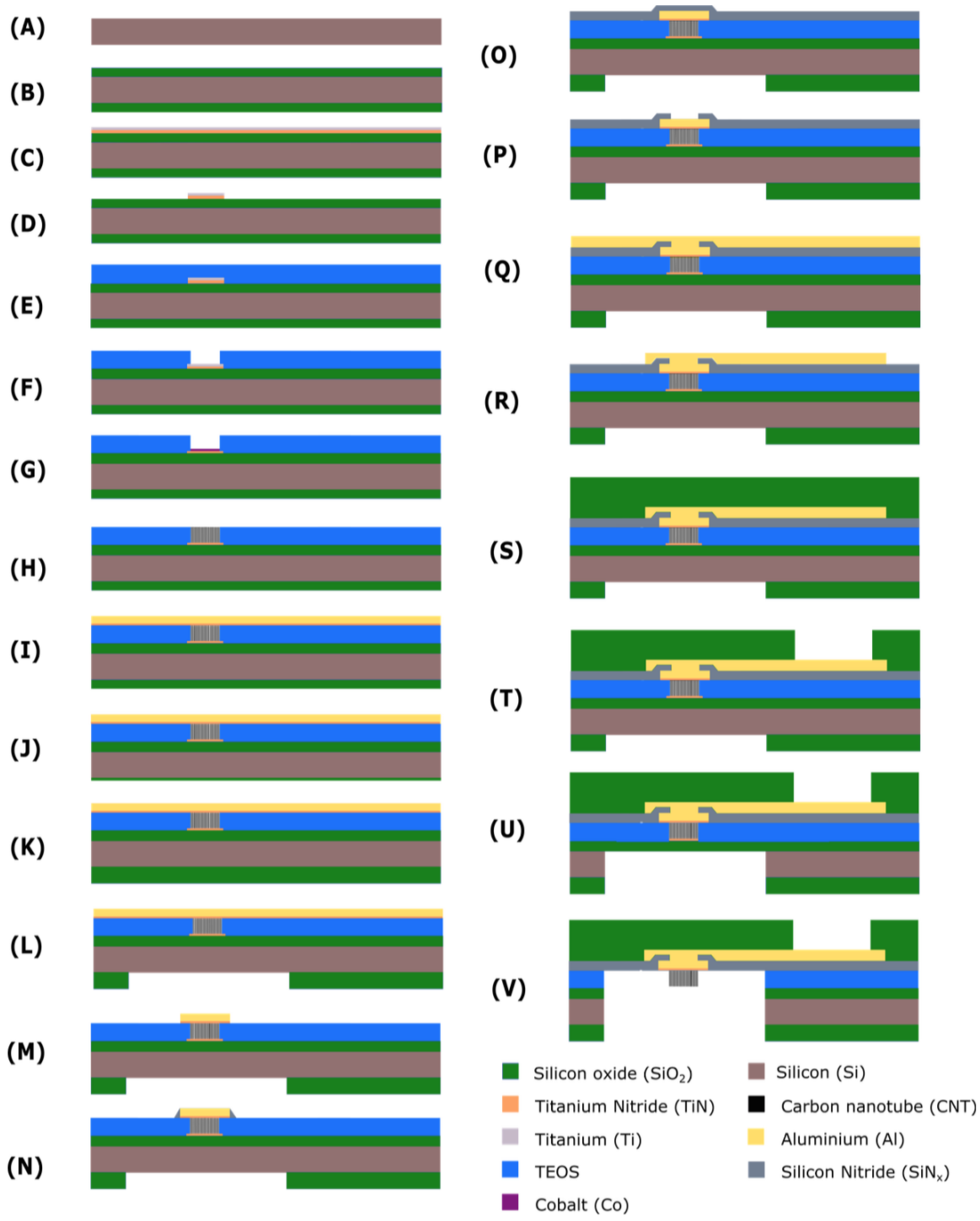

Figure 3-4: Process flow for the fabrication of Upside-down CNT MEA on rigid membrane.

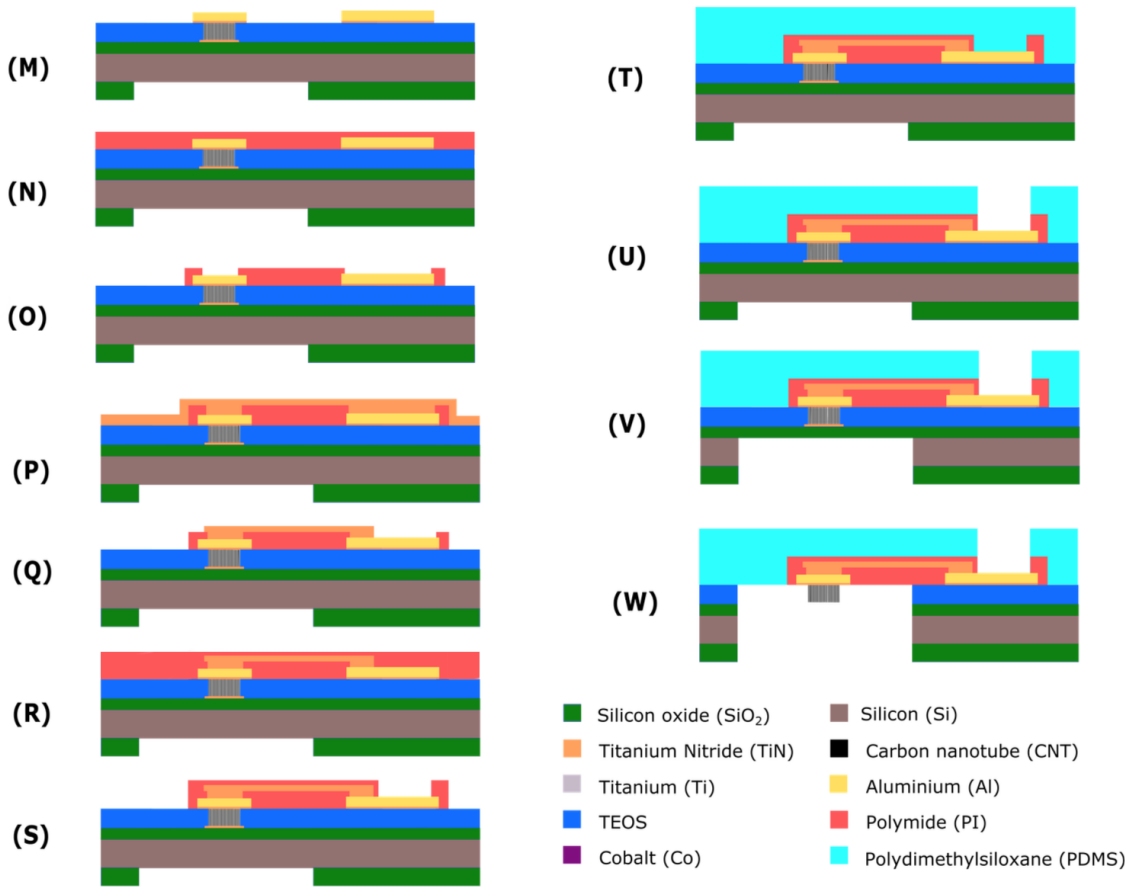

Figure 3-5: Process flow for the fabrication of Upside-down CNT MEA on stretchable membrane.

3-3 Standard CNT/TiN MEA

The fabrication of a rigid MEA started with a four inches Si wafer (doping is not influent) on top of which 1 μm of thermal SiO_2 was grown. A metal stack was sputtered on top of SiO_2 by means of a TRIKON SIGMA sputter coater (Fig. 3-3c). This was composed of 500 nm of Ti, 50 nm of TiN and 100 nm of Ti. The purpose of the first layer of Ti was to guarantee a low sheet resistance for the interconnects and a good adhesion between metal stack and SiO_2. The 50 nm of TiN were used as support layer for CNT synthesization: this thickness, like other sputtering settings, has been chosen replicating the work presented by Vollebregt et al. [34]. The top Ti layer was used as landing material during passivation etching.

The metal stack was patterned with a Trikon Omega 201 ICP etcher by means of plasma etching (Mask: C-1) and then covered with 1 μm PECVD tetraethylorthosilicate (TEOS) deposited at 350°C with Novellus Concept 1 PECVD (Fig. 3-3e). TEOS was considered more suitable compared to PECVD SiO_2 since it can stand the high temperatures required by CNT growth.

The insulator layer was then patterned in two steps. In the first one, contact pads were opened landing on Ti by means of plasma etching with a Drytek Triode 384T etcher (Mask: C-2); after this the photoresist was stripped away. In the second step electrodes were opened:

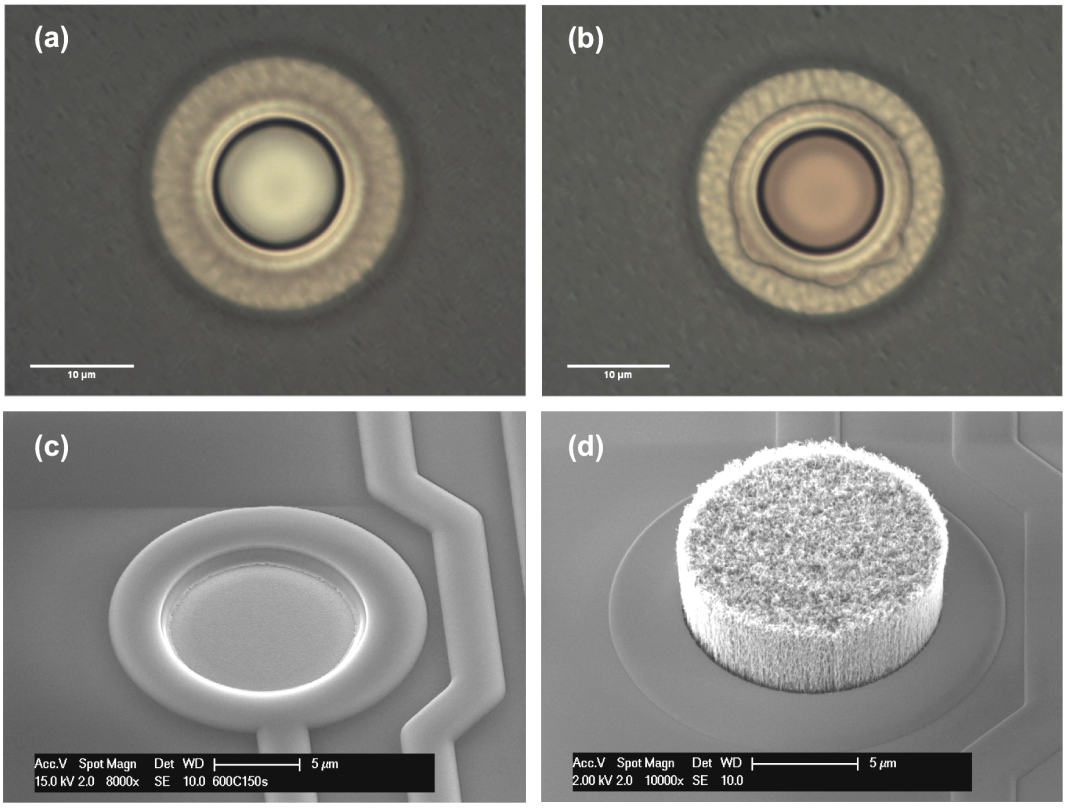

Figure 3-6: Optical image of the hole right (a) before and (b) after HF etching; (c) SEM image of the Standard TiN electrode; (d) SEM image of the Standard CNT electrode.

holes with a diameter of 12 μm were etched in TEOS in correspondence of the 12 Cytostretch electrodes. For this step an Adixen AMS100 ICP etcher was used. This machine was chosen due to its higher etching uniformity across the wafer compared to the Drytek available in Dimes Class 100. In this way it was possible to land on the Ti in every part of the wafer at the same time. Ti landing can be verified by optical microscope analysis; etching was performed in intermediate steps and stopped when holes had a grey colour as shown in Fig. 3-6a.

The top Ti layer prevented fluorine-chemistry plasma from entering in contact with TiN support layer. As proven in [42], the exposure of TiN support to plasma affects CNT alignment. The dimensions of catalyst particles activated on plasma-treated TiN are higher than those activated on a pristine surface. Catalyst-particle dimensions impact diameter and CNT density affecting also self alignment promotion.

Ti layer, was then removed by soaking the wafer in Hydrofluoric acid (HF) solution (0.55%) for 1'30". If after this step the hole colour does not turn into brown, as shown in Fig. 3-6b, it means that a thin layer of TEOS was left on Ti. This could be easily removed in buffered oxide etch (BOE) solution, however, this step implies a small gap between CNT forest and hole walls. Without stripping the photoresist, 5 nm of Co were evaporated on wafer frontside. This was patterned by means of lift off process in Tetrahydrofuran (THF) at 35°C in ultrasonic bath (Fig. 3-3h). N-Methyl-2-pyrrolidone (NMP) at 70°C, usually employed for catalyst lift off, cannot be used since it is not compatible with Co growth [4]. Lift off was not considered

optimal yet, since, after rinsing the wafer, several areas were still covered with PR residues. The problem could be solved by stripping the PR after TEOS etching and using a new PR layer for the lift off, however, misalignment between hole and the Co patterning could appear.

The process ended by growing CNTs on top of the electrodes at 500°C in CNT AIXTRON BlackMagic pro 4 inch CVD reactor (Fig. 3-3i). Growth temperature has been chosen taking in account CNT quality and alignment and trying to reduce the thermal budget as much possible. CNTs were grown for 70", reaching a length of 2-3 μm. One wafer was processed till TEOS and Ti etching, avoiding CNT growth. In this way Standard TiN MEAs were fabricated as a benchmark for electrochemical performance assessment. Fig. 3-6c and 3-6d report TiN and CNT electrodes SEM images.

3-4 Rigid Upside-down CNT MEA.

3-4-1 CNT growth

The device was fabricated on a four inches Si wafer. Two microns of SiO_2 were grown on the wafer by means of wet thermal oxidation; backside SiO_2 is be used as a stop layer for the heavy metals that could contaminate the wafer during CNT growth. A stack of metals was sputtered on wafer frontside: this consisted of 5 nm of Ti (this time only used to improve the adhesion between SiO_2 and TiN), 50 nm of TiN which acted as support layer for the catalyst, and 100 nm of Ti. The metal stack was then patterned by means of dry etching with chlorine chemistry; as opposed to the Standard MEA, it was patterned in circles (diameters 16 and 24 μm long were tested) in correspondence of the 12 Cytostretch electrodes (Fig. 3-4d, Mask: Fig. C-3). After this step, 1 μm of PECVD TEOS was deposited on the frontside: this layer was then patterned, etching holes of 12 μm in diameter on top of the Ti/TiN/Ti circles (Fig. 3-4f). Five nanometers of Co were evaporated on wafer frontside and patterned by means of lift off. CNTs were grown at 500°C in CNT AIXTRON BlackMagic pro 4 inch CVD reactor (Fig. 3-4h) filling TEOS holes as shown in Fig. 3-7.

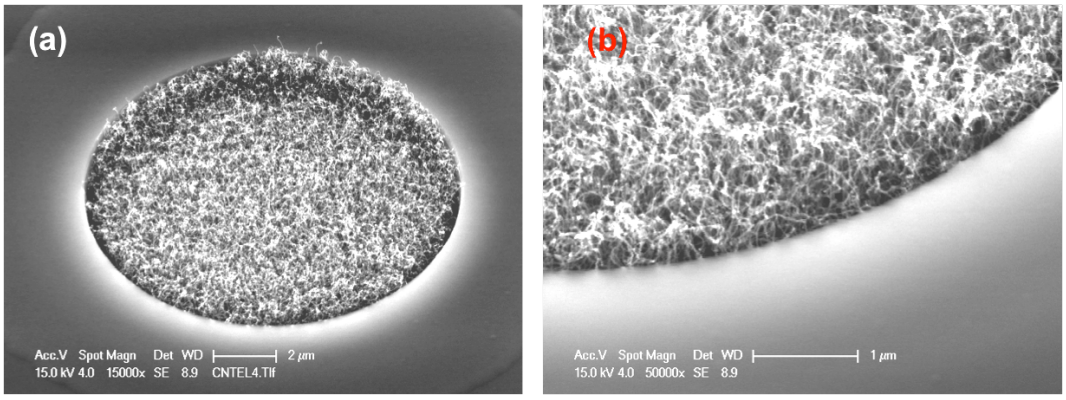

Figure 3-7: (a,b) CNT grown in TEOS hole.

3-4-2 Contamination prevention

This part of the fabrication dealt with eventual contaminations on the frontside and backside of the wafer. The latter needed to be taken in account since it has been in direct contact with the AIXTRON BlackMagic chuck (considered highly contaminated by heavy metals from previous CNT and graphene synthetizations). As already mentioned, Co is CMOS compatible; nevertheless, it is necessary to prevent CNT dispersion during following steps. For this reason, right after the growth, CNT forest was covered with a metal stack composed of 100 nm of TiN and 2 μm of Al (Fig. 3-4i). This quite thick layer of Al was required to guarantee sufficient insulation of CNTs forests. The layer was sputtered in TRIKON SIGMA sputter coater placed on a transport wafer to prevent machine contamination. Hole sealing was tested before final fabrication: this metallization provided good CNT isolation as shown in Fig. 3-8.

After this, wafer frontside was coated with a 3 μm thick PR layer; this protects the Al during the following cleaning steps. A three step cleaning was performed in dedicated baths of the Special Application Laboratory (SAL) in Clean Room (CR) Class 100. First, contaminations on the backside were removed by means of wet etching in diluted HNO_3. Second, 500 nm of thermal SiO_2 were etched in a BOE bath: this step removed the external SiO_2 which could contain eventual contaminations penetrated in wafer backside during CNT growth. Third, eventual contamination precipitation, coming from step 2, was removed form wafer backside by means of diluted HNO_3 (Fig. 3-4j). Even though the procedure was considered sufficient to process again in Clean Room Class 100, every cleaning step following this point was performed in dedicated baths in SAL; this limitation prevented eventual contaminations of CR cleaning line.

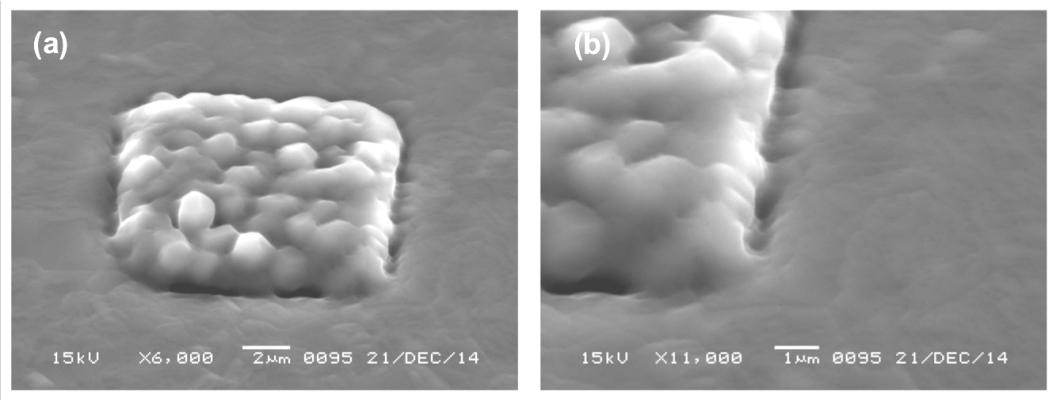

Figure 3-8: (a,b) Metallization layer composed of 100 nm of TiN and 2 μm of Al on top of CNTs.

3-4-3 Metal interconnects and membrane fabrication

Four micrometers of PECVD SiO_2 were deposited on wafer backside by means of Novellus Concept 1; the deposition was performed on a transport wafer to avoid any backside deposition. At this point the thick layer of SiO_2 on the backside was etched, patterning the dog-bone holes that will define the shape of the final membranes (Fig. 3-4l, Mask: Fig. C-4));

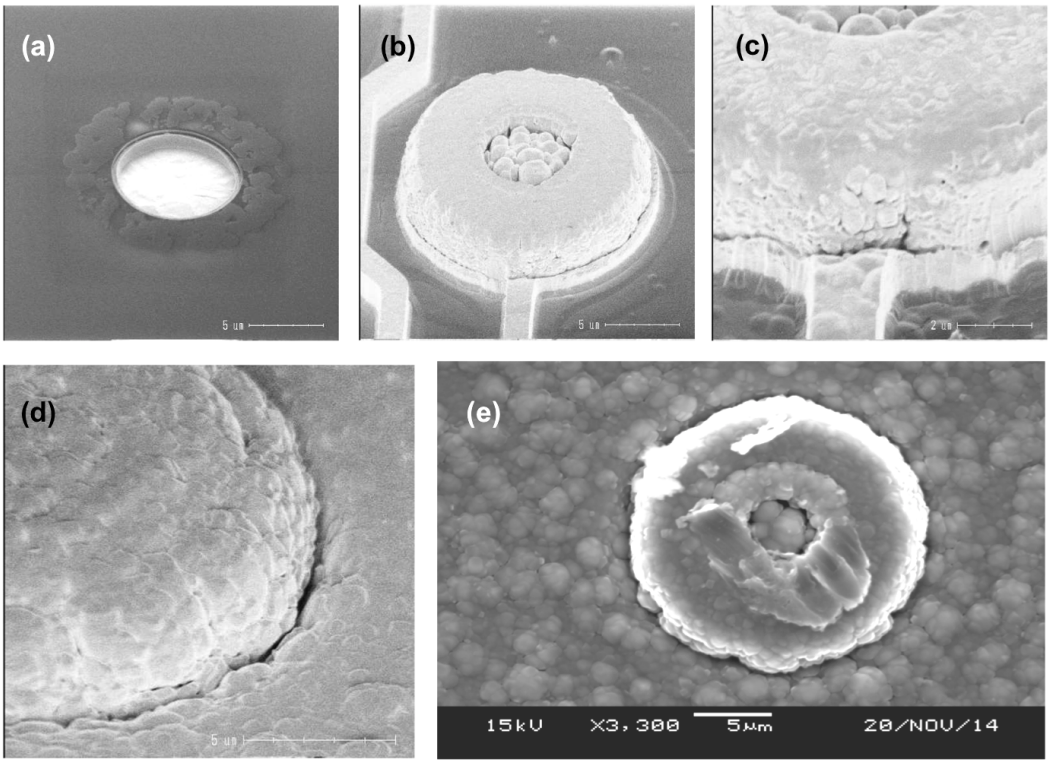

Figure 3-9: (a) SEM images during SiN etching (photoresist not stripped); (b,c) SEM image of metal interconnects 2 μm thick and sputtered at 25°C; (d) 4 μm thick Al layer on top of 2 μm step; (e) 4 μm thick Al layer on top of 2 μm step with scratch caused by measurement needle.

this SiO_2 was used as a hard mask during membrane releasing. After this step, frontside Al layer was etched, leaving only circular lids (diameter: 16 μm) on top of the CNT forests (Fig. 3-4m, Mask: Fig. C-3). Then, photoresist was stripped away with NMP at 70°C in ultrasonic bath and cleaned in HNO_3. The small dimension of the Al lids and the ultrasonic bath vibrations caused the detachment of ca 2% of the metal lids from the wafer. This situation can be easily identified with optical microscope analysis.

The process continued with the fabrication of the membrane and the metal interconnects. First, 2 μm of PECVD SiN were deposited at 400°C. This was meant to be used as stopping layer during the releasing of CNT electrodes and to insulate metal interconnects from cell culture solution. SiN layer was then patterned, etching holes on top of the electrodes: these are the vertical vias through which metal interconnects reach the correspondent electrodes (Fig. 3-4p). In order to prevent open circuit between electrodes and interconnections, SEM analysis was performed, verifying eventual charge effects on top of the Al layer (Fig. 3-9a).

Initially, metal interconnects were meant to consist of a 2 μm thick Al layer sputtered at 25°C. However, as can be seen in Fig. 3-9b,c, in this case step coverage was quite poor, showing no evident contact between the metal on top of the circular structure and the interconnects. This problem did not improve increasing Al thickness from 2 to 4 μm (Fig. 3-9d). The resistance between the Al on top of the structure and the surrounding Al layer was assessed with a two probes measurement. The resistance measured was equal to 4.3 Ω, verifying that top metal and bottom metal were actually in contact. Fig. 3-9e shows the

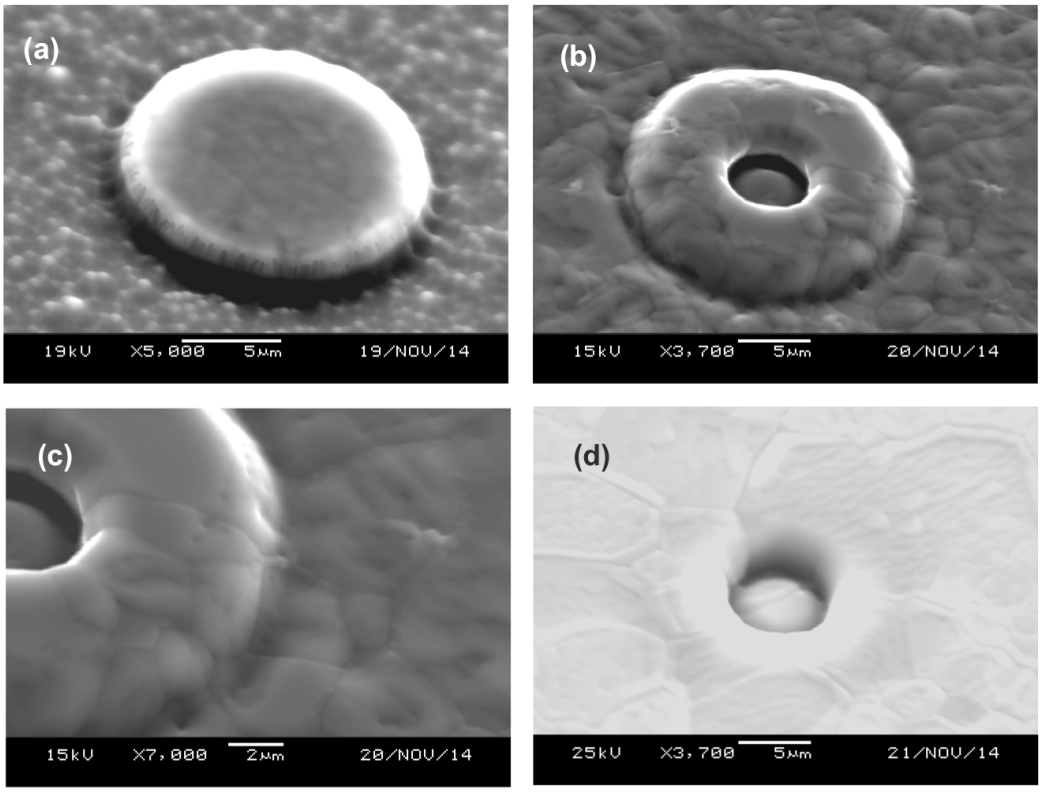

Figure 3-10: (a) SiN residues on the edge of the circular structure for spacer fabrication; (b-c) 4 μm Al layer sputtered at 350°C; (d) test hole to verify step coverage in hole 1 μm deep and with a 8 μm diameter.

scratch of the needle on top of the small structure.

Even if the two metal layer areas were in contact, few precautions were taken. A spacer was inserted in the fabrication: first, 2 μm of PECVD SiN were deposited on top of the metal lids; second, 1.5 μm of SiN were etched away leaving SiN residues around the lids to improve step coverage (Fig. 3-4n and 3-10a). The wafer was then covered with 1.5 μm of SiN which was patterned exposing the metal lids (Fig. 3-4p, Mask: Fig. C-2). After this step, 4 μm of Al were deposited on top of the structure. Deposition at 25 and 350°C was tested; the highest one provided better step coverage as can be seen in Fig. 3-10b,c; this was ascribed to the higher mobility of metal atoms during the sputtering. However, at this deposition temperature the central hole was not conformally covered. For solving this problem the diameter of the holes in SiN was increased from 6 to 8 μm, providing better step coverage in the bottom of the hole (Fig. 3-10d).

The thick layer of Al and the selectivity Trikon Omega 201 required a 6 μm thick photoresist layer to pattern the metal interconnects. As a consequence, the mask for the metal interconnects was redesigned with a higher interspace among the metal lines (Mask: Fig. C-5). After patterning the Al layer, a 10 μm thick layer of zero stress SiO_2 was deposited on the front side (Fig. 3-4s). The contact pads were then opened etching the frontside SiO_2 (Mask: Fig. C-6). The process continued on wafer backside by etching the Si underneath the membrane, landing on 2 μm of thermal SiO_2 (Fig. 3-4u); this step was performed with DRIE technology

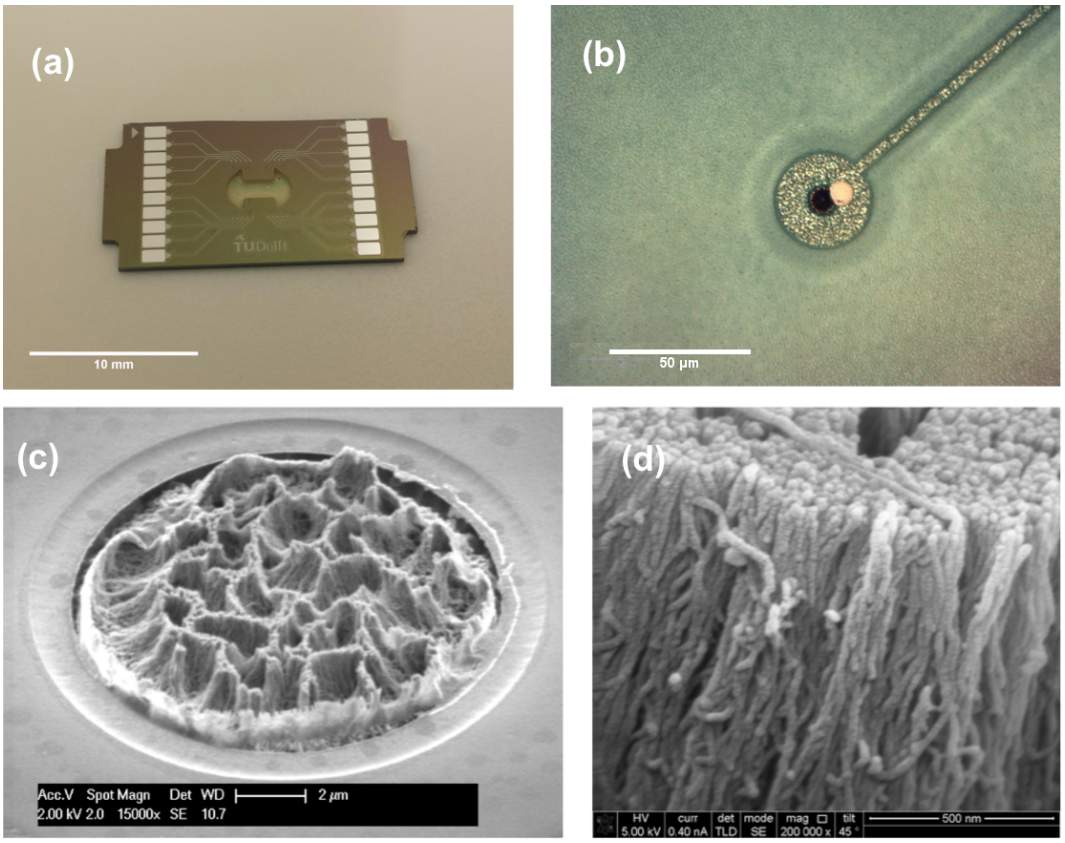

Figure 3-11: (a) Picture of the final device; (b) optical image of CNT electrode with support TiN circle detaching from CNT roots; (d-f) SEM images of Upside-down electrode.

using a Repier Omega 12L. After this step the passivation layer (teflon like layer) left during DRIE etching needed to be stripped away by means of oxygen plasma; either Trikon Omega 201 or a photoresist Stripper can be used. It is necessary to perform one of these treatments because the passivation layer is highly hydrophobic and it makes impossible for BOE solution (used in the following step) to reach the membrane backside. Another alternative for overcoming this problem is modifying the wettability of the walls by soaking the wafer in Triton right before BOE etching.

3-4-4 CNT electrodes releasing

The process ended by etching the SiO_2 around CNT forests (Fig. 3-4v). During this step wafer frontside was covered with a 12 μm thick layer of PR, making sure that Al pads are properly covered. This step was performed with BOE solution. As the solution started to etch the SiO_2 around the CNTs, TiN circles placed on the bottom of the CNT forests tended to detach from CNT roots. This was already expected, in fact, a pre-test showed that by placing a sample covered with Co-grown CNTs in BOE solution for 4-5', CNTs detach from the surface. Few TiN circles were found on the membrane at the end of the etching as can be seen in Fig. 3-11b. No difference was noticed for different dimensions of TiN circles.

In Fig. 3-11c,d Upside CNT electrodes are shown. As can be seen, CNTs tended to stick

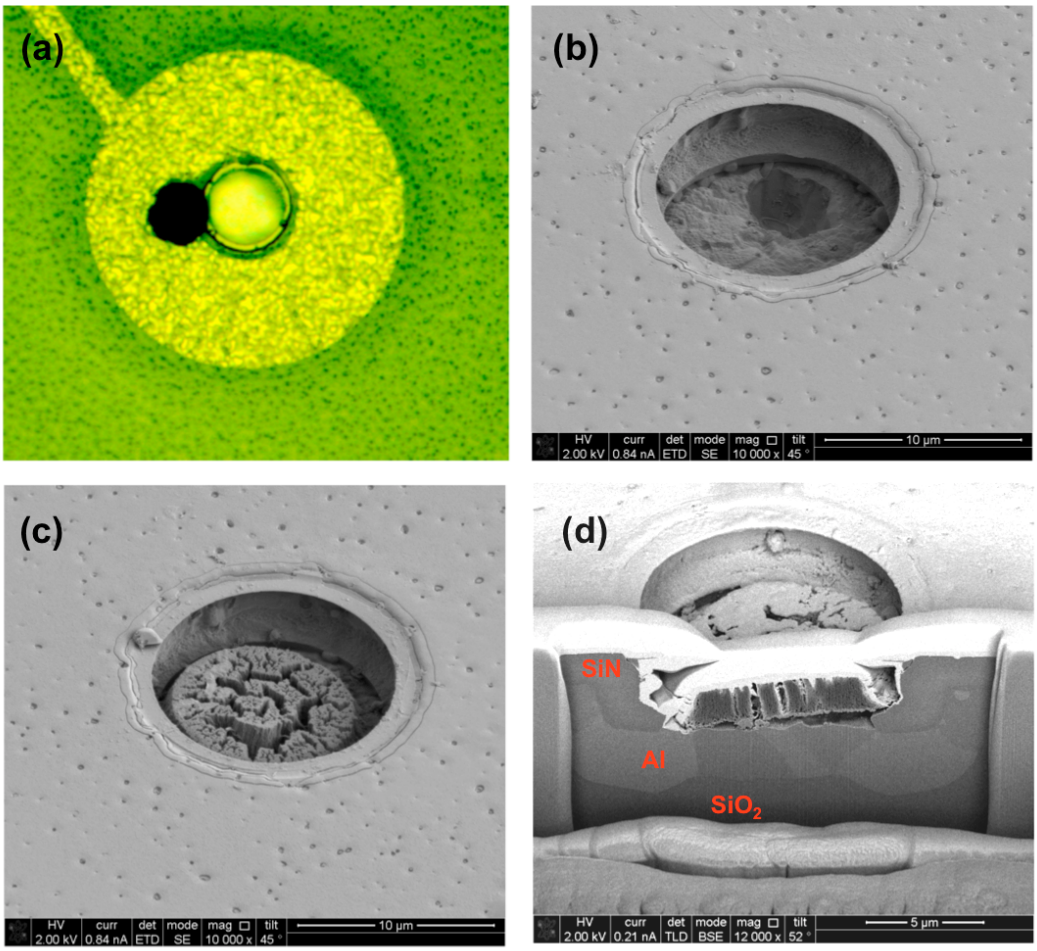

Figure 3-12: (a) Optical image of CNT island detached from the electrode; (b) SEM image of failed electrode without CNT; (c) SEM image of failed electrode with CNT island inside cavity; (d) cross section SEM image of failed electrode with CNT island inside cavity.

among each other. This situation was ascribed to BOE solution in contact with the CNTs. The effect of BOE treatment on CNTs is similar to that caused by alcohol (e.g. isopropanol). As stated by Vollebregt et al. [34], this problem is mainly due to a combination of surface tension of the liquid and strong van der Waals interactions. In several cases, during SiO_2 etching, CNT forest detached from the membrane (Fig. 3-12a,b). As can be seen in Fig. 3-12a, detached CNTs tended to stay together; this implies that CNT tips were still attached to the thin layer of TiN. This also means that the electrode failure was due to the fact that the Al on top of TiN has been etched by the BOE solution.

This theory was confirmed by a cross section of one of the failed CNT electrodes, performed with a focused ion beam (FIB)/SEM analyses (Fig. 3-12d). This electrode appeared to be covered with CNTs when checked with an optical microscope; however, when analysed with SEM microscope, it was found that the Al on top of the TiN was partially etched away. Moreover, it could be seen that CNT are kept together by the 100 nm thick layer of TiN. In Fig. 3-12c,d, a CNT island, felt in the cavity initially filled by Al, can be seen. It is worth to note that in Fig. 3-12 CNT buckling appears less severe than in Fig. 3-11.

3-5 Stretchable Upside-down CNT MEA.

The integration of the CNT MEA into a stretchable membrane follows the same process just presented till step l in Fig. 3-4. In this case, the Al is etched leaving the metal lids on top of CNT forests and the metal pads (Fig. 3-5m). Then a 2.5 μm layer of polymide is spun and patterned on wafer frontside. The thickness of this layer needs to be higher than the metal lids which are covering the CNTs. Because of planarization, polymide thickness on top of the metal will be equal to the difference between the total polymide thickness and the metal thickness. Metal interconnects are fabricated on the polymide layer and then covered by a second layer of Polymide (Fig. 3-5s). The polymide shell is meant to isolate TiN interconnects from penetrations of physiological solution during cell culture.

The structure is then covered with a 12 μm thick PDMS layer (Fig. 3-5t). Contact pads are opened in the PDMS by means of dry etching. Backside Si is etched releasing the dog-bone membranes by means of Bosch technology and. The fabrication ends by etching thermal SiO_2 and PECVD TEOS on the backside of the membrane with BOE, exposing in this way the CNT electrodes (Fig. 3-5w).

Chapter 4

Electrochemical Characterization

4-1 Methods

Two techniques have been identified as the most commonly used in the electrochemical characterization of bio-electrodes: cyclic voltammetry (CV) and electrochemical impedance spectroscopy (EIS). In the first part of the chapter, the theory behind these two techniques will be introduced. After that, the impedance spectroscopy measurements performed in High Tech Campus Eindhoven will be presented.

Cyclic voltammetry

CV is employed to identify eventual electrochemical reactions at the electrode-electrolyte interface and their nature. It is possible indeed to distinguish between Faradaic and Capacitive reactions and reversible and irreversible reactions. Moreover, CV can be also used to identify the electrode stability.

CV is performed by using three electrodes; two of them, the reference and the counter electrode, are directly soaked in electrolyte, s.a. phosphate buffered saline (PBS) solution. The third one, called test electrode (or working electrode), interfaces with the solution throughout a micro-electrode of the tested MEA. The potential difference between test and reference electrode is swept cyclically at a constant rate between two potential limits. Since the reference electrode is a non-carrying-current electrode, the current generated by these stimulations flows between test electrode and the counter electrode. This current is proportional to the reaction rate at the electrode-electrolyte interface. The result of this test is a graph showing current variations vs voltage sweeping; the shape of this graph depends on micro-electrode material, the sweep rate, the geometric area and the roughness of the micro-electrode [10].

With CV it is possible to quantify the amount of charge provided by a micro-electrode when used for electrical stimulations. This value is known as charge storage capacity (CSC) and is obtained by performing CV at slow-sweep rate over a potential range within the water electrolysis window and then integrating the measured cathodic current.

In Fig. 4-1a CVs of three electrodes made of sputtered iridium oxide film (SIROF), Pt and TiN are shown. The first piece of information can be inferred from the difference in the areas of the graphs. SIROF graph presents the largest area; this implies a higher CSC and so a higher electrochemical activity at the electrode-electrolyte interface. The approximately rectangular shape found in TiN graph is related to the Capacitive behaviour of this material. The CV of an ideal capacitor is in fact a rectangle. On the contrary, SIROF and Pt graphs present some peaks which are related to redox reactions on the surface.

In Fig. 4-1b CVs of CNT electrodes presented in [8] are reported. These have been conducted at 20, 140 and 300 mV s^{-1} in PBS. As sweep frequency increases, cycle area increases as well. CNT CVs show a rectangular shape for different sweep rates: this confirms CNT inertness and its Capacitive behaviour.

Device characterization was performed with a Metrohm Autolab potentiostat with a FRA2 module. This potentiostat performs only staircase CV, measurement that does not detect signals originated from Capacitive electrodes. For this reason, a new set up employing a Keithley Signal Measurement unit will be built to perform CV tests in the next few months.

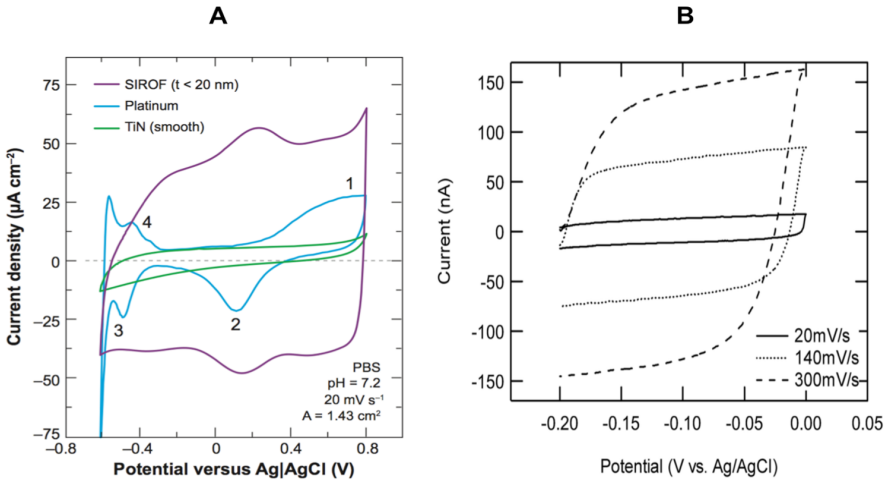

Figure 4-1: (b) CVs different materials in PBS at a sweep rate of 20 mV s^{-1} [10]; (b) CV scans of CNT coated electrodes conducted at 20, 140 and 300 mV s^{-1} in PBS [8].

Electrochemical Impedance spectroscopy

This technique measures amplitude and phase angle of the electrode/electrolyte impedance by means of sinusoidal electrical excitations. The set up of this technique is the same used for CV. In this case, the voltage between reference and working electrode is altered by means of low-amplitude sinusoidal signals. The impedance spectrum graph obtained with this test is used to characterize electrode-electrolyte interface; the impedance at 1 kHz is often used to compare different electrodes. Stimulation frequencies usually range from 1 Hz to 100 kHz. In order to have linear current-voltage response, stimulation amplitudes need to be small enough.

As already stated in Section 2-2, a rough material corresponds to higher electrical double

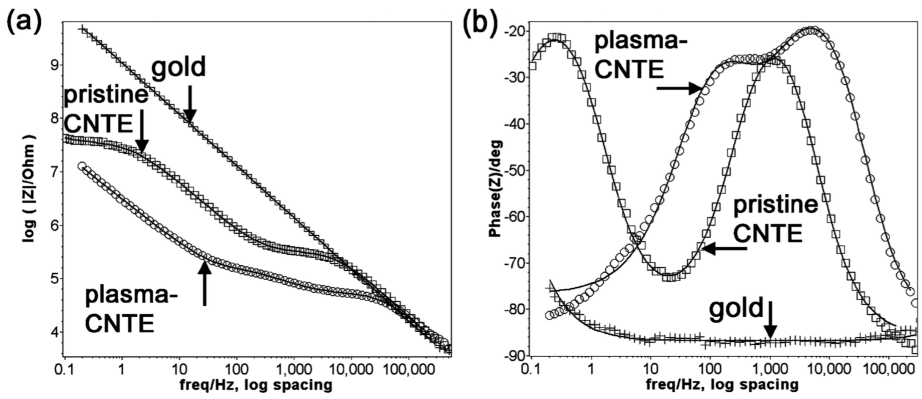

Figure 4-2: Bode plots of EIS of gold, CNT and plasma-treated CNT micro-electrodes ((a) impedance and (b) phase). Micro-electrodes have a geometric area of 116 μm^2 geometric surface area. Gold electrodes, CNT electrodes and Plasma-treated CNT electrodes show respectively an impedance of 1.3 MΩ, 260 kΩ and 79.4 kΩ.

capacitance compared to smooth micro-electrodes; this also implies smaller impedance. As shown in Fig. 4-2a the impedance of CNT electrodes shows outstanding performances when compared to smooth gold electrodes. This improvement can be seen only at low frequencies. The phenomena can be ascribed to the pore impedance which reduce ions penetration depth at higher frequencies. In Fig. 4-2, above 10 kHz the rough electrode surface behaves as a smooth surface because ions penetration is close to zero.

The Rendles circuit presented in Fig. 2-1 has shown to be not suitable for CNT electrode modelling. In this work, CNT electrodes will be modelled as metal electrodes with porous coating, using the circuit shown in Fig. 4-3. This model is often used to study the corrosion phenomena on metals covered with organic paint. The resistors R_s and R_f and the capacitance C_{dl} have the same meaning as Fig. 2-1. R_p has been interpreted as the resistance that the electrolyte faces during pore penetration. C_{CNT} can be interpreted as the capacitance of the CNT film as presented by Fung and colleagues [7]. In [7], the same model has been used, however, in that case a Walburg element was placed in series with R_f to consider in the model also ion diffusion phenomena.

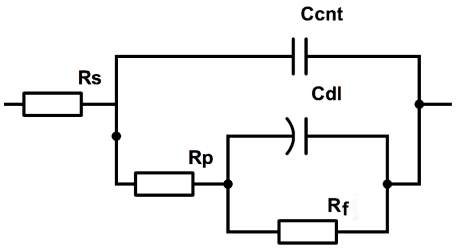

Figure 4-3: Rendles circuit used to model CNT electrodes. This correspond to the circuit often used to model metal electrodes with porous organic coating.

4-2 Electrochemical impedance spectroscopy (EIS) set up

In order to perform EIS on both Standard and Upside-down devices, plastic cylinders (internal diameter: 7 mm, external diameter, 10 mm; height: 10 mm) were attached on the devices. In order to seal the cylinders on the SiO_2/Si substrates either epoxy glue or silicone was used. Devices were left under a fume hood for 12 hours waiting for complete glue degassing to prevent any kind of interference on the measurements. These cylinder were used to contain PBS solution during electrochemical characterization and to guarantee complete isolation of the solution from device metal pads. As already mentioned in Section 4-1 EIS tests were performed with an Autohom Metrolab potentiostat with FRA2 module.

The set up was composed by three electrodes. The working electrode consisted of one of the mirco-electrodes included the MEA: this interfaced with the potentiostat by means of a crocodile cable clipped to a metal pad of the device. Counter electrode consisted of a Pt strip soaked in the electrolyte. A Silver Chloride (Ag/AgCl) electrode was used as reference electrode; compared to Pt electrodes, this kind of electrode guarantees higher stability when used as reference. A picture of the set up is shown in Fig. 4-4. Measurements were performed in a simple faraday cage composed by a cardboard box covered with Al foil and connected to the potentiostat ground through a crocodile cable.

Even though this improved the SNR, measurement performed at frequencies lower than 100 Hz were still affected by noise. For this reason final EIS measurements ranged between 100 Hz to 500 kHz. The amplitude of potential variations between working and reference electrode was equal to 20 mV. The output current signal was checked during measurements to verify eventual non-linearities caused by high-amplitude stimulations. With this voltage amplitude the output signal linearity was considered sufficient; in Fig. 4-5 input and output sinusoidal signals (ca 6 kHz) were reported.

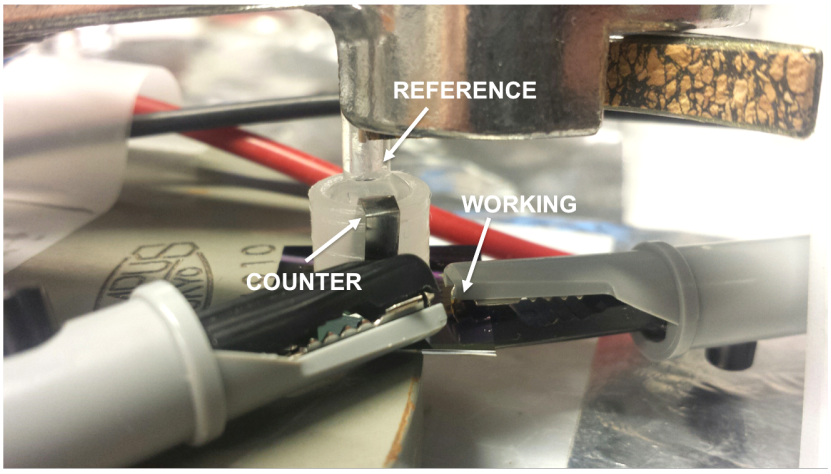

Figure 4-4: Picture of the EIS set up on a Standard CNT MEA. Three electrodes method composed by a reference, a counter and a working electrode were used.

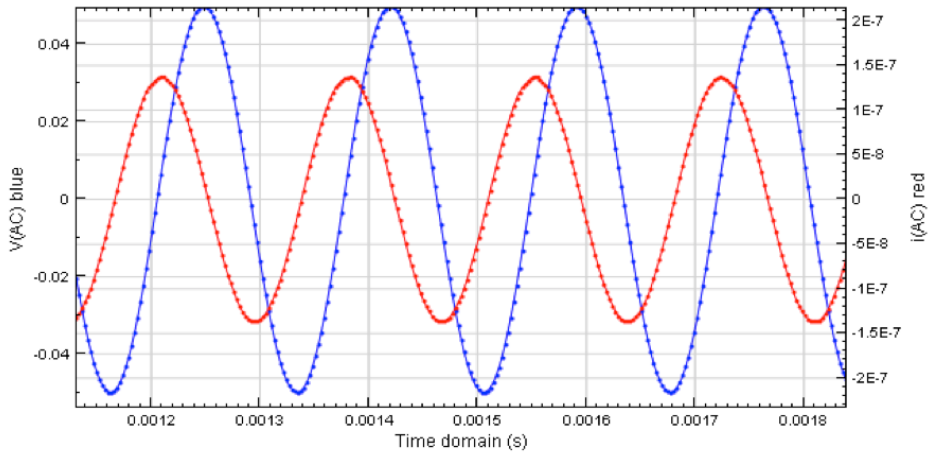

Figure 4-5: EIS measurement input and output (ca 6 kHz): Voltage stimulation signal (blue) applied across the metal/electrolyte interface and correspondent output current signal (red).

4-3 Standard MEA EIS

Impedance spectroscopy of a Standard CNT electrode and a Standard TiN MEA are shown in Fig. 4-6. The average impedance of the best three measurement was equal to 2.2 MΩ and 86.6 kΩ for TiN and CNT MEAs respectively. It is worth to note that the impedance values just mentioned were taken after having soaked CNT MEAs in PBS for 30'; this was done because it was noticed that right after covering the MEA with PBS, impedance values were unstable. Only after 30' the impedance tended to saturates to a value around 86.6 kΩ. Fig. 4-7 shows the impedance of a representative CNT electrode at 1 kHz vs time.

CNT MEAs were treated with oxygen plasma to verify eventual improvements of electrode performance. A Standard CNT MEA were placed in Europlasma stripper for 10" (power: 50 W) before sealing the plastic cylinders on top of it. A decrease in impedance was expected,

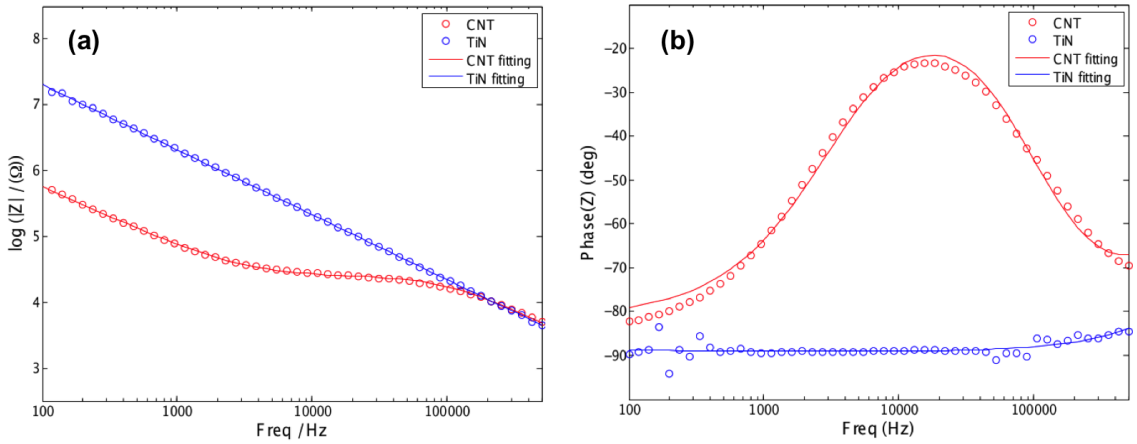

Figure 4-6: Bode graphs ((a) amplitude and (b) phase) of Standard CNT (red) and TiN (blu) electrodes. Markers show measured data, and solid lines show the fitting curve of the equivalent circuit.

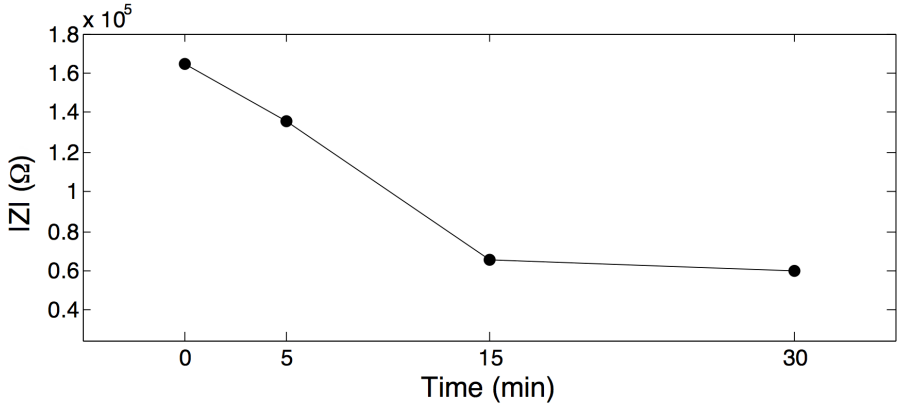

Figure 4-7: Representative CNT electrode impedance vs time.

however, no substantial improvement was verified.

The spectrum of TiN electrode was fitted with the circuit shown in Fig. 2-1 and CNT spectrum was fitted with the circuit in Fig. 4-3; NOVA software was used for this task. The average of the fitting parameters of three representative micro-electrodes is reported in Table 4-1. CNT electrodes showed a double layer capacitor five times higher than the TiN one. Moreover, as expected, CNTs showed lower α_{dl} as a consequence of high CNT roughness.

4-4 Upside-down MEA EIS

The parasitic capacitance due to the contact between the solution and the Si substrate, which affected the EIS measurement of the Cytostretch device, did not interfere with EIS measurements in the Upside-down MEA. The effect of this component in the measurements was reduced by decreasing the electrode impedance and increasing the thickness of the insulation layers under the pads. In fact, in this case between the Si substrate and the Al pads there were: 2 μm of thermal SiO_2, 1 μm of TEOS and 2 μm of PECVD SiN. The parasitic capacitance was calculated using dielectric constants for PECVD TEOS, thermal SiO_2 and PECVD SiN equal to 5, 3.9 and 7 respectively. The impedance of this parasitic element at 1 kHz was around 5.7 kΩ, a value much higher than the impedance of a Standard CNT electrode presented in Section 4-3.

The impedance spectrum of an Upside-down electrode is shown in Fig. 4-8. As can be seen Standard and Upside-down electrode spectrum show similar behaviour. The average impedance of the best three measurements was equal to: 234 kΩ. It is worth to note that several micro-electrodes did not show the expected behaviour, presenting a much higher impedance. This was ascribed to the failure of most of CNT electrodes because of Al etching (as presented in Section 3-4-4).

Compared to Standard CNT MEA, this device showed higher impedance amplitude. This could be due to the difference in CNT length and the severe CNT buckling seen in Fig. 3-11. In order to confirm this last theory, CNT buckling has been induced on a Standard CNT MEA. The effect of isopropyl alcohol (IPA) on CNT forest is shown in Fig. 4-9. The cylinder on top of the device was filled with IPA for five minutes. In order to remove IPA residues the

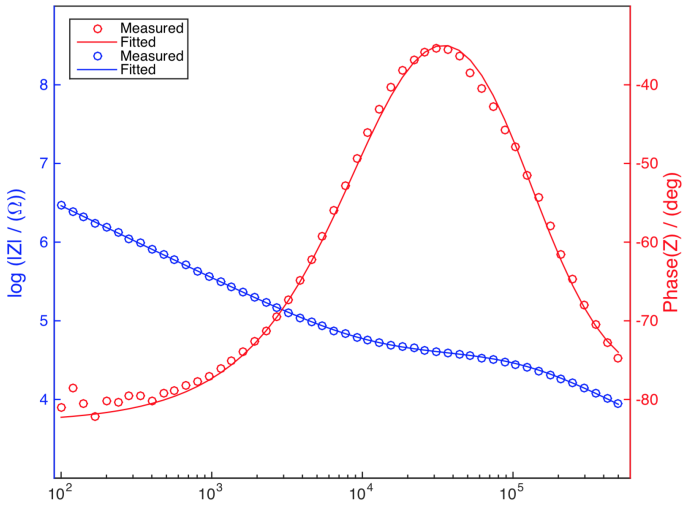

Figure 4-8: Bode plots ((blu) amplitude and (red) phase) of impedance spectra of CNT Upside-down CNT micro-electrodes. Markers show measured data, and solid lines show the fitting curve of the equivalent circuit.

device has been rinsed with PBS for three times. As can be seen in Fig. 4-10, IPA-treated CNT electrodes showed higher impedance amplitude than pristine CNT electrodes (367.1 kΩ at 1 kHz).

4-5 Discussion

TiN electrodes are showing an impedance spectroscopy two times smaller than that one measured in the Cytostretch device. This improvement is mainly due to the rough surface of TiN on the top-side of the metal layer. The impedance is supposed to further increase by optimising sputtering settings. TiN was deposited with the standard settings used to sputter CNT support layer. TiN roughness and porosity can be increased by employing the sputtering settings for the low-stress TiN presented by Creeemer et al. [43]; these enable to sputter

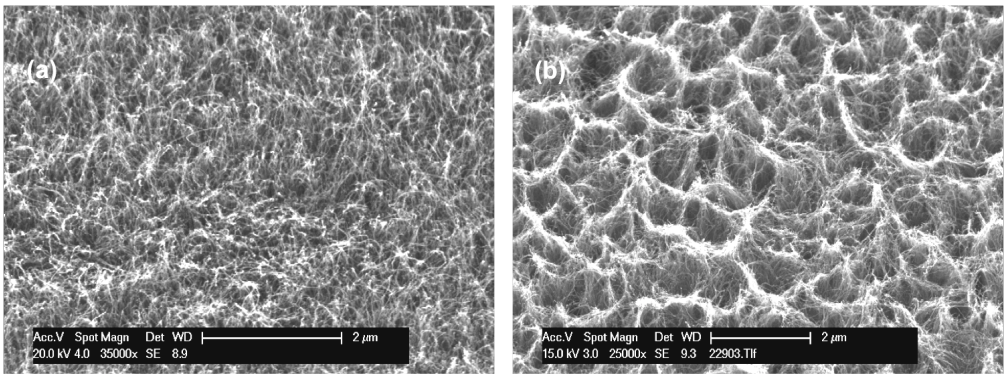

Figure 4-9: Effect of IPA on 1 μm high CNT forest: sample SEM (a) before and (b) after IPA treatment.

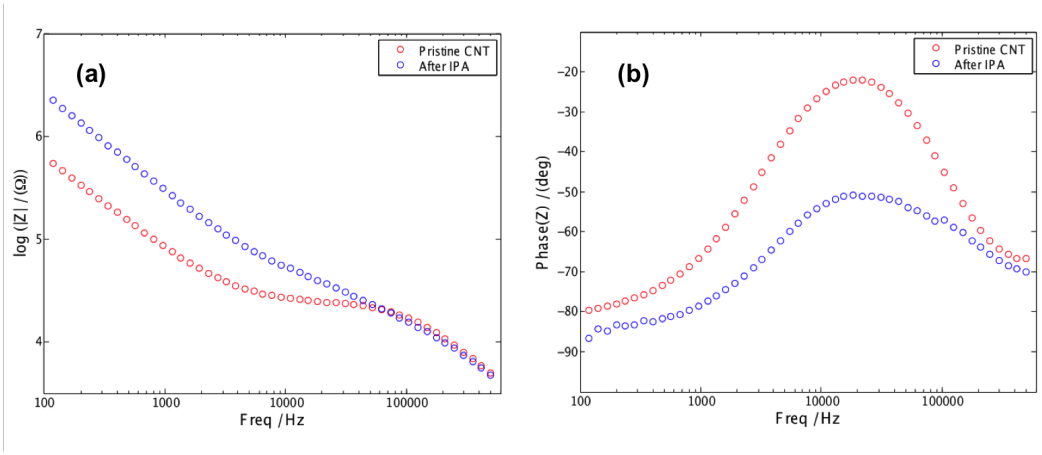

Figure 4-10: Bode plots of impedance spectra of CNT micro-electrodes after and before IPA treatment.

TiN layer with grain structure corresponding to Zone 1 of the Thornton classification. In this way, TiN assumes a highly porous structure with fibrous grains; the high number of voids in this structure should provide a further boost in the electrochemical performance of these electrodes.

Standard CNT electrodes are showing an unexpected behaviour when covered with PBS solution. The progressive decrease in impedance values was ascribed to an eventual transition of the liquid on the top of the CNTs from a Cassie-Baxter state[1] to a Wenzel state[2]; this phenomenon was already encountered by Wirth and colleagues in [44]. CNTs can be wet by substances having surface tensions lower than 200 mN m^{-1}; since PBS, like water, has a lower value, it can be driven by capillary forces among the CNTs, replacing the air pocket. The slow penetration of PBS in the air pockets increases the contact surface improving the electrochemical performance of the mirco-electrodes. Additional tests should be performed, growing CNT electrodes with growing length and verifying if the impedance decreases for longer CNTs.

CNT electrodes did not show improvement after plasma treatment. This was ascribed to the fact that after 30', PBS solution completely fills CNT air pockets. This means that making the surface superhydrophilic does not increase the contact surface area between the solution and the electrode. To the best of authors knowledge, previous papers presenting CNT MEAs have always employed randomly aligned CNTs. This could be the reason why this phenomenon has been never observed before. This theory can be also confirmed by the comparison between the impedance values measured on these electrode and the electrodes presented in [7]; this publication employs CNT electrodes with an area of 116 μm, almost the same of the area of the those presented in this project. Standard CNT electrodes right after the contact with the PBS show impedance values close to the pristine electrodes presented in [7]; after 30' they show impedance values close to the plasma-treated CNT electrodes presented in [7].

Impedances and fitting parameters of TiN, Standard CNT and Upside-down CNT are reported in Table 4-1. As can be seen, smaller impedances correspond to larger double layer

[1]State in which solution remains on top of the CNT surface with trapped air underneath.
[2]State in which the solution fully wets the CNT textured surfaces.

capacitances. With CNT electrodes, the impedance has decreased by 96% of the initial value. This good result corresponds to an increase in double layer capacitances. Another difference that can be highlighted is the decrease in α_{dl} when moving from the TiN to CNT; as already mentioned in Section 2-2 this value tends to 1 in case of smooth surfaces and decrease for rough surfaces.

Compared to Standard CNT MEA, Upside-down MEA has higher impedance value; this was ascribed to extensive CNT buckling. This impedance increase corresponds to a smaller double layer capacitance. Moreover, an increase in porous resistance (R_p) was seen. This can be due to the reduced space among CNTs. As already mentioned in Section 4-4, the relation between CNT buckling and electrode impedance was confirmed by comparing impedance spectroscopy of Standard CNT electrodes before and after IPA treatment. The severe CNT buckling can be avoided by etching the TEOS surrounding the CNT forest by means of HF vapour etching. However, this would prevent the TiN support circles from detaching from CNT roots.

Electrode	R_s (Ω)	$C_{\text{CNT}}(F)$	$R_p(\Omega)$	$K_{dl}(\Omega s^{-\alpha})$	α_{dl}	R_f (Ω)	$\|\text{Z(1 kHz)}\|$ (Ω)
TiN	482.7	n/a	n/a	$80.6 \cdot 10^{-12}$	0.99	$> 10^9$	$2.2 \cdot 10^6$
Standard	1056.7	$67.6 \cdot 10^{-12}$	$23.9 \cdot 10^3$	$4.6 \cdot 10^{-9}$	0.91	$> 10^9$	$86.6 \cdot 10^3$
Upside-down	589.7	$36.6 \cdot 10^{-12}$	$41 \cdot 10^3$	$899 \cdot 10^{-12}$	0.91	$55.3 \cdot 10^6$	$234 \cdot 10^3$

Table 4-1: Average Fitting Parameters for TiN, Standard CNT, and Upside-down CNT Electrodes

Chapter 5

Cell-device interaction

5-1 Induced pluripotential stem cells (iPSC)

The success of Organ on Chip is linked to the remarkable improvements achieved with induced pluripotential stem cells (iPSC) in the last ten years. For this reason, in this section a brief review on iPSC will be given. Different cell sources are available for *in vitro* tests: immortalized cell lines, primary cell material and stem cells [16].

Human immortalized cell lines are often used for their ability to replicate indefinitely, however, they do not carry any genetic information; this means that they cannot be employed for patient-specific studies [16]. Primary cell material enables to produce cell cultures with the same genetic characteristics of a patient by isolating the cells directly from his tissue and then proliferating them under specific conditions on a plate [45]. However, this type of cells is usually considered difficult to culture in the long term. Moreover, several organs, s.a. heart and brain, are difficult to access making cell isolation quite critical.

Stem cells solves availability and culturing problems encountered in the other two sources. However, also in this case a disadvantage is encountered: stem cells often implies difficulties in differentiating the cells and maintaining a specific phenotype [16]. Although no source can be defined as ideal, stem cells have shown to be suitable for a huge number of applications s.a. in Organ on Chips [17].

Stem cells have the ability to differentiate in any cell lineage following a particular protocol. They can be subdivided in two categories: embryonic stem cells, which carries several ethical controversies due to the use of embryos, and iPSCs. The latter are derived from somatic cells s.a. a skin sample of the patient. Cells obtained from this sample are reprogrammed altering their DNA: in this way it is possible to generate pluripotent stem cells ideally able to differentiate in any human body lineage without the use of embryos. This process provides cells that preserve the same genetic background of the patient originated from a easily accessible sample [11]. IPSCs have found several applications not only in tissue engineering, but also in disease modelling, drug testing and drug discovery as summarized in Fig. 5-1 [11].

The use of human iPSC in Organ on Chips could lead to new exciting applications. By culturing in an Organ on Chip the iPSCs of a patient, it is possible to perform costumized *in*

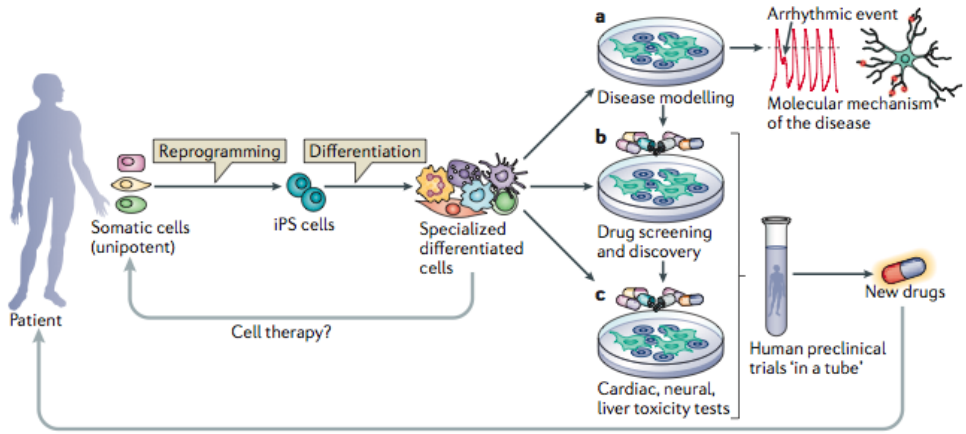

Figure 5-1: Adult somatic cells can be reprogrammed in iPSCs; after this, they can be differentiated and used for different application s.a.: (a) disease modeling, (b) drug screening and discovery and (c) toxicity tests [11].

vitro test; this scenario could boost future personal medicine advancements. Moreover iPSCs in Organ on Chips could overcome several clinical trial limitations; a good example can be found in the clinical trials of medicines for infants and children. These are usually performed on adults: in this case, the differences between adult clinical trials and infant users cause reliability problems. Including in a model specific iPSCs which represent in a better way infant cells, could avoid this issue. IPSCs could also be used to take in account the genetic peculiarities of a specific population in drug testing [20].

IPSCs can be considered as a relatively young technology, indeed, just in 2006 Yamanaka et al. [46] published the discovery that mice developed cells can be reprogrammed in stem cells; then in 2007 Yu et al. [47] published the first research in which human iPSCs have been produced. They showed how it is possible to reprogram skin cells into stem cells with almost the same characteristics of the well known embryonic stem cells, using only four factors (OCT4,SOX2,NANOG and LIN28). Most of the publications (s.a. [47]) uses integrating retroviral vectors to reprogram the somatic cells genes; this technique uses of modified viruses to transfer genes into somatic cells [48]. The safety concerns related to these viruses [48] and the variability between cell lines produced with this technique [11] have limited the use of integrating retroviral vectors in regenerative medicine. However, in 2008 Yamanaka et al. [49] reported the first generation of virus-free mice iPSCs.

5-2 CNT toxicity

CNT properties are well known as reported in Section 2-4-2. However, biocompatibility and toxicity of this material have not yet been completely characterized yet. In this work, biocompatibility is meant as "the ability of a material to perform with an appropriate host response in a specific application" as defined in [50]. From this definition it can be inferred that biocompatibility is related to a particular application. On the other hand, toxicity is a more generic concept. In this section, CNT toxicity will be discussed; then, in the following

sections, CNT biocompatibility for the specific application required in this project will be assessed in a series of tests. The effects of this material on *in vitro* and *in vivo* cultures need to be subdivided in two parts: those related to CNTs and those related to catalyst residues. In the first part of this section a review of CNT toxicity will be presented; then, the toxicity of commonly used catalysts will be discussed, mainly focusing on Co.

In literature, several inconsistencies can be verified among publications which try to assess CNT toxicity. According to Firme et al. [12], these are mainly due to the lack of Standard experimental protocols. CNT toxicity depends on several factors s.a. length, concentration, exposure duration, bond defects, CNT treatments and functionalization, and eventual catalyst residues.

A CNT floating in the extracellular medium, *in vitro* and *in vivo*, interfaces with a cell (immune cell s.a. neutrophils, macrophages and centric cells) by means of two mechanism: phagocytosis and nano penetration as shown in Fig. 5-2. In the first case, Adenosine Triphosphate (ATP) consumption is necessary. Inside the cell, CNTs can activate several signaling pathways at once and eventually lead to DNA damages. Before cytotoxicity testing, CNTs (detached from the growth support) are treated to reduce their hidrophobicity and then mixed with the culture solution. CNT wettability needs to be tuned to prevent CNTs agglomerates.

CNT functionalization can be used to avoid DNA damaging. In fact, it is possible to increase or decrease CNT toxicity by changing functional groups bound to C crystal defects [12]. CNT functionalization has also been used to deliver drugs inside a cell. CNT-DNA interactions also depend on the amount of non-hexagonal rings present along the tube. Odd-membered rings (five or seven-ring element) lead to deficit or excess of charge which alters the amount of DNA interacting with the CNT and the strength of the interactions.

The physical properties of CNTs play an important role in their toxicity. Shorter CNTs (around 0.22 μm) are easier to be engulfed into macrophages and phagocytes compared to long CNTs. This, and the amount of odd-membred rings are two sources of discrepancies in CNT toxicity assessments.

While studying *in vivo* CNT toxicity, it is necessary to take in account that different cells react to CNTs in different ways. Since one of the major concern is the impact that CNTs can have on workers who frequently are in contact with this material, most of the literature focuses on the effects of CNTs on lungs and skin. Several studies, s.a. [51], show that long exposure to CNTs can lead to lung inflammation and granuloma. Because of their diameter in order of nanometers, also long tubes (longer than 15 μm) can be inhaled, causing lung lesions. On the contrary, in contact with the skin, no irritation in the short term has been verified [52]; moreover, in [53] it was shown that, when compared to commercial black tattoo inks, CNTs have a comparable biocompatibility in implantation tests.

Regarding *in vitro* applications, Standard toxicity tests consist of plating cells in a well and inserting in the cell medium an amount of CNTs, as presented in [12]. The effect of CNTs on cardiac muscle cells in this situation has been well characterised; as presented by Garibaldi et al. [54], high purified CNTs do not affect the cells in the short period. Even though after three days CNTs were found to be bound on cell membrane, cells were still able to survive, grow and proliferate.

As already mentioned, catalyst residues play a critical role in CNT toxicity. Metal catalysts react with the oxidative species generated during the inflammatory response caused by CNT presence. This interaction leads to a redox cycling cascades which causes antioxidants lack and oxidative damage of the tissue. In particular, Co shows a high effect on CNT toxicity

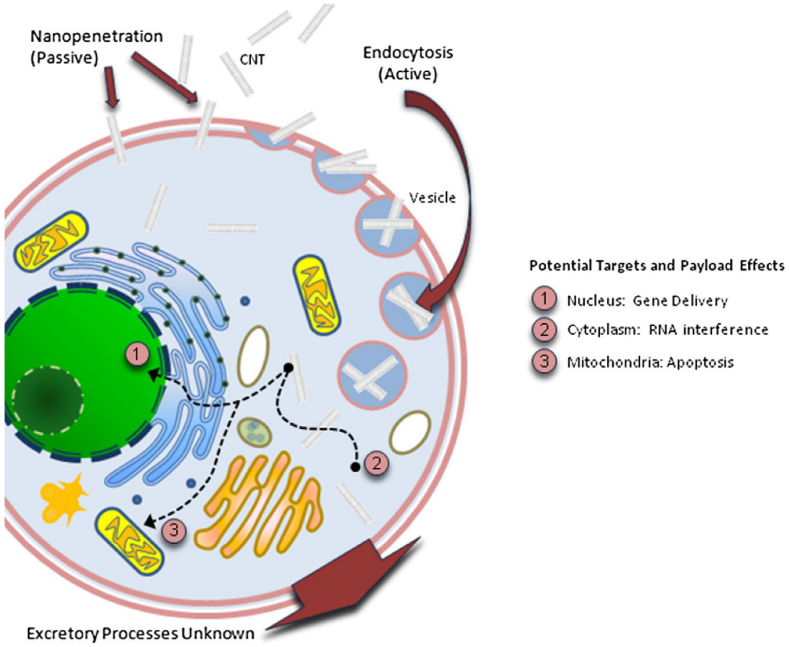

Figure 5-2: Receptor-mediated endocytosis and nanopenetration are suggested as two possible mechanisms for CNT interactions with cells [12].

which leads to chromosome damages. In large doses it is considered acutely toxic and cytotoxic leading to cell necrosis in case of *in vitro* cultures.

Even if the mechanism of Co toxicity has not been completely clarified, several causes have been identified. Co-cells interaction leads to cells oxygen deficiency, also called hypoxia, due to inhibition of crucial enzymes caused by Co affinity with sulfhydryl groups. Co toxicity is also ascribed to its interaction with Ca^{2+} channels. Moreover, Co is considered genotoxic, like the other catalysts, due to DNA damages caused by oxygen species which inhibit DNA repairment [55]. Catalyst effects can be limited by etching the particles; Co residues can be in fact easily removed with HCL or diluted HNO_3.

5-3 IPSC-derived cardiomyocytes on CNTs

As a consequence of CNT and catalyst toxicity, the devices presented in Chapter 3 need to be validated by plating human cardiac iPSC on top of Co-grown CNTs. These tests are meant to prove the biocompatibility of CNT electrode when implemented in Cytostretch device. To the best of authors knowledge, no previous work has presented a protocol for plating human iPSC on top of a substrate covered with CNT forest. The following cell culture platings were performed in the Department of Anatomy and Embryology in Leiden University Medical Centre aiming at defining a protocol for plating iPSC on top of CNT samples.

5-3-1 Substrate samples

Different samples cell plating substrates were fabricated. These can be divided in four groups:

- Samples covered with 5 nm of Ti and 50 nm of TiN;
- Samples covered with CNT forest (1 μm long) grown on Co catalyst and TiN support layer;
- Samples covered with CNT macroscopic patterns (circular islands, 1/1.5 cm in diameter) grown on Co catalyst and TiN support (Fig. 5-3a);
- Samples covered with CNT microscopic patterns (circular islands, 60 μm in diameter) grown on Co catalyst and TiN support (Fig. 5-3b);

The first two types were used during initial tests performed to define optimal coating and sterilization. The third and the fourth type were used to verify eventual migration of cardiomyocytes on top of CNT islands. This phenomenon has been observed several times in case of neuronal cells [39, 8] and it could improve signal SNR.

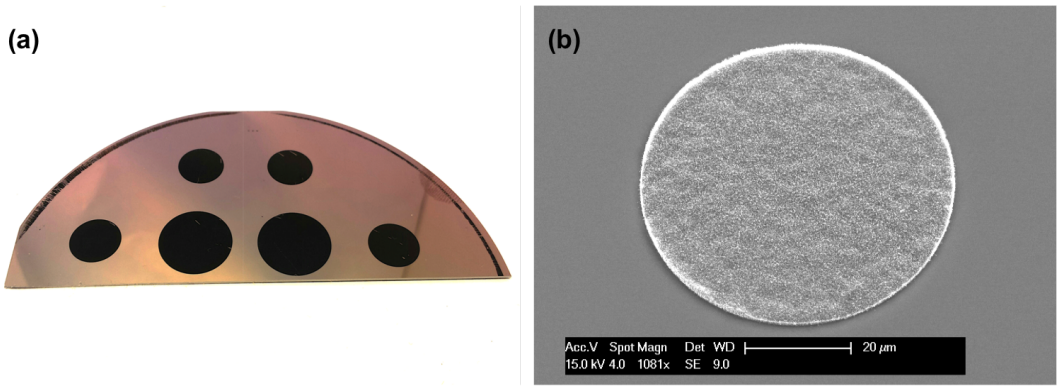

Figure 5-3: CNT patterns to verify cell migration: (a) macroscale CNT island (1/1.5 cm diameter) and (b) microscopic CNT island (60 μm diameter).

5-3-2 Sample sterilization and coating

Before plating cells on top of the samples, they needed to be sterilized; for this purpose both UV light and alcohol sterilization were tested. In case of alcohol, samples were soaked in ethylene for 30'; the UV treatment samples were placed in a Philips TUV 30 8T lamp for 20' at standard settings. After the sterilization, samples were placed in a 12 wells plate as shown in Fig. 5-4. In case of ethanol sterilization, samples were rinsed four times with PBS before proceeding with coating.

After sterilization, plating substrate needs to be coated to induce cell attachment and proliferation. Three coatings were tested for this purpose: Martigel, gelatin and Fibronecting

solutions. The first one is a gelatinous protein mixture resembling the extracellular environment found in many tissues. This was expected to provide the most suitable surface for cell plating, however, the thickness of this coating could hinder bio-signal detection. The second one is a solid substance extracted from animal collagen often used for improving cell adhesion. The third one is a high-molecular weight glycoprotein present in extracellular matrix.

As mentioned in the Section 5-3-3, sterilization and coating have been defined by plating cells on top of CNT and TiN samples. For this purpose, 16 CNT samples and 8 TiN samples were used. Eight CNT samples were sterilized with UV light and the rest with ethanol. TiN samples were sterilized only with ethanol. Every coating was used on two samples covered with UV-sterilized CNTs, two with ethanol-sterilzed CNTs and two with TiN. Cell plating without coating was tested as well. The complete set of sample combinations (sterilization/-coating/pattern) used during cell plating tests is listed in Table 5-1.

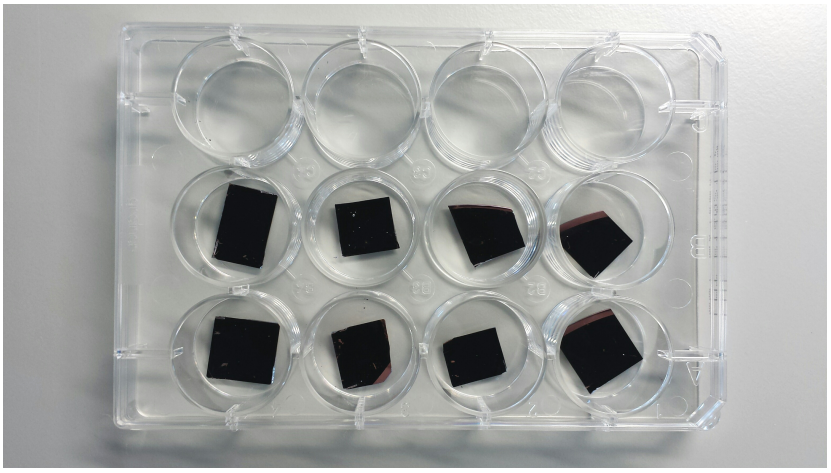

Figure 5-4: 12-well plate containing CNT samples during cell culture protocol.

5-3-3 IPSC-derived cardiomyocyte plating

IPSC-Derived Cardiomyocytes were provided by Leiden University Medical Centre in 6 wells plates. One of the cultures was dissociated by means of trypsin and PBS. The former is a pancreatic serine protease, which in contact with cell culture and in a specific environment mimicking human body (in a CO_2 incubator at 37°C), detach the cells from the culture surface. Trypsis was then stopped with a serine protease inhibitor. Cell detachment was also promoted by mechanical vibrations. Cells concentration was measured by means of a counting chamber. Live cells and dead cells were distinguished by means of Trypan blue: a vital stain which penetrate only dead cells.

Around 24'000 cells were deposited on top of each sample. These were confined in a small area of the sample by placing a plastic cylinder around it. In this way cell did not spread on the entire well surface. The cylinder was then filled with 200 μl of PBS. After plating, cell culture was checked every 24 hours to refill the PBS. After 72 hours cells cell viability, proliferation and adhesion was defined. Results and observation drawn are summarized in Section 5-3-4 and Table 5-2.

Sample	Material	Pattern	sterilization	Coating
1,2	CNT	/	Ethanol	Martigel
3,4	CNT	/	Ethanol	Gelatin
5,6	CNT	/	Ethanol	Fibronectin
7,8	CNT	/	Ethanol	/
9,10	CNT	/	UV	/
11,12	CNT	/	UV	Martigel
13,14	CNT	/	UV	Gelatin
15,16	CNT	/	UV	Fibronectin
17,18	TiN	/	Ethanol	Martigel
19,20	TiN	/	Ethanol	Gelatin
21,22	TiN	/	Ethanol	Fibronectin
23,24	CNT, TiN	1	Ethanol	Martigel
25,26	CNT, TiN	2	Ethanol	Martigel

Table 5-1: List of sample used during protocol definition

5-3-4 Protocol definition

Alcohol-sterilized samples showed the following behaviour: in case of CNT forests covered with Martigel, iPSCs showed good spreading out on both samples. Several areas of the culture were beating, confirming good cell state and differentiation of the cell culture. On the contrary, gelatin coating showed worse performances than Martigel. In this case in fact cells tended to arrange themselves in clumps, showing poor adhesion on top of the CNT. Clump presence was verified by the fact that cells islands were difficult to focus when analyzed with a microscope. Even if clumps were beating, this situation could give problems when bio-signals coming from the cells need to be read. First, the area covered by the culture is smaller, thus it is less likely that the cells get in contact with all the electrodes. Second, the part of the clumps which beats is usually the top. This means that the bottom part, eventually in contact with an electrode, hinder signal detection. Fibronectin showed to be another valid alternative for coating CNT forests. In this case good contraction and spread out were noticed.

TiN samples were used as a benchmark for assessment of cell viability and adhesion. Also Martigel-coated TiN surfaces showed to be suitable for cell plating. Monolayer islands of cells, beating in sync, showed clear electrical interconnection among each other. Gelatin, also in case of TiN, showed an inferior behaviour compared to Martigel, causing the formation of cells clumps. An inferior number of clumps and better interconnection among islands were found on Fibronecting samples. In this case cells clumps tended to be more interconnected among each other.

In general alcohol-sterilized samples showed a better adhesion than those sterilized with UV light. This difference could be either due to a difference in sterilization effectiveness or other factors s.a. the wettability modification of CNTs due to UV light and micro topographical cues caused by ethanol on the CNT forest. It is well known that cell response is highly influenced by micro and nanoscale features of the substrate [56, 57]. The microscopic pattern

in ethanol-sterilized CNTs could have improved cardioyocyte adhesion. This hypothesis has to be confirmed with high resolution SEM analysis of the cells on top of CNTs sterilized with ethanol and UV light. Martigel coated samples showed a behaviour similar to those sterilized with ethanol only in a small area of the surface. Both with gelatin and Fibronecting, clumps floating in the solution were found.

Samples used without coating showed poor cell viability both in case of TiN and CNTs substrates. It became clear from the presented results that ethanol sterilization and Martigel coating can be considered as optimal combination for cardiomyocytes iPSC plating. Even though, more tests would need to be performed to confirm these observations, they were taken in to account during cell plating on patterned CNT samples.

Sample	Viability	Monolayer/ Clumps/ Loosed/	Proliferation	Contraction	Interconnection
1,2	✓	M	+	++	-
3,4	✓	C	-	+	-
5,6	✓	M	-	+	-
7,8	✕	/	/	/	/
9,10	✕	/	/	/	/
11,12	✓	M	+	++	-
13,14	✓	L	–	+	-
15,16	✓	L	+	+	+
17,18	✓	M	+	++	++
19,20	✓	M	+	++	++
21,22	✓	C	-	+	++
23,24	✓	M	+	+	+
25,26	✓	M	+	+	+

Table 5-2: Qualitative observations about cell state 36 hours after cell plating (where ✓stands for successful, ✕stands for failed, + stands for positive result and - stands for negative result).

5-3-5 IPSC-derived cardiomyocytes on CNT pattern

Cardiac iPSCs were plated on top of patterned CNTs. In case of samples patterned with macroscopic islands (Fig. 5-3a), cells were plated on the edge of the CNT circles to verify eventual cell patterns in correspondence with CNT/TiN interface. The microscopic pattern (Fig. 5-3b) was meant to reproduce the cell migration, previously reported with neuronal cells in [39, 8].

In order to obtain as much information as possible from these cultures, cells were stained by means of 4',6-diamidino-2-phenylindole (DAPI) and cyanine dye (CY3). The first stain bind strongly to A-T rich regions in DNA, thus it is mainly used to highlight cells nucleus. The

second one is a cardiac-specify dye which highlights the cytoskeletal network of cardyomyocyte. These two stains add to the green fluorescent protein (GFP) marker already featured in the available iPSCs. Staining procedure is presented in following paragraphs.

Cell staining: After washing cell culture for three times with PBS, cells were fixed to the surface by means of paraformaldehyde which kills the cells and prevents cell putrification. After this, cells were washed and permealized by means of Triton X-100 diluted in PBS. This guaranteed dies penetration into the cells. Then, cells were pre-incubated by means of normal goat serum in PBS for one hour to prevent background staining.

CY3 staining was then performed. This was done in two steps: in the first one, cells are incubated with an antibody which binds to α actinin proteins inside the cadiomyocyte cells. In the second step, cells were incubated with a fluorescent antibody that binds with the first one. DAPI staining was performed in a single step by incubating the cells in DAPI diluted in PBS. This procedure ended by rinsing the samples in PBS.

Results Fluorescent images of stained cells on samples covered with macroscopic and microscopic CNT patterns are shown in Fig. 5-5 and 5-6. The figures were created merging only CY3 (in red) and DAPI (in blue) signals. As shown in Fig. 5-5, cardiomyocytes in proximity (a) and on top (b) of CNTs, cells presented a well developed cross-striated sarcomeric structure as revealed by CY3 expression.

Bright field images are not included, however CNT patterns are highlighted with white dotted lines/circles. As can be seen in Figure 5-6b, with microscopic CNT pattern, cell spread out without showing relevant migration on top of CNT islands. It seems that cells neither avoid or prefer CNT surface. The same thing can be said about the macroscopic pattern.

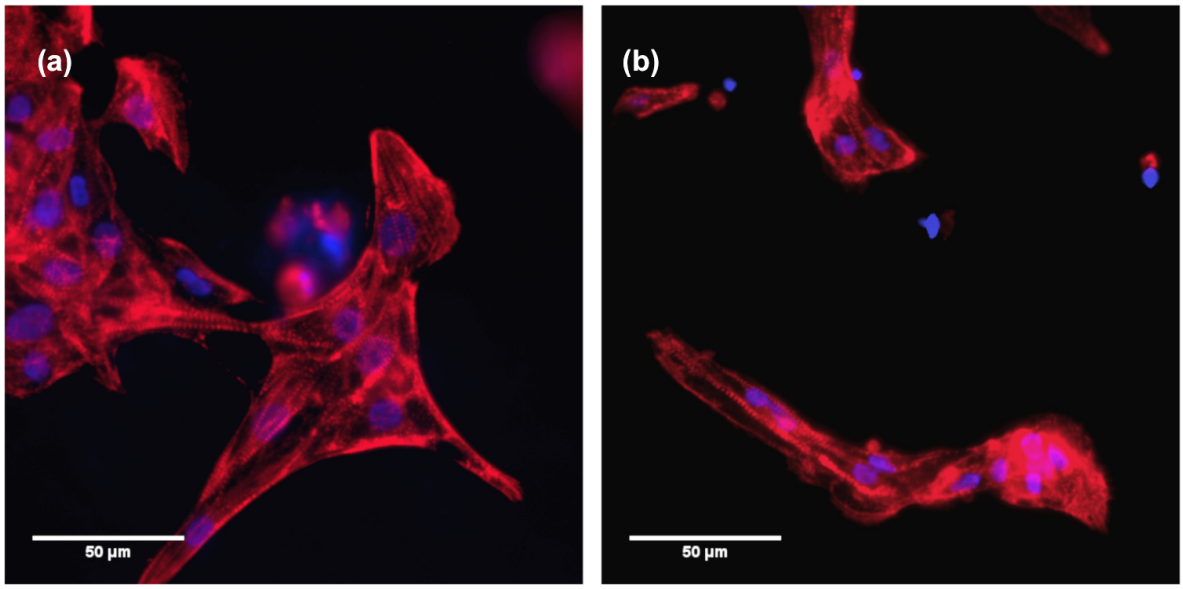

Figure 5-5: Merged fluorescent images of cardiac iPSCs stained with DAPI (blue) and CY3 (red) and plated (a) on top and (b) in proximity of CNTs.

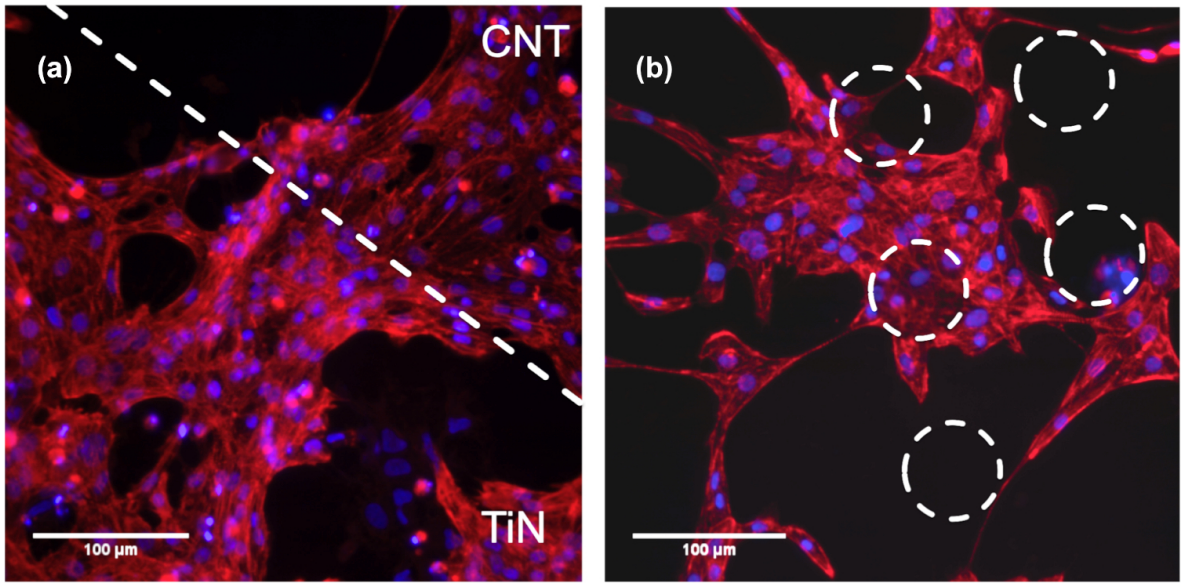

Figure 5-6: Merged fluorescent images of cardiac iPSC plated on patterned CNTs ((a): macroscopic pattern, (b) microscopic pattern) and stained with DAPI (blue) and CY3 (red).

As shown in Fig 5-6a, there is no relevant pattern in the cardiomyocyte layer at the interface between CNTs and TiN.

5-4 Extracellular recording

In order to test the performance of CNT electrodes detecting cells field potential, Cardiomyocyte cells were plated on an Upside-down CNT MEA and a Cytostretch device provided by DIMES center. Both dies were mounted over an acrylic culturing chamber. In this case, cell adhesion was promoted by sterilising both devices with a low-power (25 mW) oxygen plasma for 1'. As proved in Section 2-4-3, such a low power treatment does not affect CNT quality. PDMS and SiN surfaces were covered with Martigel coating for optimal cell adhesion.

Cells were plated on the membrane backside. Fig. 5-7 shows the tested MEAs covered with cardiomyocytes where cell coverage appeared superior on the Cytostretch device. This was ascribed to the good bio-functionality of PDMS promoted by the oxygen plasma treatment. This treatment makes PDMS surface hydrophilic by converting $SiCH_3$ groups on the surface into SiOH groups.

Cardiomyocyte potential field was recorded with the aid of a Multi Channel System (MCS) USB-MEA-System. Devices interface with this system through a printed circuit board as presented in [58]. Signals detected from a Cytostretch electrode and an Upside-down CNT electrode are reported in Fig. 5-8a,b and Fig. 5-8c,d respectively. The signals were filtered with Matlab using a bandstop filter for 50 Hz, a low pass filtered at 200 Hz and a 2 Hz high pass filter.

Fig. 5-8b,d represents the field potential variations measured with the two devices corresponding to the initial phase of membrane action potential. In Fig. 5-8a,c a series of field potential peaks is shown corresponding to cell beating. Measurements were extremely limited

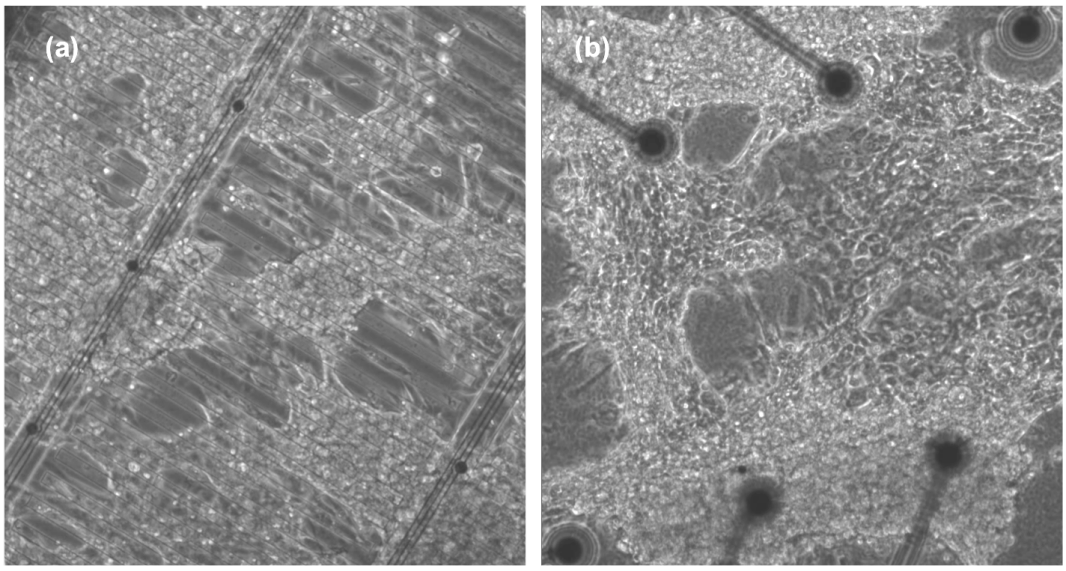

Figure 5-7: Optical images of cardiac iPSC (a) on top of cytrostretch device and (b) Upside-down CNT MEA.

by the high noise in both devices and by the limited amount of working CNT electrodes. As can be inferred from Fig. 5-8b and 5-8d, the used CNT electrode showed a noise level even higher than the Cytostretch device.

5-5 Discussion

CNTs and Co catalyst have been defined as toxic materials in the initial part of this chapter. Nevertheless, the biocompatibility of Co-grown CNTs was tested. In order to do this, a cell plating protocol was defined. Results proved that cardiac human iPSCs can be successfully plated on top of a CNT forest. Viability, adhesion and differentiation do not seem to be influenced by CNT substrate. This ensures that CNTs would not interfere with the cell culture plated on top of the device during *in vitro* testing.

IPSCs were also plated on patterned CNTs. No migration on top of the CNTs was seen. This phenomenon could guarantee higher SNR, since it promotes a close contact between cell culture and CNT electrodes. The absence of cell migration can be ascribed to the fact that this work employs cardiac cells rather than neuronal cells. Neurons migration was caused by the high roughness of CNT electrodes; even though, CNT roughness was compromised by BOE buckling on these devices.

CNT electrodes were also tested for detecting field potential variations generated by cardiac cells plated on the device. Few tested electrodes showed poor performance, almost in the same order of the Cytostretch device in contrast with the good electrochemical performance presented in Chapter 4. This problem could be either due to detachment of CNTs from the membrane or severe CNT buckling. Another factor that could have compromised the comparison between Cytostretch and Upside-down CNT MEA is the difference in membrane material. Bio-functionality differences between SiN and PDMS could cause a different adhesion between cell cultures and substrates affecting also the SNR during signal detection.

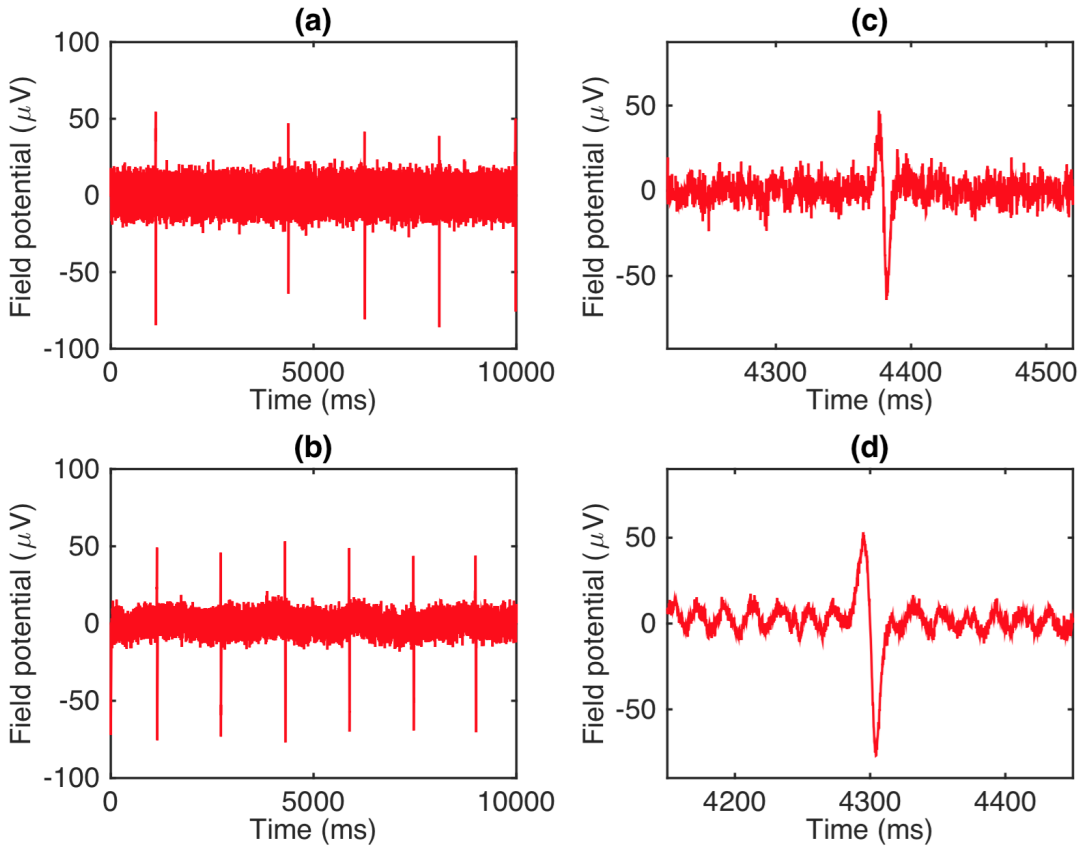

Figure 5-8: Field potential of cardiomyocytes recorded using (a,b) Upside-down CNT MEA and (c,d) Cytostretch device. Signals were obtained after filtering the signal measured by MEA amplifier to remove 50 Hz noise, the frequencies above 200 Hz and below 2 Hz.

Chapter 6

Conclusion

The MEA embedded in the Heart on Chip fabricated by Pakazad et al. [1] showed an insufficient electrochemical behaviour; this can be improved by increasing the SSA of the electrodes. The high aspect ratio of CNTs makes this material a valid solution for increasing the SSA of Cytostretch electrodes. This thesis aimed to assess the performance of these electrodes. Moreover, a novel technique for embedding CNT electrodes in the Cytostretch PDMS membrane was presented. The objectives defined in Section 1-3 were achieved: these, and the related results, are summarized in the following paragraphs.

- This work focused only on Co-grown CNTs. This catalyst choice guarantees two advantages: firstly, Co is CMOS compatible, as opposed to Fe and Cu. Secondly, Co, when used as CNT catalyst, has a low activation energy that guarantees CNT growth at low temperature: this low energy budget guarantees the possibility of including integrated circuits around the device before the CNT growth. The temperature at which the CNTs were grown is 500°C. The vertical alignment of CNTs grown at this temperature is sufficient to guarantee good mechanical and electrical CNT/metal contact. This hypothesis was confirmed by mechanical and electrical tests.
  Co-grown CNTs synthesized at 500°C showed an $I_{D/G}$ ratio of 1.27. Even though they grew at lower temperature, these CNTs showed the same quality of CNTs used as electrode coating in previous works s.a. [7]. Wettability tests verified CNT super-hydrophobicity. When CNTs are used as electrode coating, this property can limit the electrochemical performance of the MEA. For this reason, it was verified that a brief oxygen-plasma treatment can move CNTs from a super-hydrophobic to a super-hydrophilic state.

- In order to prove that Co-grown VACNTs are a valid option for improving MEA impedance, Standard CNT electrodes were fabricated and tested with EIS measurements. These showed outstanding performance with an impedance around 86.6 kΩ at 1 kHz. With these electrodes, the Cytostretch electrodes could have an impedance two order of magnitudes smaller than actual TiN electrodes.
  The EIS measurements, were performed only after soaking the MEA in PBS for 30'.

This was done because electrode impedance showed an unstable behaviour with a value that slowly decrease till it saturates around 86.6 kΩ. This phenomenon was ascribed to the wetting transition of the CNT forest on the top of the electrodes. This was probably not verified by other publications because previous works employed long random aligned CNT; the transition from Cassie to Wenzel regime was previously seen on short and vertically aligned CNTs. Oxygen plasma treatment did not improve the impedance of these electrodes: this is probably due to the fact that CNT pores are completely filled with PBS after 30', thus, the impedance cannot be further improved.

- In order to embed CNTs in a polymer membrane, a novel structure was designed. During this project the CNT MEA was embedded in a rigid membrane rather than a flexible one. Even if it is not a stretchable membrane, this proves that it is possible to embed CNT electrodes in a PDMS membrane. CNTs are first grown in SiO_2 holes, and then covered them with metal lids. These are are embedded in a membrane which also includes the metal interconnects through which the field potential variations coming from a cell culture can be read. The membrane is then released by means of DRIE etching and BOE wet etching. The TiN support layer, on the top of which CNTs were grown, is detached from CNT roots by employing the poor adhesion between CNTs and the metal support during backside SiO_2 etching.
  Previous works have already embedded CNT electrodes in PDMS membranes, however, none achieved large-scale fabrication. This work proves that this goal is feasible. EIS measurement performed on the novel MEA structure (Upside-down CNT electrodes) showed an impedance around 230 kΩ at 1 kHz. These presented an inferior performance compared to Standard CNT electrodes because of different CNT length and CNT buckling. This second theory was confirmed by treating Standard CNT electrodes with IPA; after this treatment CNT electrodes showed an increase in electrode impedance.

- The cytotoxicity of CNTs and Co required to assess the biocompatibility of Co-grown CNT MEAs. For this reason human iPSCs were plated on top of CNT islands to verify if cells viability could be affected by CNTs and Co catalyst. In order to do this, a protocol for plating cardiac iPSC was defined. Cells showed to adhere better to CNT sterilized with ethylene. Moreover, Fibronectin and Matrigel were identified as the best coating options; the first one is the more suitable for MEA coating. Besides the definition of the process, eventual cell migration on the top of CNT islands was assessed. However, it seems that cardiac iPSCs do not migrate on the top of CNTs as neuronal cells do. At the end, iPSCs were grown on top of Cytostretch devices and Upside-down CNT MEAs and bio-electrical signals were detected.

6-1 Recommendations and future work

This Master project was meant to prove that CNTs are a valid solution for improving electrochemical performance of the Cytostretch device and present a novel technique for embedding CNTs in the device. For this reason, the fabrication of PDMS membranes embedding Upside-down CNT electrodes will be the obvious following step of the project: in order to do this, the thickness of metal interconnects and the polyimide which protect them need to be adapted to the thick metal lids on top of CNTs.

Several improvements need to be considered during the fabrication of the final device. As proven by the large amount of failed Upside-down CNT electrodes, the actual CNT metallization is not compatible with BOE releasing. Al layer could be replaced by a thick layer of TiN. TiN sputtering settings should be optimized to reduce the step coverage during the deposition; this would guarantee CNT forest sealing. Using only TiN would prevent oxidations of the metal on top of the CNTs guaranteeing good electrical contact between electrodes and interconnects. Other materials s.a. Molybdenum (Mo) and Gold (Au) will also be considered for replacing Al.

This problem could be also avoided by etching the TEOS around CNTs by means of HF vapour etching. This technique does not etch Al, preventing CNT island detachment. However, this alternative does not remove the TiN support circles attached to CNT roots. Replacing the support layer made of TiN with a material which etches in vapour HF (s.a. Ti) would solve this problem. Another interesting improvement that could be tested is to coat CNTs with a thin layer of TiN by means of atomic layer deposition (ALD). This prevents CNTs from buckling and so it guarantees higher electrochemical performance. TiN coating should not reach CNT roots to avoid sealing CNT roots with TiN support circles. CNT buckling could be also avoided by freeze-drying the wafer right after BOE etching.

Co-grown CNTs can be considered a valid option for CNT MEA, however, the process showed few limits during lift off procedure. Alternatives to THF need to be identified. Ni grown CNTs could be a valid option for replacing Co. This would also make the device suitable for implantable applications s.a. cochlear implants and neural stimulators. The use of Ni grown PECVD CNTs synthesized on SiO_2 would provide an additional advantage: these CNTs can be grown directly on SiO_2 so the electrode realising could be performed with HF vapour etching [34].

In order to prove that CNT electrodes are detecting field potential variations through Capacitive reactions, CV needs to be performed on Standard and Upside-down CNT electrodes. Moreover, CSC for TiN and CNT electrodes could be calculated and compared, giving an additional proof of the superior electrochemical properties of CNTs.

Last but not least, only after the fabrication of stretchable Upside-down CNT MEAs, it will be possible to assess the performance of the novel structure in bio-signal detection. A MEA completely covered with CNTs and embedded in a PDMS substrate would indeed increase the probability of having an optimal electrode/cells contact, improving in this way the SNR during signal detection.

Appendix A

Standard MEA

A-1 Starting material

Use single side polished test wafers with the following specifications:

Type:	P-type, Boron
Orientation:	1-0-0, 0 deg of orientation
Resistivity	525 $\pm$ 15 μm
Diameter	100.0 $\pm$ 0.2 mm

Table A-1: Wafer Specifications

Wafers taken out of an already opened box must be cleaned before processing, according to the standard procedure. Wafers taken out of an unopened wafer box do not have to be cleaned before processing.

A-2 Flowchart summary

1. **Lithography - Alignment markers (Frontside)**
2. **Dry etching - Alignment markers (Frontside)**
3. **Cleaning**
4. **Thermal oxidation**
5. **Ti, TiN and Ti deposition (Frontside)**
6. **Lithography - Ti, TiN and Ti patterning**
7. **Dry etching - Ti, TiN and Ti patterning**
8. **Cleaning**
9. **Deposition TEOS PECVD (Frontside)**
10. **Lithography - TEOS patterning - Contact pads**
11. **Dry etching - TEOS patterning - Contact pads**
12. **Wet etching Ti**
13. **Cleaning**
14. **Lithography - TEOS patterning - Electrodes**
15. **Dry etching - TEOS patterning - Electrodes**
16. **Wet etching Ti**
17. **Catalyst evaporation (Co) (CR class 10000)**
18. **Lift-off (SAL)**
19. **CNT growth (CR class 10000)**

A-3 Detailed flowchart

If not differently specified, the process has been performed in Clean Room Class 100.

1. **Coating and backing**

   Use the EVG 120 coater/developer to coat the wafers with resist and follow the instructions specified for this equipment. The process consists of a treatment with HMDS (hexamethyldisilazane) vapor with nitrogen as a carrier gas, spin coating with Shipley SPR3012 positive photoresist (spin velocity 3450 RPM; spin time 30"), and a soft bake at 95°C for 1.5'. Always check the temperature of the hotplate and the relative humidity ($48 \pm 2\%$) in the room first.

   Use coating Co-3012-zero layer (resist thickness: 1.4 μm).

2. **Alignement and exposure**

   Processing will be performed on the ASML PAS5500/80 automatic wafer stepper.
   Follow the operating instructions from the manual when using this machine.

   Expose masks COMURK and FWAM, with job "20X20COMURK0.0"+ "FWAM" and the correct exposure energy 150 mJ.

3. **Development**

   Use the EVG 120 Coater/developer to develop the wafers, and follow the instructions specified for this equipment. The process consists of a post-exposure bake at $115°C$ for 1.5', followed by a development step using Shipley MF322 developer (single puddle process), and a hard bake at 100°C for 1.5'. Always check the temperature of the hotplates first.

   Use development program: Dev - SP.

4. **Photoresist inspection**

   Visually inspect the wafers through a microscope. Check if there are PR residues in exposed parts.

5. **Plasma etching of alignment marks**

   Use the Trikon Ωmega 201 plasma etcher. Follow the operating instructions from the manual when using this machine.

   Use sequence URK_NPD (with a platen temperature of 20°C) to etch 120 nm deep ASM URK's into the Si.

Step	Gasses and flows	Pressure	Platen RF	ICP RF	Platen temp.	Etch time
breakthrough	CF_4/O_2 = 40/20 sccm	5 mTorr	60 W	500 W	20°C	0'10"
gasstab	Cl_2/HBr = 80/40 sccm	60 mTorr	0 W	0 W	20°C	0'10"
bulk etch	Cl_2/HBr = 80/40 sccm	60 mTorr	20 W	500 W	20°C	0'40"

Table A-2: Process conditions from chamber recipe URK_ETCH

6. **Cleaning procedure: Tepla + HNO_3 100% and 65%**

   (a) Plasma strip: Use the Tepla plasma system to remove the photoresist in an oxygen plasma. Follow the instructions specified for the Tepla stripper, and use the quartz carrier.
   Use program 1: 1000 W power and automatic endpoint + 2' overetching.

   (b) Cleaning: Use wet bench "HNO_3 (100%)" and the carrier with the red dot. Leave wafers in bath for 10'.

   (c) QDR: Rinse in the QDR with the standard program until the resistivity is 5 MΩ.

   (d) Cleaning: Use wet bench "HNO3 (65%)" and the carrier with the red dot. Leave in bath for 10'.

   (e) QDR: Rinse in the QDR with the standard program until the resistivity is 5 MΩ.

   (f) Drying: Use the Semitool "rinser/dryer" with the standard program, and the white carrier.

7. **Thermal SiO_2**

   - Equipment: Furnace D1
   - Recipe: WETOXID.
   - Temperature: 1100°C
   - Time: 8h15'.

8. **Measurement of Thickness**

   Use the Leitz MPV-SP measurement system to measure the oxide thickness.

   Program: Th. SiO2 on Si, >50 nm auto5pts.

9. **Ti, TiN and Ti deposition**

   Use the TRIKON SIGMA sputter coater for the deposition of the Ti and TiN metal layer on the process wafers. The target must exist of 100% Ti. Follow the operating instructions from the manual when using this machine.

   Use recipe Ti500TiN50 350C to reactively sputter 500 nm Ti followed by 50 nm TiN (to function as barrier for Fe diffusion). Add dummy wafers in-between as required. Temperature = 350°C
   Perform a target clean and deposit an additional 100 nm of Ti (100 nm at 350°C) to act as sacrificial layer.

10. **Coating and backing**

    Processing will be performed on the EVG 120 wafer track automatically: this includes a HMDS (hexa methyl disilazane) treatment with nitrogen carrier gas, the coating with Shipley SPR 3012 resist (spin velocity 3450 RPM ; spin time 30"), and prebaking for 1.5' at 95°C. Follow the instructions specified for this equipment, and always check the temperature of the hotplates first.

    Use Coating Program "CO-3012-1.4mu" (resist thickness: 1.4 μm at 48% RV).

11. **Alignement and exposure**

    Processing will be performed on the ASML PAS5500/80 automatic wafer stepper.
    Follow the operating instructions from the manual when using this machine.

    Use METAL (Box 456), job g20a-1 exposure energy 200 mj.

12. **Development**

Use the EVG 120 Coater/developer to develop the wafers, and follow the instructions specified for this equipment. The process consists of a post-exposure bake at $115°C$ for 1.5', followed by a development step using Shipley MF322 developer (single puddle process), and a hard bake at 100°C for 1.5'. Always check the temperature of the hotplates first.

Use development program: Dev -SP.

13. **Photoresist inspection**

Visually inspect the wafers through a microscope. Check if there are PR residues in exposed parts.

14. **Plasma etching of interconnects and contact pads**

Use the Trikon Ωmega 201 plasma etcher. Follow the operating instructions from the manual when using this machine.

Use sequence TiTiNTi1 (with a platen temperature of 25°C) to etch Ti and TiN.

Step	Gasses and flows	Pressure	Platen RF	ICP RF	Platen temp.	Etch time
Bulk	Cl2/HBr = 30/40 sccm	5 mTorr	40 W	500 W	20°C	0'78"
overetch	Cl2/HBr = 30/40 sccm	5 mTorr	40 W	500 W	20°C	0'10"

Table A-3: Process conditions from chamber recipe TiTiNTi1

Etching program includes end-point detection.

15. **Cleaning procedure: Tepla + HNO_3 100% for green metals**

(a) Plasma strip: Use the Tepla plasma system to remove the photoresist in oxygen plasma. Follow the instructions specified for the Tepla stripper, and use the quartz carrier.
Use program 1: 1000 W power and automatic endpoint + 2' overetching.

(b) 10 ' in fuming nitric acid at ambient temperature. This will dissolve organic materials.
Use wet bench "HNO_3 99% (metal)" and the carrier with a red and yellow dot.

(c) QDR: Rinse in the QDR with the standard program until the resistivity is 5 MΩ.

(d) Drying: Use the Semitool "rinser/dryer" with the standard program, and the white carrier.

16. Deposition 1 μm TEOS

Use the Novellus PECVD reactor to deposit a 1 μm thick TEOS-based silicon oxide. Follow the operating instructions from the manual when using this machine.

Use recipe xxxnmTEOS at 350°C. Change the deposition time (seconds per station) according to log-book.

Gasses and flows	Pressure	HF power	LF power	Temp.	Time
O_2/TEOS = 5/1.8 ml/m	2.2 Torr	500 W	500 W	350°C	ca 40"

Table A-4: Process conditions from chamber recipe xxxnmTEOS

17. Measurement of Thickness

Use the Leitz MPV-SP measurement system to measure the oxide thickness.

Program: NOVELLUS Std TEOS on Si.

18. Coating and backing

Processing will be performed on the EVG 120 wafer track automatically:
this includes a HMDS (hexa methyl disilazane) treatment with nitrogen carrier gas , the coating with Shipley SPR 3027 resist (spin velocity 2480 RPM; spin time 30"), and prebaking. Follow the instructions specified for this equipment, and always check the temperature of the hotplate first.

Use Coating Program "CO-3027-3.1um" (resist thickness: 3.1 μm at 48% RV).

19. Alignment and exposure

Processing will be performed on the EV420 Contact Aligner. Follow the operating instructions from the manual when using this machine.

Use mask ORGAN_V3 (BOX 453) exposure time _____ (perform test before proceeding), Program 1.

20. Development

Use the EVG 120 Coater/developer to develop the wafers, and follow the instructions specified for this equipment. The process consists of a post-exposure bake at $115°C$ for 1.5', followed by a development step using Shipley MF322 developer (single puddle process), and a hard bake at 100°C for 1.5'. Always check the temperature of the hotplates first.

Use development program: Dev -SP.

21. Photoresist inspection

Visually inspect the wafers through a microscope. Check if there are PR residues in exposed parts.

22. Plasma etching: SiO_2

Use the Drytek Triode 384T plasma etcher.
Follow the operating instructions from the manual when using this machine.
The process parameters of the etch program may not be changed.

Copy the program StdSiO2 in 'magwegNG' changing the time for etching windows into the oxide layer and landing on titanium.

Gasses and flows	Pressure	RF power	He pressure	Etch time
C_2F_6/CHF_3 = 36/144 sccm	180 mTorr	300 W	12 Torr	ca 2'

Table A-5: Process conditions from chamber recipe Stdsio2

23. Cleaning procedure: Tepla + HNO_3 100% for green metals

(a) Plasma strip: Use the Tepla plasma system to remove the photoresist in an oxygen plasma. Follow the instructions specified for the Tepla stripper, and use the quartz carrier.
Use program 1: 1000 W power and automatic endpoint + 2' overetching.

(b) 10 ' in fuming nitric acid at ambient temperature. This will dissolve organic materials.
Use wet bench "HNO_3 99% (metal)" and the carrier with a red and yellow dot.

(c) QDR: Rinse in the QDR with the standard program until the resistivity is 5 MΩ.

(d) Drying: Use the Semitool "rinser/dryer" with the standard program, and the white carrier.

24. Coating and backing

Processing will be performed on the EVG 120 wafer track automatically:
this includes a HMDS (hexa methyl disilazane) treatment with nitrogen carrier gas , the coating with Shipley SPR 3027 resist (spin velocity 2480 RPM ; spin time 30"), and prebaking. Follow the instructions specified for this equipment, and always check the temperature of the hotplate first.

Use Coating Program "CO-3027-3.1um_noEBR" (resist thickness: 3.1 μm at 48% RV). Check eventual PR on backside.

25. Alignment and exposure

Processing will be performed on the ASML PAS 5500/80 automatic wafer stepper. Follow the operating instructions from the manual when using this machine.

Use CNT (box 449) job g20a-1, exposure energy: 300 mJ.

26. Development

Use the EVG 120 Coater/developer to develop the wafers, and follow the instructions specified for this equipment. The process consists of a post-exposure bake at 115°C for 1.5', followed by a development step using Shipley MF322 developer (single puddle process), and a hard bake at 100°C for 1.5'. Always check the temperature of the hotplates first.

Use development program: Dev -SP.

27. **Photoresist inspection**

Visually inspect the wafers through a microscope. Check if there are PR residues in exposed parts.

28. **Plasma Etching: TEOS**

Use the Alcatel GIR300 F etcher. Follow the operating instructions from the manual when using this machine.
Use the following settings:

Gasses and flows	Pressure	Power	Etch time.
CF4/CHF3/He = 50/25/40 sccm	0.05 mBar	60 W	25'

Table A-6: Process conditions from chamber recipe: SiO_2 etching (Alcatel)

Perform this process in more than one step for avoiding PR burning (s.a. 10' + 10' + 5').

29. **Via Hole etching: HF**

Use wet bench "HF (0.55%)" for green metals at ambient temperature, and the carrier with the red black dot.
The bath contains a standard 0.55% HF solution (Merck, VLSI selectipur).
Rinse the wafers in DI and dry. Use the Avenger "rinser/dryer" in etching line with the standard program, and the white carrier with a black dot. Leave in HF for ca 2'.
Brownish colour has to be seen in the holes.

30. **Catalyst deposition (CR class 10000)**

Use the CHA Solution e-beam evaporator to deposit 5 nm Co directly on the TiN surface. Use dedicated contaminated shields. Deposition rate: 0.2 Å/sec.
Remark: After this step use dedicated contaminated box (GREEN BOX).

31. **Lift off (SAL)**

Perform lift-off procedure with THF solvent. First heat water to 35°C and put in ultrasonic bath. Than put the THF in a beaker inside the bath and wait 20' for warming up the solvent. Use special holder to put wafers in bath and perform ultrasonic stripping for 20'. Use dedicated beaker from Cu corner. Refresh often THF (ca 4wafer/1l).

32. **Rinse and dry (SAL)**

Rinse the wafers in DI and dry using manual dryer with special Cu chuck.

33. **Inspection (SAL)**

Visually inspect the wafers through a microscope, check if catalyst layer remained in the holes. Put paper under wafer and throw away paper after use.

34. **CNT growth (CR class 10000)**

Use the AIXTRON BlackMagic Pro to grow CNTs using LPCVD at temperatures at 500°C for Co catalyst layers.

Use recipe: lpcvd_subref_v3_500
Growth rate: ca 30.83 nm/sec.

35. **SEM of CNT height**

SEM of CNT height in Class 100. Use a dedicated transport wafer to prevent contamination.

Appendix B

Upside-down CNT MEA

B-1 Starting material

Use single side polished test wafers with the following specifications:

See Table A-1.

Wafers taken out of an already opened box must be cleaned before processing, according to the standard procedure. Wafers taken out of an unopened wafer box do not have to be cleaned before processing.

B-2 Flowchart summary

1. **Lithography - Alignment markers (Frontside)**
2. **Dry etching - Alignment markers (Frontside)**
3. **Cleaning**
4. **Thermal oxidation**
5. **Ti, TiN and Ti deposition (Frontside)**
6. **Lithography - Ti, TiN and Ti patterning**
7. **Dry etching - Ti, TiN and Ti patterning**
8. **Cleaning**
9. **Deposition TEOS PECVD (Frontside)**
10. **Lithography - TEOS patterning - Electrodes**
11. **Dry etching - TEOS patterning - Electrodes**
12. **Wet etching Ti**
13. **Catalyst evaporation (Co) (CR class 10000)**
14. **Lift-off (SAL)**
15. **CNT growth (CR class 10000)**
16. **TiN and Al deposition (Frontside)**
17. **PR Coating (Frontside)**
18. **Backside contamination cleaning (SAL)**
19. **Cleaning (SAL)**
20. **Deposition SiO_2 PECVD (Backside)**
21. **Lithography - SiO_2 patterning - Hard Mask - (Backside)**
22. **Dry etching - SiO_2 patterning - Hard Mask - (Backside)**
23. **Cleaning (SAL)**
24. **Lithography - Al and TiN patterning - Metal lids**
25. **Dry etching - Al and TiN patterning - Metal lids**
26. **Cleaning (SAL)**
27. **Deposition SiN PECVD (Frontside)**

28. **Dry etching - SiN - Spacer (Frontside)**
29. **Deposition SiN PECVD (Frontside)**
30. **Lithography - SiN patterning - Electrode-interconnection contact (Frontside)**
31. **Dry etching - SiN patterning - Electrode-interconnection contact (Frontside)**
32. **Cleaning (SAL)**
33. **Al deposition (Frontside)**
34. **Lithography - Al patterning - Interconnects**
35. **Dry etching - Al patterning - Interconnects**
36. **Cleaning (SAL)**
37. **Deposition zerostress SiO_2 PECVD (Frontside)**
38. **Lithography - zerostress SiO_2 patterning - Contact pads (Frontside)**
39. **Dry etching - zerostress SiO_2 patterning - Contact pads - (Frontside)**
40. **Cleaning (SAL)**
41. **DRIE etching - Si (Backside)**
42. **PR Coating (Frontside)**
43. **Triton treatment (SAL)**
44. **Wet etching - SiO_2 (Backside)**
45. **PR strip (SAL)**

B-3 Detailed flowchart

If not differently specified, the process has been performed in Clean Room Class 100.

1. **Coating and backing**

   Use the EVG 120 coater/developer to coat the wafers with resist, and follow the instructions specified for this equipment. The process consists of a treatment with HMDS (hexamethyldisilazane) vapor with nitrogen as a carrier gas, spin coating with Shipley SPR3012 positive photoresist (spin velocity 3450 RPM; spin time 30"), and a soft bake at 95°C for 1.5'. Always check the temperature of the hotplates and the relative humidity ($48 \pm 2\%$) in the room first.

   Use coating Co-3012-zero layer (resist thickness: 1.4 μm). Look at the list for the correct program.

2. **Alignement and exposure**

   Processing will be performed on the ASML PAS5500/80 automatic wafer stepper.
   Follow the operating instructions from the manual when using this machine.

   Expose masks COMURK and FWAM, with job "20X20COMURK0.0"+ "FWAM" and the correct exposure energy 150 mJ.

3. **Development**

   Use the EVG 120 Coater/developer to develop the wafers, and follow the instructions specified for this equipment. The process consists of a post-exposure bake at $115^{\circ}C$ for 1.5', followed by a development step using Shipley MF322 developer (single puddle process), and a hard bake at 100°C for 1.5'. Always check the temperature of the hotplates first.

   Use development program: Dev - SP.

4. **Photoresist inspection**

   Visually inspect the wafers through a microscope. Check if there are PR residues in exposed parts.

5. **Plasma etching of alignment marks**

   Use the Trikon Ωmega 201 plasma etcher. Follow the operating instructions from the manual when using this machine.

   Use sequence URK_NPD (with a platen temperature of 20°C) to etch 120 nm deep ASM URK into the Si.

   See Table A-2

6. Cleaning procedure: Tepla + HNO_3 99% and 65%

(a) Plasma strip: Use the Tepla plasma system to remove the photoresist in an oxygen plasma. Follow the instructions specified for the Tepla stripper, and use the quartz carrier.
Use program 1: 1000 W power and automatic endpoint + 2' overetching.

(b) Cleaning: Use wet bench "HNO_3 (99%)" and the carrier with the red dot. 10' in fuming nitric acid (Merck: HNO_3 99% selectipur) at ambient temperature.

(c) QDR: Rinse in the QDR with the standard program until the resistivity is 5 MΩ.

(d) Cleaning: Use wet bench "HNO3 (65%)" and the carrier with the red dot. Leave wafers in the bath for 10'.

(e) QDR: Rinse in the QDR with the standard program until the resistivity is 5 MΩ.

(f) Drying: Use the Semitool "rinser/dryer" with the standard program, and the white carrier.

7. Thermal SiO_2

- Equipment: Furnace D1
- Recipe: WETOXID.
- Temperature: 1100°C
- Time: ca 8h15'.

8. Measurement of Thickness

Use the Leitz MPV-SP measurement system to measure the oxide thickness.

Program: Th. SiO2 on Si, >50 nm auto5pts.

9. Ti, TiN and Ti deposition

Use the TRIKON SIGMA sputter coater for the deposition of the Ti and TiN metal layer on the process wafers. The target must exist of 100% Ti. Follow the operating instructions from the manual when using this machine.

Use recipe Ti10TiN50at350C to reactively sputter 500 nm Ti followed by 50 nm TiN (to function as barrier for Fe diffusion). Add dummy wafers in-between as required. Temperature = 350°C
Perform a target clean and deposit an additional 100 nm of Ti (100 nm at 350°C) to act as sacrificial layer.

10. Coating and backing

Processing will be performed on the EVG 120 wafer track automatically: this includes a HMDS (hexa methyl disilazane) treatment with nitrogen carrier gas , the coating with Shipley SPR 3012 resist (spin velocity 3450 RPM ; spin time 30"), and prebaking for 1.5' at 95°C. Follow the instructions specified for this equipment, and always check the temperature of the hotplate first.

Use Coating Program "CO-3012-1.4mu" (resist thickness: 3.1 μm at 48% RV).

11. Alignement and exposure

Processing will be performed on the ASML PAS5500/80 automatic wafer stepper.
Follow the operating instructions from the manual when using this machine.

Use mask Ti (box 449) (alternative: Ti2 (box 449)), job g20a-1 exposure energy 200 mJ.

12. Development

Use the EVG 120 Coater/developer to develop the wafers, and follow the instructions specified for this equipment. The process consists of a post-exposure bake at 115°C for 1.5', followed by a development step using Shipley MF322 developer (single puddle process), and a hard bake at 100°C for 1.5'. Always check the temperature of the hotplates first.

Use development program: Dev -SP.

13. Photoresist inspection

Visually inspect the wafers through a microscope. Check if there are residues in exposed parts.

14. Plasma etching of Ti,TiN and Ti stack

Use the Trikon Ωmega 201 plasma etcher. Follow the operating instructions from the manual when using this machine.

Use sequence TiTiNTi2 (with a platen temperature of 25°C) to etch Ti and TiN.
Etching program includes end-point detection.

Step	Gasses and flows	Pressure	Platen RF	ICP RF	Platen temp.	Etch time
Bulk	Cl2/HBr = 30/40 sccm	5 mTorr	40 W	500 W	20°C	0'30"
overetch	Cl2/HBr = 30/40 sccm	5 mTorr	40 W	500 W	20°C	0'10"

Table B-1: Process conditions from chamber recipe TiTiNTi2

15. Cleaning procedure: Tepla + HNO_3 99% for green metals

(a) Plasma strip: Use the Tepla plasma system to remove the photoresist in an oxygen plasma. Follow the instructions specified for the Tepla stripper, and use the quartz carrier.
Use program 1: 1000 W power and automatic endpoint + 2' overetching.

(b) 10' in fuming nitric acid at ambient temperature. This will dissolve organic materials.
Use wet bench "HNO_3 99% (metal)" and the carrier with a red and yellow dot.

(c) QDR: Rinse in the QDR with the standard program until the resistivity is 5 MΩ.

(d) Drying: Use the Semitool "rinser/dryer" with the standard program, and the white carrier.

16. Deposition 1 μm TEOS

Use the Novellus PECVD reactor to deposit a 1 μm thick TEOS-based silicon oxide. Follow the operating instructions from the manual when using this machine.

Use recipe xxxnmTEOS at 350°C. Change the deposition time (seconds per station) according to logbook.

See Table A-4.

17. **Measurement of Thickness**
Use the Leitz MPV-SP measurement system to measure the oxide thickness. Perform measurement on test wafer.

Program: NOVELLUS Std TEOS on Si.

18. **Coating and backing**

Processing will be performed on the EVG 120 wafer track automatically:
this includes a HMDS (hexa methyl disilazane) treatment with nitrogen carrier gas , the coating with Shipley SPR 3027 resist (spin velocity 2480 RPM; spin time 30"), and prebaking. Follow the instructions specified for this equipment, and always check the temperature of the hotplate first.

Use Coating Program "CO-3027-3.1um_noEBR" (resist thickness: 3.1 μm at 48% RV). Check eventual PR on backside.

19. **Alignment and exposure**

Processing will be performed on the ASML PAS 5500/80 automatic wafer stepper. Follow the operating instructions from the manual when using this machine.

Use CNT (box 449) job g20a-1, exposure energy: 300 mJ.

20. **Development**

Use the EVG 120 Coater/developer to develop the wafers, and follow the instructions specified for this equipment. The process consists of a post-exposure bake at $115°C$ for 1.5', followed by a development step using Shipley MF322 developer (single puddle process), and a hard bake at 100°C for 1.5'. Always check the temperature of the hotplates first.

Use development program: Dev -SP.

21. **Photoresist inspection**

Visually inspect the wafers through a microscope. Check if there are PR residues in exposed parts.

22. **Plasma Etching: TEOS**

Use the Alcatel GIR300 F etcher. Follow the operating instructions from the manual when using this machine.
Use the following settings:

See Table A-6.

Perform the etching in more than one step for avoiding PR burning. (10' + 10' + 5')

23. **Via Hole etching: HF**

Use wet bench "HF (0.55%)" for green metals at ambient temperature, and the carrier with the red black dot.
The bath contains a standard 0.55% HF solution (Merck, VLSI selectipur).
Rinse the wafers in DI and dry. Use the Avenger "rinser/dryer" in etching line with the standard program, and the white carrier with a black dot. Leave in HF for 2'.
Brownish colour has to be seen in the holes.

24. **Catalyst deposition (CR class 10000)**

Use the CHA Solution e-beam evaporator to deposit 5 nm Co directly on the TiN surface. Use dedicated conta'ated shields. Deposition rate: 0.2 Å/sec.
Remark: After this step use dedicated conta'ated box (GREEN BOX).

25. **Lift off (SAL)**

Perform lift-off procedure with THF solvent. First heat water to 35°C and put in ultrasonic bath. Than put the THF in a beaker inside the bath and wait 5' for warming up the solvent. Use special holder to put wafers in bath and perform ultrasonic stripping for 20'. Use dedicated beaker from Cu corner. Refresh often THF (ca 4wafer/1l).

26. **Rinse and dry (SAL)**

Rinse the wafers in DI and dry using manual dryer with special Cu chuck.

27. **Inspection (SAL)**

Visually inspect the wafers through a microscope, check if catalyst layer remained in the holes. Put paper under wafer and throw away paper after use.

28. **CNT growth (CR class 10000)**

Use the AIXTRON BlackMagic Pro to grow CNTs using LPCVD at temperatures at 500°C for Co catalyst layers.

Use recipe: lpcvd_subref_v3_500.
Growth time: ca 0'38".

29. **Metallization**

Use the TRIKON SIGMA sputter coater for the deposition of the TiN and Al/Si metal layer on the process wafers.
Follow the operating instructions from the manual when using this machine. Use a dedicated transport wafer to prevent contamination.

Use recipe TiN 100nm AlSi2um_50C to sputter a 0.100 ± 0.1 μm thick layer of TiN at 25C (1 kW) followed by 2 μm of Al at 25°C (3 kW).

Add a test wafer. Deposition needs to be performed on transport wafers for avoiding contaminations

30. **Coating and baking**

Use the Lanz manual coater with Cu chuck to coat the front side with 3 μm of SPR3027 photoresist and perform a hard bake at 115°C in Memmert oven for 30'. Use dedicated Cu chuck and a dummy wafer underneath during the bake.

Coating program: 1600 RPM for 30".

31. **Wet etching Co catalyst (SAL)**

(a) Etch: Use a dedicated bath in SAL contaminated corner with "HNO_3:H2O = 1:1" at ambient temperature, and contaminated carrier.
The dedicated bath contains a HNO_3 solution.

(b) Time: 5'.

(c) Rinse: Rinse flowing water for 5'.

32. Wet etching BHF: Etch 0.5 μm Thermal SiO_2 (SAL)

(a) Etch: Use a dedicated bath in SAL contaminated corner with "BHF 1:7 (Metal)" at ambient temperature, and and contaminated carrier.
The bath contains a buffered HF solution.

(b) Time: 5'

(c) Rinse:Rinse flowing water for 5'.

33. Wet etching Co catalyst (SAL)

(a) Etch: Use a dedicated bath in SAL contaminated corner with "HNO_3:H2O = 1:1" at ambient temperature, and contaminated carrier.
The dedicated bath contains a HNO_3 solution.

(b) Time: 5'.

(c) Rinse: Rinse flowing water for 5'.

(d) Change carrier (not contaminated).

(e) Rinse: Rinse flowing water for 5' in SAL standard bench.

Move wafers in a standard white box.

34. Cleaning: Acetone + HNO_3 99% for green metal (SAL)

(a) Acetone: Dissolve the photoresist in acetone at RT in a glass beaker. Time = 5'.

(b) Clean: 10' nitric acid at ambient temperature. This will dissolve organic materials. Use standard bath bench containing HNO_3 (99%).

(c) Rinse: Rinse in flowing DI water for 5'.

(d) Dry: Use the single dryer with the standard program, and the Si holder.

35. Deposition 4 μm SiO_2 backside

Use the Novellus PECVD reactor to deposit a 4 μm thick silicon oxide. Follow the operating instructions from the manual when using this machine.

Use recipe xxxnmsiostd at 400°C. Change the deposition time (seconds per station) according to logbook. Load wafer on top of transport wafer. (Use dedicated cassette and load only one wafer).

Gasses and flows	Pressure	HF power	LF power	Temp.	Time
N2/SiH4/N2O = 3150/210/6000 sccm	2.2 Torr	1000 W	0 W	400°C	ca 0'80"

Table B-2: Process conditions from chamber recipe xxxsiostd

36. Measurement: Silicon oxide thickness

Use the Leitz MPV-SP measurement system for layer thickness measurements.
Follow the operating instructions from the manual when using this equipment.
Measure on test wafer the thickness.

Use program: NOVELLUS Std SiO2.

37. Coating and backing

Use the EVG 120 coater/developer to coat the wafers with resist, and follow the instructions specified for this equipment. The process consists of a treatment with HMDS (hexamethyldisilazane) vapor with nitrogen as a carrier gas, spin coating with Shipley SPR3027 positive photoresist (spin velocity 2480 RPM; spin time 30"), and a soft bake at 95°C for 1.5'. Always check the temperature of the hotplate and the relative humidity ($48 \pm 2\%$) in the room first.

Use coating "Co-3027-3.1um" (resist thickness: 3.1 μm). Look at the list for the correct program.

38. Alignment and exposure

Processing will be performed on the ASML PAS 5500/80 automatic wafer stepper. Follow the operating instructions from the manual when using this machine.

Use BACK (box 437) job $Diesize\_20mm/bg20a - 11$, exposure energy: 1200 mJ.

39. Development

Use the EVG 120 Coater/developer to develop the wafers, and follow the instructions specified for this equipment. The process consists of a post-exposure bake at $115°C$ for 1.5', followed by a development step using Shipley MF322 developer (single puddle process), and a hard bake at 100°C for 1.5'. Always check the temperature of the hotplates first.

Use development program: Dev - SP.

40. Photoresist inspection

Visually inspect the wafers through a microscope. Check if there are residues in exposed parts. Put paper under wafer and throw away paper after use.

41. Plasma etching: SiO_2

Use the Drytek Triode 384T plasma etcher.
Follow the operating instructions from the manual when using this machine.
The process parameters of the etch program may not be changed.

Copy the program StdSiO2 in 'magwegNG' changing the time for etching windows into the oxide layer and landing on titanium.

Use recipe to etch the oxide. Settings presented in Table A-5. Time: ca 13'.

42. Layer stripping (SAL)

Perform PR stripping procedure with NMP solvent. First heat water to 80°C and put in ultrasonic bath. Than heat NMP to 70°C and put it in a beaker inside the bath. Use special holder to put wafers in bath and perform ultrasonic stripping for 5'.
Rinse: Rinse in flowing DI water for 5'.

43. Cleaning procedure: HNO_3 99% for green metal (SAL)

(a) 10' nitric acid at ambient temperature. This will dissolve organic materials. Use standard bench in SAL bench containing HNO_3 (99%) (metal).

(b) Rinse: Rinse in flowing DI water for 5'.

(c) Dry: Use the single dryer with the standard program, and the Si holder.

44. Coating and backing

Use the EVG 120 coater/developer to coat the wafers with resist, and follow the instructions specified for this equipment. The process consists of a treatment with HMDS (hexamethyldisilazane) vapor with nitrogen as a carrier gas, spin coating with Shipley SPR3012 positive photoresist (spin velocity 1575 RPM; spin time 30"), and a soft bake at 95°C for 1.5'. Always check the temperature of the hotplate and the relative humidity ($48 \pm 2\%$) in the room first.

Use coating "Co-3012-2.1um" (resist thickness: 2.1 μm). Look at the list for the correct program.

45. Alignment and exposure

Processing will be performed on the ASML PAS 5500/80 automatic wafer stepper. Follow the operating instructions from the manual when using this machine.

Use Ti2 (box 449) job g20a-1, exposure energy: 315 mJ. + Use open rectlicle 20x20, job g20a1edgefull exposure energy 315 mJ.

46. Development

Use the EVG 120 Coater/developer to develop the wafers, and follow the instructions specified for this equipment. The process consists of a post-exposure bake at $115°C$ for 1.5', followed by a development step using Shipley MF322 developer (single puddle process), and a hard bake at 100°C for 1.5'. Always check the temperature of the hotplates first.

Use development program: Dev - SP.

47. Photoresist inspection

Visually inspect the wafers through a microscope. Check if there are residues in exposed parts. Put paper under wafer and throw away paper after use.

48. Plasma etching Al and TiN

Use the Trikon Ωmega 201 plasma etcher. Follow the operating instructions from the manual when using this machine.

Use sequence al2T01gf (with a platen temperature of 25°C) to etch Al and TiN.

Step	Gasses and flows	Pressure	Platen RF	ICP RF	Platen temp.	Etch time
Breakthrough	Cl2/HBr = 30/40 sccm	5 mTorr	50 W	500 W	25°C	0'15"
Al	Cl2/HBr = 30/40 sccm	5 mTorr	35 W	500 W	25°C	3'15"
Ti	Cl2/HBr = 30/40 sccm	5 mTorr	40 W	500 W	25°C	0'21"

Table B-3: Process conditions from chamber recipe al2T01gf

Etching program includes end-point detection.

49. **Layer stripping (SAL)**

Perform PR stripping procedure with NMP solvent. First heat water to 80°C and put in ultrasonic bath. Than heat NMP to 70°C and put it in a beaker inside the bath. Use special holder to put wafers in bath and perform ultrasonic stripping for 5'.
Rinse: Rinse in flowing DI water for 5'.

50. **Cleaning procedure: HNO_3 99% for green metal (SAL)**

(a) 10' nitric acid at ambient temperature. This will dissolve organic materials. Use standard bath in SAL bench containing HNO_3 (99%) (metal).

(b) Rinse: Rinse in flowing DI water for 5'.

(c) Dry: Use the single dryer with the standard program, and the Si holder.

51. **Deposition 2 μm SiN**

Use the Novellus PECVD reactor to deposit a 2 μm thick Silicon Nitride. Follow the operating instructions from the manual when using this machine.

Use recipe xxxnmsinstd at 400°C. Change the deposition time (seconds per station) according to logbook.

Gasses and flows	Pressure	HF power	LF power	Temp.	Time
N2/SiH4/NH3 = 1000/280/1000 sccm	2.8 Torr	320 W	480 W	400°C	110"

Table B-4: Process conditions from chamber recipe xxxnmsinstd

52. **Measurement of Thickness**

Use the Leitz MPV-SP measurement system to measure the silicon nitride thickness.

Program: NOVELLUS std SiN, >50 nm. Perform measurement on test wafer.

53. **Plasma Etching: SiN**

Use the Alcatel GIR300 F etcher. Follow the operating instructions from the manual when using this machine.
Use the following settings:

Gasses and flows	Pressure	Power	Etch time.
CF4/SF6/O2 = 70/10/10 sccm	0.05 mBar	60 W	10'

Table B-5: Process conditions from chamber recipe: SiN etching (Alcatel)

54. Deposition 1.5 μm SiN

Use the Novellus PECVD reactor to deposit a 2 μm thick Silicon Nitride. Follow the operating instructions from the manual when using this machine.

Use recipe xxxnmsinstd at 400°C. Change the deposition time (seconds per station) according to logbook.
Settings in Table B-4; Time: ca 85"

55. Measurement of Thickness

Use the Leitz MPV-SP measurement system to measure the silicon nitride thickness. Perform measurement on test wafer.

Program: NOVELLUS std SiN, >50 nm

56. Coating and backing

Processing will be performed on the EVG 120 wafer track automatically:
this includes a HMDS (hexa methyl disilazane) treatment with nitrogen carrier gas , the coating with Shipley SPR 3027 resist (spin velocity 2480 RPM; spin time 30"), and prebaking. Follow the instructions specified for this equipment, and always check the temperature of the hotplate first.

Use Coating Program "CO-3027-3.1um" (resist thickness: 3.1 μm at 48% RV). Check eventual PR on backside.

57. Alignement and exposure

Processing will be performed on the ASML PAS5500/80 automatic wafer stepper.
Follow the operating instructions from the manual when using this machine.

Use mask SiN (box 459), job g20a-1 exposure energy 420 mJ, focus -12

58. Development

Use the EVG 120 Coater/developer to develop the wafers, and follow the instructions specified for this equipment. The process consists of a post-exposure bake at $115°C$ for 1.5', followed by a development step using Shipley MF322 developer x2 (double puddle process), and a hard bake at 100°C for 1.5'. Always check the temperature of the hotplates first.

Use development program: DP1.

59. Photoresist inspection

Visually inspect the wafers through a microscope. Check if there are residues in exposed parts. Put paper under wafer and throw away paper after use.

60. Plasma Etching: SiN

Use the Alcatel GIR300 F etcher. Follow the operating instructions from the manual when using this machine.
Use settings shown in B-5. Time: ca 25' (10'+10'+5').

61. Layer stripping (SAL)

Perform PR stripping procedure with NMP solvent. First heat water to 80°C and put in ultrasonic bath. Than heat NMP to 70°C and put it in a beaker inside the bath. Use special holder to put wafers in bath and perform ultrasonic stripping for 5'.
Rinse: Rinse in flowing DI water for 5'.

62. Cleaning procedure: HNO_3 99% for green metal (SAL)

(a) 10' nitric acid at ambient temperature. This will dissolve organic materials. Use standard bath in SAL bench containing HNO_3 (99%).

(b) Rinse: Rinse in flowing DI water for 5'.

(c) Dry: Use the single dryer with the standard program, and the Si holder.

63. Al deposition

Use the TRIKON SIGMA sputter coater for the deposition of the Al metal layer on the process wafers.The target must exist of AlSi. Follow the operating instructions from the manual when using this machine. Use recipe Al4mu-RF-350C to reactively sputter 4 μm Al. Temperature = 350°C

64. Coating and backing

Processing will be performed on the EVG 120 wafer track automatically:
this includes a HMDS (hexa methyl disilazane) treatment with nitrogen carrier gas , the coating with AZ9260 resist, and prebaking. Follow the instructions specified for this equipment, and always check the temperature of the hotplate first.

Use Coating Program "Co-AZ9260-Syr-6um-no EBR" (resist thickness: 6 μm at 48% RV). Check eventual PR on backside.
Before starting check if syring in the EVG 120 is empty and change holder.

65. Alignement and exposure

Processing will be performed on the ASML PAS5500/80 automatic wafer stepper.
Follow the operating instructions from the manual when using this machine.

Use mask METAL2 (box 460), job g20a-1 exposure energy 350 mJ, focus -2

66. Development

Use the EVG 120 Coater/developer to develop the wafers, and follow the instructions specified for this equipment. The process consists of a post-exposure bake at $115°C$ for 1.5', followed by a development step using Shipley MF322 developer (DOUBLE puddle process), and a hard bake at 100°C for 1.5'. Always check the temperature of the hotplates first.

Use development program: DP1.

67. Photoresist inspection

Visually inspect the wafers through a microscope. Check if there are residues in exposed parts. Put paper under wafer and throw away paper after use.

68. **Plasma etching of Al interconnects**

Use the Trikon Ωmega 201 plasma etcher. Follow the operating instructions from the manual when using this machine.

Use sequence AL4MU350 (with a platen temperature of 25°C) to etch Al.

Step	Gasses and flows	Pressure	Platen RF	ICP RF	Platen temp.	Etch time
Breakthrough	Cl2/HBr = 30/40 sccm	5 mTorr	50 W	500 W	25°C	0'15"
Bulk	Cl2/HBr = 30/40 sccm	5 mTorr	35 W	500 W	25°C	5
Overetch	Cl2/HBr = 30/40 sccm	5 mTorr	35 W	500 W	25°C	Step2 60%

Table B-6: Process conditions from chamber recipe AL4MU350

Etching program includes end-point detection.

69. **Layer stripping (SAL)**

Perform PR stripping procedure with NMP solvent. First heat water to 80°C and put in ultrasonic bath. Than heat NMP to 70°C and put it in a beaker inside the bath. Use special holder to put wafers in bath and perform ultrasonic stripping for 5'.
Rinse: Rinse in flowing DI water for 5'.

70. **Cleaning procedure: HNO_3 99% for green metal (SAL)**

(a) 10' nitric acid at ambient temperature. This will dissolve organic materials. Use standard bath in SAL containing HNO_3 (99%) (metal).

(b) Rinse: Rinse in flowing DI water for 5'.

(c) Dry: Use the single dryer with the standard program, and the Si holder.

71. **Deposition 10μm Zerostress SiO_2**

Use the Novellus PECVD reactor to deposit a 10 μm thick zero-stress SiO_2. Follow the operating instructions from the manual when using this machine.

Use recipe *zero_stress_sio*2 at 400°C. Change the deposition time (seconds per station) according to logbook.

Gasses and flows	Pressure	HF power	LF power	Temp.	Time
$SiH_4/N_2O/N_2$ = 300/9500/1500	2.4 Torr	0.75 W	0 W	400°C	ca 150"

Table B-7: Process conditions from chamber recipe *zero_stress_sio*2

72. Measurement of Thickness

Use the Leitz MPV-SP measurement system to measure the oxide thickness. Perform measurement on test wafer.

Program: NOVELLUS std SiO2

73. Coating and backing

Processing will be performed on the EVG 120 wafer track automatically:
this includes a HMDS (hexa methyl disilazane) treatment with nitrogen carrier gas , the coating with AZ9260 resist (spin velocity 950 RPM ; spin time 30"), and prebaking. Follow the instructions specified for this equipment, and always check the temperature of the hotplate first.

Use Coating Program "Co-AZ9260-Syr-12μm-no EBR" (resist thickness: 12 μm at 48% RV). Check eventual PR on backside.

Before starting check if siring in the EVG 120 is empty and change holder.

74. Alignement and exposure

Processing will be performed on the EV420 Contact Aligner. Follow the operating instructions from the manual when using this machine.

Use mask ORGAN_V3, BOX 453, exposure time ____ (perform test before proceeding), Program 1.

75. Development

Use the EVG 120 Coater/developer to develop the wafers, and follow the instructions specified for this equipment. The process consists of a post-exposure bake at 115°C for 1.5', followed by a development step using Shipley MF322 developer (single puddle process), and a hard bake at 100°C for 1.5'. Always check the temperature of the hotplates first.

Use development program: Dev-sp.

76. Photoresist inspection

Visually inspect the wafers through a microscope. Check if there are residues in exposed parts. Put paper under wafer and throw away paper after use.

77. Plasma etching: SiO_2

Use the Drytek Triode 384T plasma etcher.
Follow the operating instructions from the manual when using this machine.
The process parameters of the etch program may not be changed.

Copy the program StdSiO2 in 'magwegNG' changing the time for etching windows into the oxide layer and landing on Al. (bulk etch rate 0.5 μm/sec)

Use recipe to etch the oxide. Settings presented in Table A-5. Time: ca 20'. Perform the etching in more than one step. It is also possible to reduce the dry etching time by partially etch with BHF.

78. Layer stripping (SAL)

Perform PR stripping procedure with NMP solvent. First heat water to 80°C and put in ultrasonic bath. Than heat NMP to 70°C and put it in a beaker inside the bath. Use special holder to put wafers in bath and perform ultrasonic stripping for 5'.
Rinse: Rinse in flowing DI water for 5'.

79. **Cleaning procedure: HNO_3 99% for green metal (SAL)**

(a) 10' nitric acid at ambient temperature. This will dissolve organic materials. Use standard bath in SAL bench containing HNO_3 (99%) (metal).

(b) Rinse: Rinse in flowing DI water for 5'.

(c) Dry: Use the single dryer with the standard program, and the Si holder.

80. **Plasma etching Si backside**

Use the Rapier Omega i2L plasma etcher. It is not allowed to change the process conditions from the etch recipe. Change only number of cycles.
Landing in SiO2.
Use sequence EP_pox_through (with a platen temperature of 20°C) to etch the Si layer and stop on SiO_2. Ca 500 cycles.
Etching program includes end-point detection.

81. **Triton Treatment in (SAL)**

Treat hole walls by soaking for few seconds the wafer in Triton in a dedicated bath. (6 drops per liter)

82. **Wet etching BHF: Etch landing Thermal SiO_2 and TEOS layer (SAL)**

(a) Etch: Use a dedicated bath in SAL contaminated bench with "BHF 1:7 (Metal)" at ambient temperature, and contaminated carrier.
The bath contains a buffered HF solution.

(b) Time: ca 25'

(c) Rinse: Rinse flowing water for 5'.

83. **Inspection (SAL)**

Visually inspect the wafers through a microscope, check if CNT holes have been released. Put paper under wafer and throw away paper after use. Repeat BHF etching till all electrodes are clearly black.

84. **Layer stripping**

Perform Acetone stripping procedure. Heat acetone to 40°C in a beaker. Use special holder to put wafers in bath and perform stripping for 5'.
Rinse: Rinse in flowing DI water for 5'.

Appendix C

Mask set

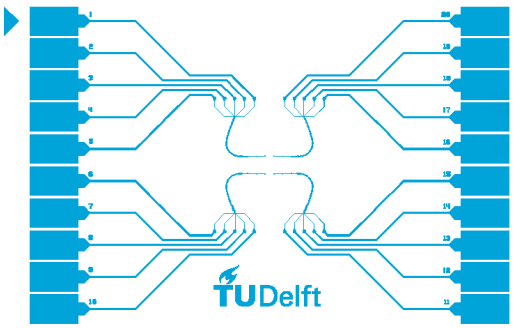

(a) Full view

(b) Zoom in on micro-electrode array.

Figure C-1: Mask: METAL. Blue area not exposed.

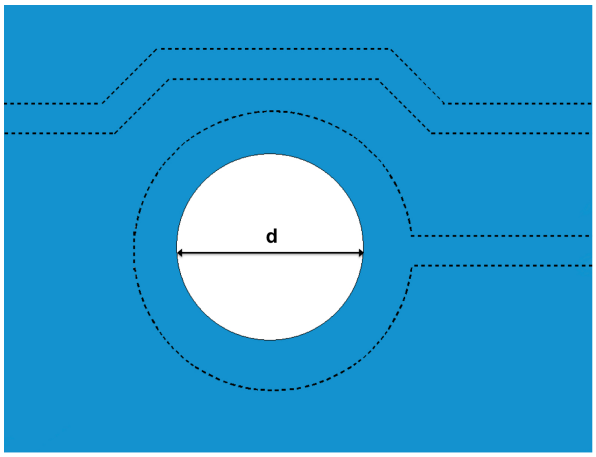

Figure C-2: Mask: CNT/SiN. CNT: d=12 μm, SiN: d= 6 μm. Blue area not exposed. Mask METAL reported with black dotted lines.

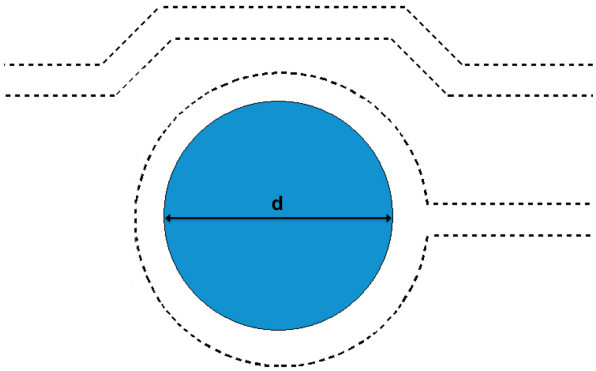

Figure C-3: Mask: Ti/Ti2. Ti: d=14 μm, Ti2: d= 24 μm. Blue areas not exposed. Mask METAL reported with black dotted lines.

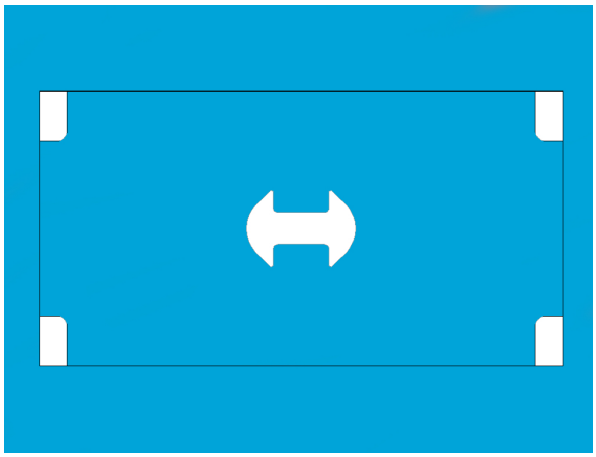

Figure C-4: Mask: BACK. Blue area not exposed. Scribe lines reported in black.

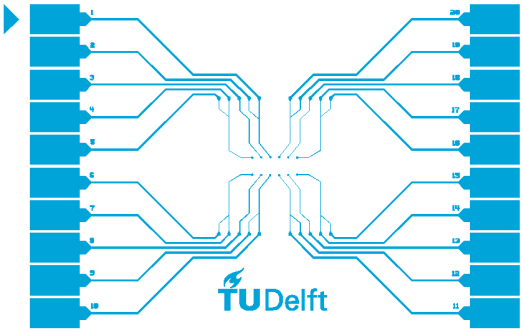

(a) Full view

(b) Zoom in on micro-electrode array.

Figure C-5: Mask: METAL2. Blue area not exposed.

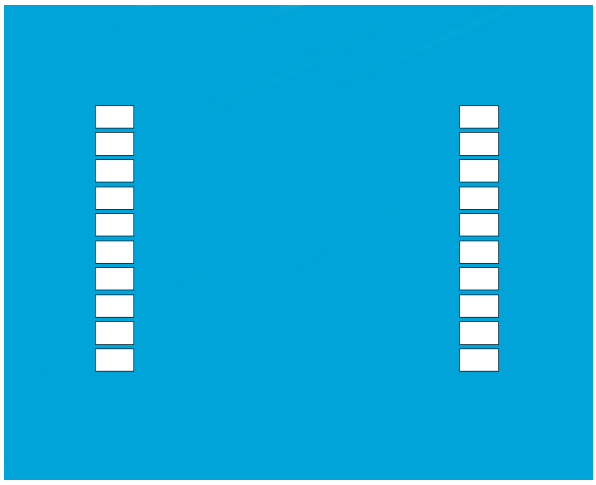

Figure C-6: Maks: ORGAN_V3. Blue area not exposed.

Bibliography

[1] S. K. Pakazad, A. Savov, A. van de Stolpe, and R. Dekker, "A novel stretchable microelectrode array (smea) design for directional stretching of cells," *Journal of Micromechanics and Microengineering*, vol. 24, no. 3, p. 034003, 2014.

[2] v. d. S. B. M. D. Pakazad, Savov, "A stretchable micro-electrode array for in vitro electrophysiology," *IEEE International Conference on Micro Electro Mechanical Systems - MEMS*, pp. 829–832, 2012.

[3] K.-L. Yang, S. Yiacoumi, and C. Tsouris, "Electrical double-layer formation," *Dekker Encyclopedia Of Nanoscience And Nanotechnology*, p. 1001, 2004.

[4] S. Vollebregt, *Carbon Nanotubes as Vertical Interconnects in 3D Integrated Circuits*. PhD thesis, TU Delft.

[5] A. I. Aria, *Control of wettability of carbon nanotube array by reversible dry oxidation for superhydrophobic coating and supercapacitor applications*. PhD thesis, California Institute of Technology, 2013.

[6] M. P. Pujadó, *Carbon nanotubes as platforms for biosensors with electrochemical and electronic transduction*. Springer Science & Business Media, 2012.

[7] A. O. Fung, C. Tsiokos, O. Paydar, L. H. Chen, S. Jin, Y. Wang, and J. W. Judy, "Electrochemical properties and myocyte interaction of carbon nanotube microelectrodes," *Nano letters*, vol. 10, no. 11, pp. 4321–4327, 2010.

[8] T. Gabay, M. Ben-David, I. Kalifa, R. Sorkin, R. A. ZeâĂŹev, E. Ben-Jacob, and Y. Hanein, "Electro-chemical and biological properties of carbon nanotube based multi-electrode arrays," *Nanotechnology*, vol. 18, no. 3, p. 035201, 2007.

[9] M. David-Pur, L. Bareket-Keren, G. Beit-Yaakov, D. Raz-Prag, and Y. Hanein, "All-carbon-nanotube flexible multi-electrode array for neuronal recording and stimulation," *Biomedical microdevices*, vol. 16, no. 1, pp. 43–53, 2014.

[10] S. F. Cogan, "Neural stimulation and recording electrodes," *Annu. Rev. Biomed. Eng.*, vol. 10, pp. 275–309, 2008.

[11] G. M. Bellin, Marchetto, "Induced pluripotent stem cells: the new patient?," *Nature Reviews*, vol. 13, pp. 713–723, 2012.

[12] C. P. Firme III and P. R. Bandaru, "Toxicity issues in the application of carbon nanotubes to biological systems," *Nanomedicine: Nanotechnology, Biology and Medicine*, vol. 6, no. 2, pp. 245–256, 2010.

[13] A. Norlin, J. Pan, and C. Leygraf, "Investigation of electrochemical behavior of stimulation/sensing materials for pacemaker electrode applications i. pt, ti, and tin coated electrodes," *Journal of the Electrochemical Society*, vol. 152, no. 2, pp. J7–J15, 2005.

[14] I. A. S. Olsson, N. H. Franco, D. M. Weary, and P. Sandøe, "The 3rs principle–mind the ethical gap!," *ALTEX*, pp. 333–336, 2011.

[15] D. J. Wells, "Animal welfare and the 3rs in european biomedical research," *Annals of the New York Academy of Sciences*, vol. 1245, no. 1, pp. 14–16, 2011.

[16] v. d. B. van der Meer, "Organs-on-chips: breaking the in vitro impasse," *The Royal Society of Chemistry 2012*, vol. 4, no. 5, pp. 451–576, 2012.

[17] d. T. van de Stolpe, "Workshop meeting report organs-on-chips: human disease models," *The Royal Society of Chemistry 2013*, 2013.

[18] R. v. N. Y. Zhang, Zhao, "Towards a human-on-chip: Culturing multiple cell types on a chip with compartmentalized microenvironments," *The Royal Society of Chemistry 2009*, vol. 9, no. 22, pp. 3165–3312, 2009.

[19] J. P. Wikswo, E. L. Curtis, Z. E. Eagleton, B. C. Evans, A. Kole, L. H. Hofmeister, and W. J. Matloff, "Scaling and systems biology for integrating multiple organs-on-a-chip," *Lab on a Chip*, vol. 13, no. 18, pp. 3496–3511, 2013.

[20] G. Hamilton, "Body parts on a chip, tedxboston 2013." https://www.ted.com/talks/geraldine_hamilton_body_parts_on_a_chip. [Online; accessed 8-October-2014].

[21] S. R. Braam, L. Tertoolen, A. van de Stolpe, T. Meyer, R. Passier, and C. L. Mummery, "Prediction of drug-induced cardiotoxicity using human embryonic stem cell-derived cardiomyocytes," *Stem cell research*, vol. 4, no. 2, pp. 107–116, 2010.

[22] D. E. Ingber, "Cellular mechanotransduction: putting all the pieces together again," *The FASEB journal*, vol. 20, no. 7, pp. 811–827, 2006.

[23] D.-H. Kim, P. K. Wong, J. Park, A. Levchenko, and Y. Sun, "Microengineered platforms for cell mechanobiology," *Annual review of biomedical engineering*, vol. 11, pp. 203–233, 2009.

[24] N. Wang, J. D. Tytell, and D. E. Ingber, "Mechanotransduction at a distance: mechanically coupling the extracellular matrix with the nucleus," *Nature reviews Molecular cell biology*, vol. 10, no. 1, pp. 75–82, 2009.

[25] B. Van Meer, *Design of Cytostretch Skin A human cell based stretchable, flexible and mass-producible skin tissue model for drug development.* PhD thesis, Delft University of Technology, 2014.

[26] W. F. Boron and E. L. Boulpaep, *Medical Physiology, 2e Updated Edition: with STUDENT CONSULT Online Access.* Elsevier Health Sciences, 2012.

[27] M. R. Neuman, "Biopotential amplifiers," *Medical instrumentation: application and design*, pp. 316–318, 1998.

[28] L. Bareket-Keren and Y. Hanein, "Carbon nanotube-based multi electrode arrays for neuronal interfacing: progress and prospects," *Frontiers in neural circuits*, vol. 6, 2012.

[29] W. Franks, I. Schenker, P. Schmutz, and A. Hierlemann, "Impedance characterization and modeling of electrodes for biomedical applications," *Biomedical Engineering, IEEE Transactions on*, vol. 52, no. 7, pp. 1295–1302, 2005.

[30] E. Huigen, A. Peper, and C. Grimbergen, "Investigation into the origin of the noise of surface electrodes," *Medical and biological engineering and computing*, vol. 40, no. 3, pp. 332–338, 2002.

[31] C. Chen, H. Su, S. Chuang, S. Yen, Y. Chen, Y. Lee, T. Yew, H. Chen, S. Yeh, Y. Chang, *et al.*, "Hydrophilic modification of multi-walled carbon nanotubes based neural microelectrode array," in *Solid-State Sensors, Actuators and Microsystems Conference, 2009. TRANSDUCERS 2009. International*, pp. 967–970, IEEE, 2009.

[32] H.-S. P. Wong and D. Akinwande, *Carbon nanotube and graphene device physics.* Cambridge University Press, 2011.

[33] Q. Zhang, G. Chen, S. Yoon, J. Ahn, S. Wang, Q. Zhou, Q. Wang, J. Li, *et al.*, "Thermal conductivity of multiwalled carbon nanotubes," *Physical Review B*, vol. 66, no. 16, p. 165440, 2002.

[34] S. Vollebregt, C. Beenakker, and R. Ishihara, "Carbon nanotubes as vertical interconnects in 3d integrated circuits," 2014.

[35] X. Zhang, Q. Li, Y. Tu, Y. Li, J. Y. Coulter, L. Zheng, Y. Zhao, Q. Jia, D. E. Peterson, and Y. Zhu, "Strong carbon-nanotube fibers spun from long carbon-nanotube arrays," *Small*, vol. 3, no. 2, pp. 244–248, 2007.

[36] P. Li, X. Lim, Y. Zhu, T. Yu, C.-K. Ong, Z. Shen, A. T.-S. Wee, and C.-H. Sow, "Tailoring wettability change on aligned and patterned carbon nanotube films for selective assembly," *The Journal of Physical Chemistry B*, vol. 111, no. 7, pp. 1672–1678, 2007.

[37] M. E. RamoÌĄn, A. Gupta, C. Corbet, D. A. Ferrer, H. C. Movva, G. Carpenter, L. Colombo, G. Bourianoff, M. Doczy, D. Akinwande, *et al.*, "Cmos-compatible synthesis of large-area, high-mobility graphene by chemical vapor deposition of acetylene on cobalt thin films," *ACS nano*, vol. 5, no. 9, pp. 7198–7204, 2011.

[38] G. Gabriel, R. Gómez-Martínez, and R. Villa, "Interface impedance improvement with carbon nanotubes," in *13th International Conference on Electrical Bioimpedance and the 8th Conference on Electrical Impedance Tomography*, pp. 296–299, Springer, 2007.

[39] M. Shein, A. Greenbaum, T. Gabay, R. Sorkin, M. David-Pur, E. Ben-Jacob, and Y. Hanein, "Engineered neuronal circuits shaped and interfaced with carbon nanotube microelectrode arrays," *Biomedical microdevices*, vol. 11, no. 2, pp. 495–501, 2009.

[40] C.-M. Lin, Y.-T. Lee, S.-R. Yeh, and W. Fang, "Flexible carbon nanotubes electrode for neural recording," *Biosensors and Bioelectronics*, vol. 24, no. 9, pp. 2791–2797, 2009.

[41] H.-L. Hsu, I.-J. Teng, Y.-C. Chen, W.-L. Hsu, Y.-T. Lee, S.-J. Yen, H.-C. Su, S.-R. Yeh, H. Chen, and T.-R. Yew, "Flexible uv-ozone-modified carbon nanotube electrodes for neuronal recording," *Advanced Materials*, vol. 22, no. 19, pp. 2177–2181, 2010.

[42] S. Vollebregt, R. Ishihara, J. Derakhshandeh, J. van der Cingel, H. Schellevis, and C. Beenakker, "Integrating low temperature aligned carbon nanotubes as vertical interconnects in si technology," in *Nanotechnology (IEEE-NANO), 2011 11th IEEE Conference on*, pp. 985–990, IEEE, 2011.

[43] J. Creemer, D. Briand, H. Zandbergen, W. Van der Vlist, C. de Boer, N. F. de Rooij, and P. Sarro, "Microhotplates with tin heaters," *Sensors and Actuators A: Physical*, vol. 148, no. 2, pp. 416–421, 2008.

[44] C. Wirth, S. Hofmann, and J. Robertson, "Surface properties of vertically aligned carbon nanotube arrays," *Diamond and Related Materials*, vol. 17, no. 7, pp. 1518–1524, 2008.

[45] L. Technologies, "GibcoÅą cell culture basics." http://www.invitrogen.com/site/us/en/home/References/gibco-cell-culture-basics.html. [Online; accessed 16-July-2013].

[46] Y. Takahashi, "S. induction of pluripotent stem cells from mouse embryonic and adult fibroblast cultures by defined factors. cell," *Science*, vol. 126, p. 663ÃŘ676, 2006.

[47] S.-O. A.-B. F. T. N. J. R. S. S. T. Yu, Vodyanik, "Induced pluripotent stem cell lines derived from human somatic cells," *Science*, vol. 318, pp. 1917–1919, 2007.

[48] ScienceDaily, "Eliminating viral vector in stem cell reprogramming." http://www.invitrogen.com/site/us/en/home/References/gibco-cell-culture-basics.html, 2008. [Online; accessed 16-July-2013].

[49] H.-I. Y. Okita, Nakagawa, "Generation of mouse induced pluripotent stem cells without viral vectors," *Science*, vol. 322, pp. 949–952, 2008.

[50] D. F. Williams, *The Williams dictionary of biomaterials*. Liverpool University Press, 1999.

[51] D. B. Warheit, B. Laurence, K. L. Reed, D. Roach, G. Reynolds, and T. Webb, "Comparative pulmonary toxicity assessment of single-wall carbon nanotubes in rats," *Toxicological sciences*, vol. 77, no. 1, pp. 117–125, 2004.

[52] S. Smart, A. Cassady, G. Lu, and D. Martin, "The biocompatibility of carbon nanotubes," *Carbon*, vol. 44, no. 6, pp. 1034–1047, 2006.

[53] K. Hara, K. Aoki, Y. Usui, M. Shimizu, N. Narita, N. Ogihara, K. Nakamura, N. Ishigaki, K. Sano, H. Haniu, *et al.*, "Evaluation of cnt toxicity by comparison to tattoo ink," *Materials Today*, vol. 14, no. 9, pp. 434–440, 2011.

[54] S. Garibaldi, C. Brunelli, V. Bavastrello, G. Ghigliotti, and C. Nicolini, "Carbon nanotube biocompatibility with cardiac muscle cells," *Nanotechnology*, vol. 17, no. 2, p. 391, 2006.

[55] L. O. Simonsen, H. Harbak, and P. Bennekou, "Cobalt metabolism and toxicologyâĂŤa brief update," *Science of the Total Environment*, vol. 432, pp. 210–215, 2012.

[56] A. Von Recum and T. Van Kooten, "The influence of micro-topography on cellular response and the implications for silicone implants," *Journal of Biomaterials Science, Polymer Edition*, vol. 7, no. 2, pp. 181–198, 1996.

[57] J. Park, P. Kim, W. Helen, A. J. Engler, A. Levchenko, D.-H. Kim, *et al.*, "Control of stem cell fate and function by engineering physical microenvironments," *Integrative Biology*, vol. 4, no. 9, pp. 1008–1018, 2012.

[58] S. Agrawal, *Assessment of Cytostretch-A Heart-On-Chip device. Experiments on Cardiomyocytes*. PhD thesis, TU Delft, Delft University of Technology, 2014.

Glossary

List of Acronyms

PDMS	PolyDiMethylSiloxane
CNT	Carbon Nanotube
VACNT	Vertically Aligned Carbon Nanotube
SWCNT	Single-Walled Carbon Nanotube
CVD	Chemical Vapour Deposition
MWCNT	Multi-Walled Carbon Nanotube
iPSC	Induced Pluripotential Stem Cell
ECTM	Laboratory of Electronic Components, Technology and Materials
DIMES	Delft Institute of Microsystems and Microelectronics
EMA	European Medicines Agency
EURL ECVAM	European Union Reference Laboratory for Alternatives to Animal Testing
FEM	Finite-Element Model
PECVD	Plasma Enhanced Chemical Vapour Deposition
DRIE	Deep Reactive Ion Etching
SSA	Specific Surface Area
MEA	Micro-Electrode Array
GSA	Geometric Surface Area
AC	Alternating Current
SNR	Signal to Noise Ration

EIS	Electrochemical Impedance Spectroscopy
PBS	Phosphate Buffered Saline
TEM	Transmission Electron Microscopy
FWHM	Full Width at Half Maximum
TEOS	TetraEthyl OrthoSilicate
PR	PhotoResist
SAL	Special Application Laboratory
CR	Clean Room
BOE	Buffered Oxide Etch
SEM	Scanning Electron Microscope
FIB	Focused Ion Beam
CV	Cyclic Voltammetry
CSC	Charge Storage Capacity
ATP	Adenosine Triphosphate
DAPI	4',6-DiAmidino-2-PhenylIndole
CY3	Cyanine dye
SIROF	Sputtered Iridium Oxide Film
GFP	Green Fluorescent Protein
ALD	Atomic Layer Deposition
THF	TetraHydroFuraan
CPE	Constant Phase Element
IPA	IsoPropAnol

List of Symbols

α_{dl}	Empirical constant [0-1]
K_{dl}	CPE parameter
C_{CNT}	CNT film capacitance
C_{dl}	Double layer capacitor
R_f	Faradaic resistance

R_p	Pore resistance
R_s	Solution resistance
V_m	Membrane potential
V_t	Threshold voltage